

# Ligand Chemistry of Inorganic Lead Halide Perovskite Nanocrystals

Nadesh Fiuza-Maneiro, Kun Sun, Iago López-Fernández, Sergio Gómez-Graña, Peter Müller-Buschbaum, and Lakshminarayana Polavarapu\*



Cite This: *ACS Energy Lett.* 2023, 8, 1152–1191



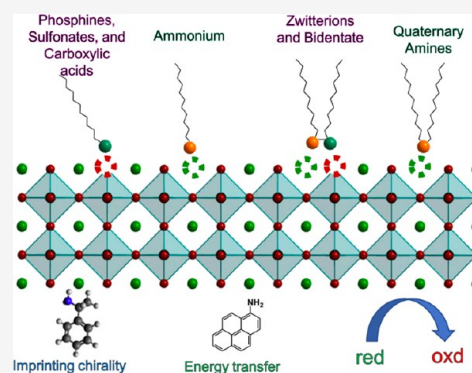
Read Online

ACCESS |

Metrics & More

Article Recommendations

**ABSTRACT:** Lead halide perovskite nanocrystals (LHP NCs) have emerged as next-generation semiconductor materials with outstanding optical and optoelectronic properties. Because of the high surface-to-volume ratio, the optical and optoelectronic performance and the colloidal stability of LHP NCs largely depend on their surface chemistry, especially the ligands and surface termination. On one hand, the capping ligands improve the colloidal stability and luminescence; on the other hand the highly dynamic binding nature of ligands is detrimental to the colloidal stability and photoluminescence of LHP NCs. In addition, the surface functionalization with desired molecules induces new functionalities such as chirality, light harvesting, and triplet sensitization through energy/electron transfer or use as X-ray detectors. In this review, we present the current understanding of an atomic view of the surface chemistry of colloidal LHP NCs, including crystal termination, vacancies, and different types of capping ligands. Furthermore, we discuss the ligand-induced functionalities, including photocatalysis and chirality.



Colloidal nanocrystals are ligand-capped tiny particles with at least one of their dimensions in the range of 1–100 nm and are constituted of hundreds to thousands of atoms.<sup>1–5</sup> Because of their extremely small size, they exhibit a high surface-to-volume ratio; thus, the surfaces play a vital role in their optical, electronic, and catalytic properties.<sup>4,6–9</sup> Importantly, materials at the nanoscale exhibit unique size-dependent properties that can be harnessed for a variety of applications.<sup>5,8,10,11</sup> Semiconductor quantum dots (QDs) are one of the most important classes of materials that exhibit size and shape-dependent optical properties.<sup>4,12</sup> Over the last few decades, colloidal semiconductor QDs with the compositions of II–VI and III–V groups have been greatly investigated regarding their synthesis and optoelectronic applications.<sup>10,13,14</sup> The emission color of QDs is precisely tunable across the visible spectrum of light by their size without changing the composition.<sup>10,13–15</sup> However, these classical QDs require an epitaxially coated wide-bandgap inorganic shell that passivates the surface traps to achieve high photoluminescence quantum yields (PLQY), while the organically passivated QDs exhibit low PLQY because of surface-related trap states. Over the last 7–8 years, the research focus has been partially shifted to the newly emerged colloidal lead halide perovskite (LHP) nanocrystals (NCs) because of their remarkable optical and optoelectronic properties, such as

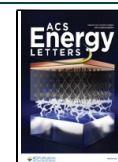
near-unity PLQY, narrow emission line widths, tunable emission color by halide composition and by accessing quantum confinement effects, suppressed blinking, and defect tolerant nature.<sup>8,16–25</sup> Unlike classical core–shell QDs, organic ligand-capped colloidal halide (Br and I) perovskite NCs without an inorganic shell exhibit extremely high PLQY because of their defect-tolerant nature.<sup>20,26</sup> These interesting properties confer them a multitude of applications, including light-emitting diodes (LEDs), near-eye displays for augmented and virtual reality (AR and VR), single-photon emission, photodetectors, lasers, and photovoltaics.<sup>8,19,27–30</sup>

Halide perovskites exhibit  $ABX_3$  crystal structure, typically in cubic or orthorhombic phases, in which the divalent cation “B” is coordinated to six halides (X) in an octahedral fashion, while the monovalent cation “A” sits in and occupies the cuboctahedral cavity of eight  $BX_6$  octahedral units.<sup>8</sup> The A is either an organic [typically methylammonium ( $MA^+$ ) or formamidinium ( $FA^+$ )] or inorganic (usually  $Cs^+$ ) cation; B

Received: October 19, 2022

Accepted: January 5, 2023

Published: January 26, 2023



is  $\text{Pb}^{2+}$ ,  $\text{Sn}^{2+}$  or  $\text{Ge}^{2+}$ ; and X is a halide ( $\text{Cl}^-$ ,  $\text{Br}^-$ , or  $\text{I}^-$ ). The optical properties of metal halide perovskite NCs are tunable across the visible spectrum to near-infrared by varying the composition of the three constituents (A, B, and X). After the early reports,<sup>21–23,25,31,32</sup> perovskite NCs have been greatly exploited regarding their synthesis with a wide range of A, B, and X compositions, properties, and applications.<sup>8</sup> In particular, inorganic lead halide perovskite NCs received special interest because of their superior stability and the ability to synthesize them with excellent shape control, along with high monodispersity and crystallinity compared with organic–inorganic hybrid counterparts. These NCs are being significantly studied regarding their use as light-emitting and -harvesting materials in LEDs and solar cells, respectively.<sup>8,20,27,29,33,34</sup> The power conversion efficiency (PCE) and electroluminescence quantum efficiency (EQE) of halide perovskite NC-based solar cells and LEDs have continued to rise over the years and have surpassed 17% and 23%, respectively.<sup>20,27</sup> However, the optical properties of halide perovskite NCs are often hampered by halide vacancies on the surface and the defects formed by ligand detachment. The ligand binding to the surface of halide perovskite NCs is highly dynamic because of its ionic nature and, thus, leads to a detachment of ligands and removal of surface halides during the purification process that is necessary for device applications. Despite the defect tolerance nature, the detachment of ligands and halide atoms from the surface significantly reduces the PLQY because of the formation of nonradiative surface traps.<sup>8,20,35,36</sup> The surface ligands not only affect the PLQY of NCs but also the shape and size, along with their colloidal stability and assembly into thin films, which is crucial for device applications. Therefore, ligands and the passivation of surface traps play an essential role in modulating stability, luminescence, or charge carrier transport and perhaps even in the induction of new functionalities.<sup>8,20,37–39</sup> Interestingly, the surface traps are removable by postsynthetic chemical treatments. Currently, understanding the surface chemistry through different characterization techniques, testing different ligands, postsynthetic surface treatment, ligand exchange, and surface functionalization for the introduction of new properties and improvement of the stability and PLQY of LHP NCs are the most active research directions in the field.<sup>8</sup> A large number of ligands and passivation approaches have been reported for improving the colloidal and phase stability and PLQY of LHP NCs (see Table 1).<sup>8,20,39,40</sup>

Ligands and the passivation of surface traps play an essential role in modulating stability, luminescence, or charge carrier transport and perhaps even in the induction of new functionalities.

This review presents a state-of-the-art understanding of the atomic and molecular view of the surface chemistry of ligand-capped colloidal LHP nanocrystals. We first present the possible mechanisms of ligand binding to the surface of LHP NCs and the defects formed upon the detachment of ligands and surface atoms and their consequences on the optical properties. The structural characterization of surfaces by different experimental techniques is presented. We then discuss the surface passivation mechanisms via in situ synthesis

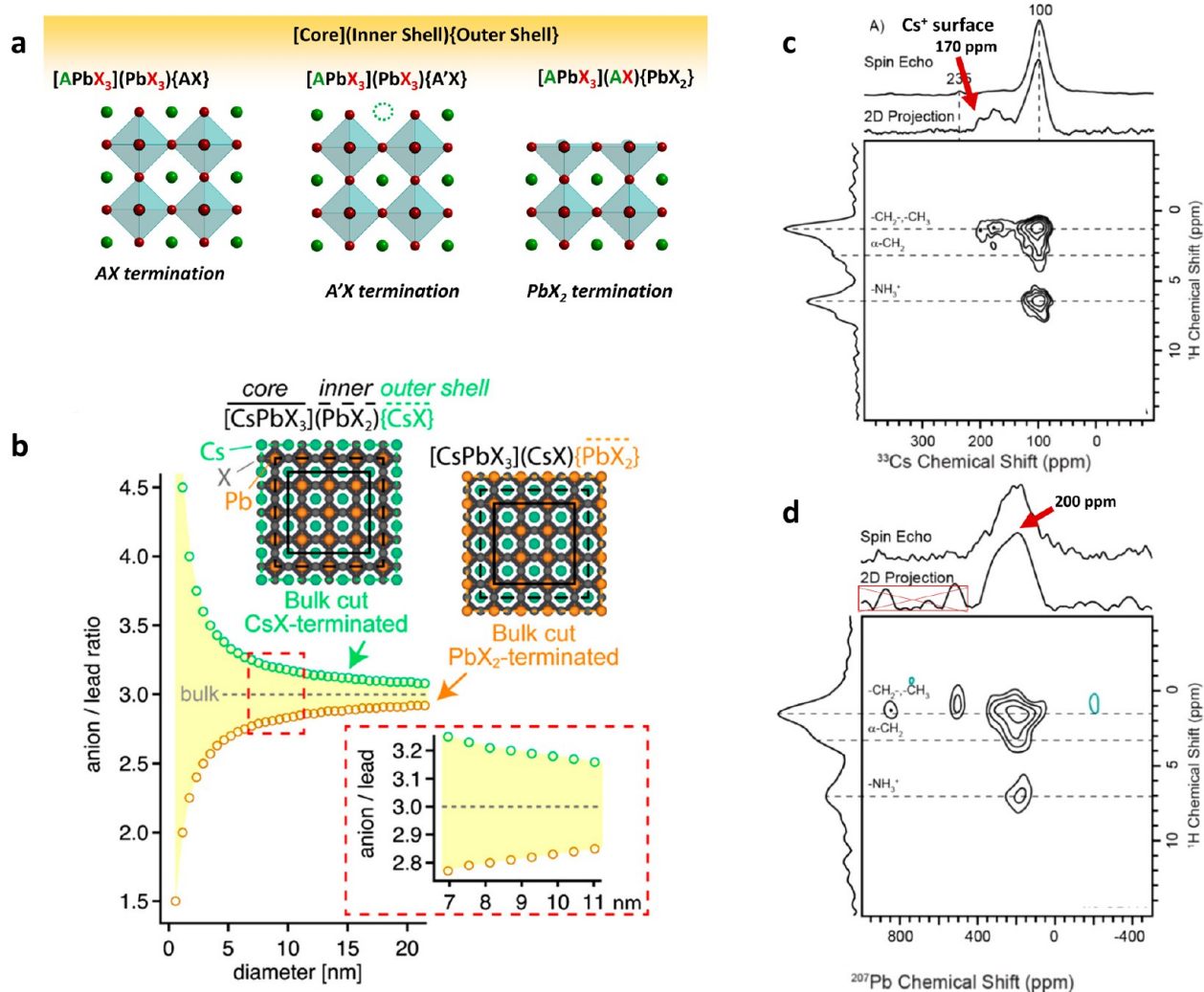
or postsynthetic ligand exchange and various strongly bounded ligands used to improve the stability and PLQY of LHP NCs. The functionalization of surfaces with different functional ligands for imparting new properties into LHP NCs is presented. Finally, we provide a brief outlook and future research directions with outstanding questions that remain in understanding surface chemistry, ligand exchange, and surface functionalization of LHP NCs.

## ■ ATOMIC VIEW OF SURFACE TERMINATION

As discussed in the introduction, the surface atoms and ligands of colloidal semiconductor NCs play an important role in their optical and chemical properties because of their high surface-to-volume ratio.<sup>6,8,41,42</sup> In particular, for LHP NCs, the ionic nature and weak interactions with ligands make them vulnerable to detachment of surface atoms and ligands, which leads to the formation of defects and, thus, the introduction of trap states that stimulate nonradiative recombination processes. However, the ionic character of the capping ligands allows the modification of the NC surface along with their properties and colloidal stability. Therefore, an atomic-level understanding of the surfaces of LHP NCs, in terms of crystal structure, surface defects, and surface termination, is the prerequisite for enabling a better tuning of their optical properties.<sup>8,40,43,44</sup>

An atomic-level understanding of the surfaces of LHP NCs, in terms of crystal structure, surface defects, and surface termination, is the prerequisite for enabling a better tuning of their optical properties.

Accordingly, several studies have proposed the possibility of the existence of two different surface terminations for the typical orthorhombic phase 9–12 nm  $\text{CsPbBr}_3$  NCs.<sup>38,45–49</sup> The two types of terminations are CsBr (or Cs atoms substituted with ammonium ligands) and  $\text{PbBr}_2$ , which are illustrated in Figure 1.<sup>46</sup> In this regard, Bodnarchuk et al. used density functional theory (DFT) calculations to analyze the atomistic stoichiometry of the surface terminations and their inherent optoelectronic properties for  $\text{CsPbBr}_3$  NCs.<sup>38</sup> They proposed the two surface terminations on the basis of the X/Pb ratio, which can be measured by XPS or ICP mass spectrometry.<sup>50,51</sup> The ratio of X/Pb and X/Cs at the surface of typical 9–12 nm  $\text{CsPbX}_3$  NCs is usually different (typically varies between about 2.7 and 3.3) from that of bulk ( $\sim 3$ ).<sup>38</sup> The surface X/Pb ratio significantly increases with a decrease in the size of NCs because of the high surface-to-volume ratio. For an ideal cubic phase (or orthorhombic phase), the NCs adapt an  $(\text{APbX}_3)(\text{PbX}_2)$  (AX)-type structure at a high X/Pb ratio ( $>3$ ), which corresponds to an  $\text{APbX}_3$  core terminated by an inner shell of  $\text{PbX}_2$  with an outer shell composed of monovalent cations (A:  $\text{Cs}^+$ ,  $\text{FA}^+$ , or  $\text{MA}^+$ ) and X anions (X: halides or carboxylic acid ligands).<sup>38</sup> However, the substitution of some of the A cations by ammonium ligands ( $\text{A}'$ ) results in an  $\text{A}'\text{X}$ -type stoichiometry on the surface with an  $(\text{APbX}_3)-(\text{PbX}_2)\text{A}'\text{X}$ -type structure (Figure 1a). For a low X/Pb ratio ( $<3$ ), the NCs adapt an  $(\text{APbX}_3)(\text{AX})(\text{PbX}_2)$ -type structure with a  $\text{PbX}_2$  surface termination.<sup>38</sup> In this case, the ligands most likely bind to the  $\text{PbX}_2$  terminal, and the structure



**Figure 1.** (a) Three typical possible surface terminations for cubic/orthorhombic  $\text{APbX}_3$  NCs. The A, B, and X atoms are labeled in green, black, and red, respectively. The dotted circle represents the A cation vacancies. The NCs can be modeled with an inorganic core and AX or  $\text{PbX}_2$  surface termination. The replacement of A with an ammonium ligand gives an A'X terminated surface. (b) Size-dependent anion/lead (X/Pb) ratio of  $\text{CsPbX}_3$  NCs, where Cs, Pb, and X atoms are labeled in green, orange, and gray spheres, respectively. Reproduced with permission from ref 52. Copyright 2019 American Chemical Society. (c) Solid-state  $^{133}\text{Cs}$  spin-echo and 2D  $^1\text{H} \rightarrow ^{133}\text{Cs}$  CP-HETCOR NMR spectra of  $\text{CsPbBr}_3$  NCs. (d) Solid-state  $^{207}\text{Pb}$  spin-echo and 2D  $^1\text{H} \rightarrow ^{207}\text{Pb}$  CP-HETCOR NMR spectra of  $\text{CsPbBr}_3$  NCs. The  $^{207}\text{Pb}$  NMR signals at 500 and 850 ppm are from  $t_1$  noise. The panels (a), (c), and (d) are reproduced with permission from ref 53. Copyright 2020 American Chemical Society.

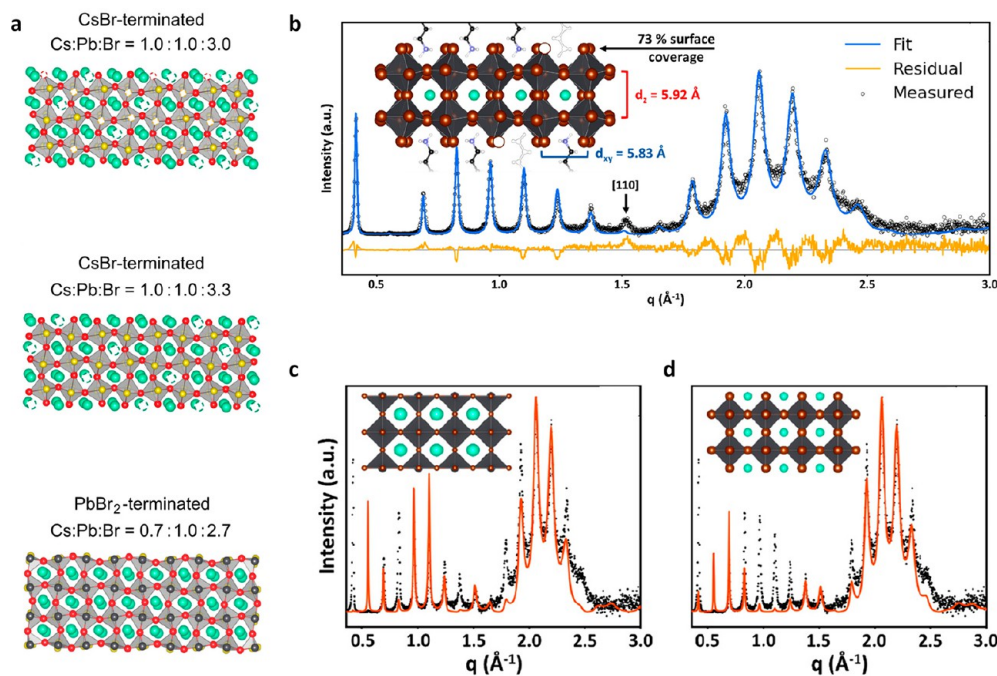
becomes  $(\text{APbX}_3)(\text{AX})(\text{PbX}'_2)$ -type, where  $\text{X}'$  is an oleate ligand. However, this  $\text{PbX}'_2$  termination is unlikely because it requires a dense packing of ligands to passivate the Pb surface atoms, which leads to steric hindrance and disturbs the  $\text{Pb}^{2+}$  octahedral coordination.<sup>38</sup>

Furthermore, it is predicted that the  $\text{PbX}'_2$ -type of termination leads to the formation of charge traps after the loss of only 25% of the ligands.<sup>53</sup> Therefore, the most realistic surface termination constitutes the  $(\text{APbX}_3)(\text{PbX}_2)[(\text{A} + \text{A}')\text{X}]$  structure, in which  $(\text{A} + \text{A}')$  is a mixture of A cations and alkylammonium cation ligands that provides colloidal stability. In addition, the  $(\text{APbX}_3)(\text{PbX}_2)[\text{A}(\text{X} + \text{X}')]$  structure is also proposed, in which  $(\text{X} + \text{X}')$  is a mixture of halides and oleate ligands. The  $(\text{APbX}_3)(\text{PbX}_2)[(\text{A} + \text{A}')\text{X}]$ -type structure was further supported by  $^{133}\text{Cs}$  direct excitation (spin echo) and surface-selective 2D dipolar  $^1\text{H} \rightarrow ^{133}\text{Cs}$  cross-polarization heteronuclear correlation (CP-HETCOR) NMR experiments (Figure 1c).<sup>53</sup> The spin-echo spectra consists of three main

signals: (1) a high intensity one at 100 ppm, which was assigned to bulk  $\text{CsPbBr}_3$ ; (2) a very low-intensity signal around 235 ppm, which was assigned to zero-dimensional  $\text{Cs}_4\text{PbBr}_6$  crystals; and (3) a low-intensity broad peak at around 170 ppm, which was attributed to cesium present on the surface. The signal attributed to surface Cs (170 ppm) shows higher relative intensity in a surface selective 2D  $^1\text{H} \rightarrow ^{133}\text{Cs}$  CP-HETCOR spectrum because such sites are likely coordinated to carboxylate or phosphonate ligands. The  $^1\text{H}$  dimension 2D  $^1\text{H} \rightarrow ^{133}\text{Cs}$  CP-HETCOR NMR spectrum shows signals corresponding to the  $-\text{NH}_3$  (6.5 ppm) and neighboring carbons of the carboxyl group ( $\alpha\text{-CH}_2$ , 3.0 ppm). The  $\text{CH}_2$  along the alkyl chain (1.2 ppm) is expected to have higher intensities because the groups are adjacent to the surface of the  $\text{CsPbBr}_3$  QDs and increase the dipole coupling to the surface.

Additionally, the  $^{207}\text{Pb}$  spin-echo spectrum (Figure 1d) shows a single peak at 200 ppm similar to that reported for bulk





**Figure 2.** (a) Orthorhombic crystal structure of CsPbBr<sub>3</sub> perovskite nanoplattlets with different surface terminations. Reproduced with permission from ref 57. Copyright 2019 American Chemical Society. (b) Diffraction pattern (with best-fit) of colloidal CsPbBr<sub>3</sub> nanoplattlets with Br<sup>-</sup>/R–NH<sub>3</sub><sup>+</sup> termination. The signal at  $q \approx 1.5 \text{ \AA}^{-1}$  corresponds to a peak of a misaligned fraction of nanoplattlets. The inset illustrates the structure of nanoplattlets showing the tilted octahedral and partially occupied surface layer. The Cs<sup>+</sup>, Br<sup>-</sup>, and Pb<sup>2+</sup> atoms are colored in light blue, brown, and dark gray, respectively. Structural refinement of Cs–Pb–Br nanoplattlets with the surface terminations of PbBr<sub>2</sub> (c) and CsBr (d). The panels (b), (c), and (d) are reproduced with permission from ref 58. Copyright 2021 American Chemical Society.

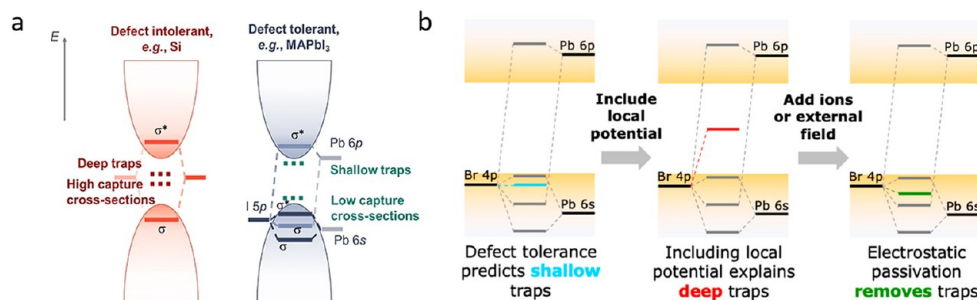
MAPbBr<sub>3</sub> (400 ppm) and CsPbBr<sub>3</sub> (250 ppm).<sup>54,55</sup> Surface-selective <sup>207</sup>Pb NMR spectra obtained through <sup>207</sup>Pb → <sup>1</sup>H CP-HETCOR experiments enabled the detection of the lead atoms proximate to the surface.<sup>56</sup> The similarity in the Pb projection of the surface selective 2D <sup>207</sup>Pb → <sup>1</sup>H CP-HETCOR spectrum and the <sup>207</sup>Pb spin-echo spectrum suggests that most of the lead atoms are present in a bulk environment, which corresponds to the complete PbBr<sub>6</sub> octahedra.<sup>53</sup> In addition, the <sup>1</sup>H → <sup>133</sup>Cs and the <sup>207</sup>Pb → <sup>1</sup>H 2D NMR correlation experiment spectra indicate the presence of –NH<sub>3</sub><sup>+</sup> and α-CH<sub>2</sub> protons of the oleate and alkylammonium surface ligands.<sup>53</sup> Taking into account that signals related to surface ligands could only be observed for <sup>133</sup>Cs, as previously described, a preferential termination of Cs could be assumed.<sup>53</sup> Additionally, RESPDOR experiments determined the internuclear distances between –NH<sub>3</sub><sup>+</sup> protons to Cs and Pb atoms, where the simulation of multispin RESPDOR dipolar dephasing curves indicate a (CsPbBr<sub>3</sub>)-(PbBr<sub>2</sub>)(ABr) termination, where A is Cs or alkylammonium.<sup>53</sup>

High-resolution transmission electron microscopy (HRTEM) is usually used to retrieve the surface characterization of lead halide perovskites. However, there are two main drawbacks hampering the acquisition of HRTEM images of perovskite NCs.<sup>59–61</sup> One is the structural instability of the perovskite NCs under the electron beam; another is the limitation of detecting the tilt of the PbX<sub>6</sub> octahedra. Therefore, noninvasive and versatile X-ray scattering methods, ranging from common XRD measurements to GISAXS and GIWAXS, are applied as complementary probes for HRTEM.<sup>8</sup> We also would like to refer readers to a previous review, which

shed light on the necessity and importance of applying X-ray scattering, especially real-time investigations, on perovskite films.<sup>62</sup> For instance, through the use of synchrotron X-ray total scattering, Bertolotti et al.<sup>57</sup> proposed three structural models by varying the stoichiometry and termination and found that the dominant surface termination is CsBr in the fully stoichiometric composition of CsPbBr<sub>3</sub> (Figure 2a). In contrast to PbX<sub>2</sub> and CsX terminations, Manna et al. discerned the surface termination of perovskite NCs consisting of Br<sup>-</sup> and R–NH<sub>3</sub><sup>+</sup> by multilayer diffraction, along with proper modeling (Figure 2b). By comparing the experimental and calculated patterns that resulted from tuning the Pb–Pb distance, stacking disorder, and other fitting parameters, it was possible to discard the PbBr<sub>2</sub><sup>-</sup> and CsBr<sup>-</sup> terminations (fitting plot in Figures 2c,d) and ascertain the Br<sup>-</sup> and R–NH<sub>3</sub><sup>+</sup> termination (Figure 2b). Likewise, by taking advantage of the sensitivity of multilayer diffraction to interparticle spacing, they demonstrated that no discernible change is found in a diffractogram with the introduction of erucic acid, while the interparticle distance and stacking disorder decreased in the octylamine-containing sample, which means there was no influence of oleic acid (OA) on the surface passivation.<sup>58</sup> This finding is in accordance with the work of De Roo et al.,<sup>35</sup> which is explained in more detail in [Ligand Binding to Nanocrystal Surface](#).

## ■ SURFACE DEFECTS AND DEFECT TOLERANCE

The soft ionic nature of LHPs confers their preference for ionic surface ligands that exhibit highly dynamic binding and tend to detach from the surface by washing, aging, or dilution of colloidal NCs.<sup>8,35,41,50,64</sup> In addition, these processes result in



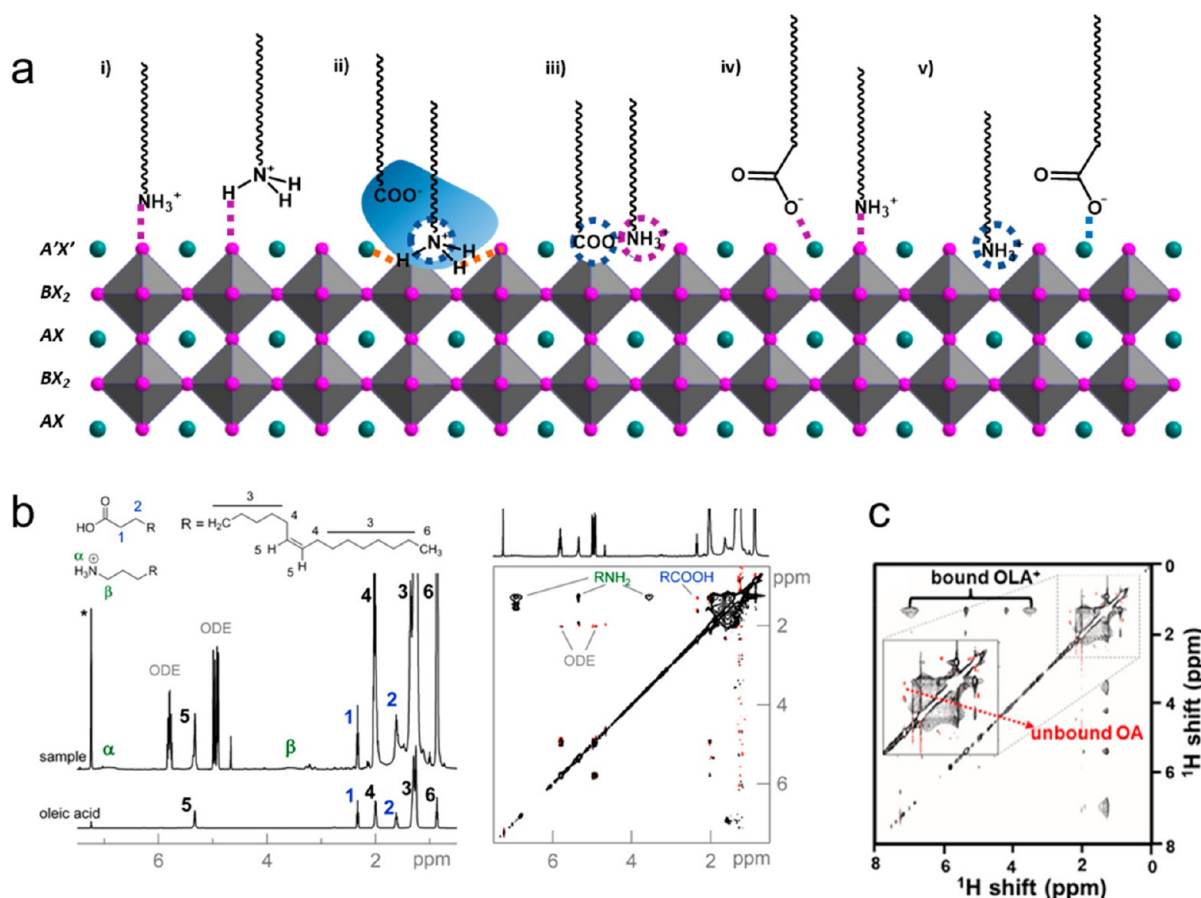
**Figure 3.** (a) Illustration of the electronic structures of classical semiconductors, e.g. Si, and lead halide perovskites, e.g. MAPbI<sub>3</sub>, regarding the formation of defect-induced states. Left: The traps in defect-intolerant materials (e.g., silicon) form deep electronic states within the band gap and have high-capture cross sections. Right: In defect-tolerant materials (e.g., MAPbI<sub>3</sub>), the defects form shallow traps with low-capture cross sections. Reproduced under Creative Commons CC-BY license from ref 20. Copyright 2021 The Authors, Wiley-VCH GmbH. (b) Electronic structure of lead halide perovskites showing the formation of shallow and deep traps and their removal by electronic passivation. Reproduced with permission from ref 63. Copyright 2022 American Chemical Society.

the dissolution or degradation of surface atoms, which leads to a disordered surface with considerable defects that reduces the long-term stability and PLQY.<sup>20,35,50,64–66</sup> The defects act as trap sites for optically excited, as well as electrically injected, charge carriers and excitons. These surface defects are more relevant in perovskite NCs than in bulk because of their higher proportion of surface atoms and reduced size.<sup>40</sup> Generally, LHPs are expected to be highly defect-tolerant materials unlike classical semiconductors, such as Si, GaAs, CdTe, CdSe, and InP, where a small population of defects can be extremely detrimental for PLQY and charge carrier mobility.<sup>19,26,67,68</sup> This is because the majority of intrinsic defects (A and X site vacancies) of LHPs are associated with the shallow states (the localized levels within or close to the valence and conduction bands); thus, they do not affect the optical, and optoelectronic properties (Figure 3a).<sup>8,18,69,70</sup> The defect-tolerant nature of LHPs enables the fabrication of highly efficient perovskite solar cells with polycrystalline films, which are crystallized at relatively low temperatures and ambient conditions and are characterized by a high density of defects. Similarly, colloidal LHP NCs with near-unity PLQY can be prepared at room temperature using technical grade reagents and without any surface passivation, which is compulsory to prepare highly luminescent classical colloidal quantum dots.<sup>8</sup> Despite significant studies on the defect tolerance of LHPs, this complex phenomenon has not been fully understood, especially for colloidal inorganic LHP NCs. Several studies show that the PLQY of CsPbX<sub>3</sub> LHPs is very sensitive to surface defects caused by the detachment of ligands and surface atoms (X, Cs, and Pb) and is significantly reduced after aging or washing. A theoretical evaluation of the ligand desorption and the consequent formation of vacancies on (APbX<sub>3</sub>)(PbX<sub>2</sub>)(AX′)-type surface termination shows structural integrity without the formation of localized states even after 75% loss of the (AX′) shell.<sup>38</sup> However, this effect is not appreciated for the PbX<sub>2</sub> surface termination, in which structural deformation and the presence of localized states were observed at only 25% detachment of the (PbX<sub>2</sub>) shell.<sup>38</sup> This suggests that the dangling bonds caused by halide vacancies and ligand detachment on the surface of LHP NCs can create trap states under certain circumstances. In this regard, density functional theory calculations by du Fossé et al.<sup>63</sup> suggest that the defect states are pushed into the bandgap by a destabilizing local electrostatic potential (Figure 3b). Besides, the defect tolerance of LHP NCs is strongly

dependent on the lattice parameter and, thus, the size of the halide. The lattice constant of MAPbX<sub>3</sub> perovskites decreases with the change of halide from I to Br to Cl and, thus, leads to stronger interactions between halide and Pb<sup>2+</sup> dangling bonds. This causes the formation of deep traps upon the detachment of surface chloride ions. However, the formation energies of surface defects in CsPbI<sub>3</sub> are low, and their energy levels do not form midgap states.<sup>71</sup> Therefore, iodine and bromide-based perovskites exhibit high defect tolerance compared with chloride perovskites.<sup>72–74</sup> Furthermore, ab initio calculations on surface halide vacancies of CsPbX<sub>3</sub> (X = I, Br, Cl) show that the halide defects are shallow in CsPbI<sub>3</sub>, a little deeper in CsPbBr<sub>3</sub>, and midgap in CsPbCl<sub>3</sub>.<sup>74</sup> This is consistent with the low PLQY of CsPbCl<sub>3</sub> NCs (PLQY = ~1–5%) compared with that of CsPbBr<sub>3</sub> and CsPbI<sub>3</sub> NCs (PLQY = ~80–90%), regardless of their synthesis approach.<sup>24,75</sup> The influence of halide ion vacancies on the PLQY of LHP NCs was further studied by the deliberate creation of surface defects, and it was found that the defect tolerance is in the order of CsPbI<sub>3</sub> > CsPbBr<sub>3</sub> > CsPbCl<sub>3</sub>.<sup>74</sup> However, interestingly, the shallow states near the valence band maximum and conduction band minimum, as well as the deep traps, can be removed by passivation with appropriate ligands and reconstruction of the surface with metal halides (Figure 3b).<sup>70</sup> Various postsynthetic surface treatments using different ligands have been developed to recover the photoluminescence of LHP NCs, as well as to improve their long-term stability through strong NC–ligand interactions.<sup>8,40,76</sup>

## ■ LIGAND BINDING TO NANOCRYSTAL SURFACE

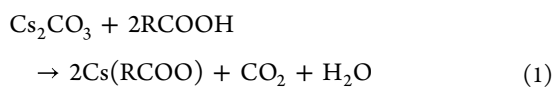
It is fundamentally necessary to understand how capping ligands bind to the surface of nanocrystals to have control over the surface chemistry of new ligands used for strong surface-to-ligand interactions and surface functionalization with desired ligands and, thus, improve the optical and long-term stability of colloidal LHP NCs.<sup>8,78–80</sup> The capping ligands of LHP NCs can be classified into three types, as per covalent bond classification: (1) L-type [two-electron donor ligands (Lewis bases)], (2) Z-type [two-electron acceptor ligands (Lewis acids)], and (3) X-type (one-electron donor ligands).<sup>40,81</sup> Because the surface of an LHP NC is ionic, the surface ligands are ionic and they fall into the X-type category (e.g. alkylammonium, alkyl carboxylates). The most widely used capping ligands are long-chain alkylamines and alkylacids, of which oleylamine (OAm) and oleic acid (OA) as the most



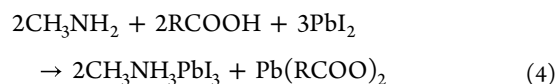
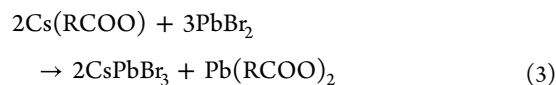
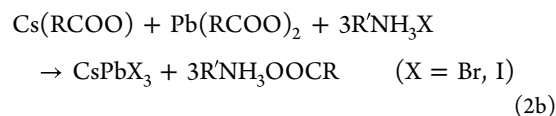
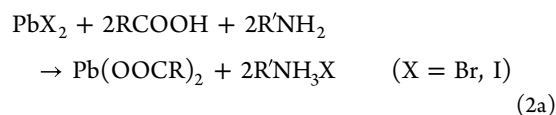
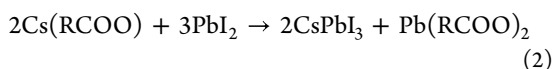
**Figure 4.** (a) Schematic illustration of the different binding modes of oleylamine and oleic acid to a lead halide perovskite NC surface. (b) Left:  $^1\text{H}$  NMR spectrum of purified  $\text{CsPbBr}_3$  NCs. The impurities of octadecene (ODE) are also indicated from the reference spectrum of oleic acid. Right: NOESY spectrum of the purified  $\text{CsPbBr}_3$  NCs in  $\text{CDCl}_3$ . The panel (b) is reproduced with permission from ref 35. Copyright 2016 American Chemical Society. (c) NOESY spectrum of  $\text{CsPbBr}_3$  NCs in  $\text{CDCl}_3$ . The magnified NOESY spectrum shows the correlation of oleylammonium ( $\text{OAm}^+$ ) to the surface of the NCs, whereas the oleate does not bind. Reproduced with permission from ref 51. Copyright 2017 American Chemical Society.

widespread pair.<sup>23,24,28</sup> The OAm/OA ligand pair for the synthesis of LHP NCs was first employed by Protesescu et al. in 2015<sup>23</sup> and showed great promise for tuning the size, shape, and halide composition of colloidal perovskite NCs with excellent monodispersity and high photoluminescence quantum yield.<sup>8,17,82</sup> The OA/OAm acid–base pair first transforms into an oleate anion and oleylammonium cation through proton transfer, and then, these ions are likely to bind to the surface of LHP NCs.<sup>83</sup> In addition, ligands help to dissolve the precursors in a solvent medium and, thus, initiate the reaction that leads to colloidal perovskite NCs.<sup>75,77,84</sup> The typical synthesis of LHP NCs by hot injection using the OAm/OA ligand pair involves various reactions, as shown in eqs 1–4 for  $\text{CsPbBr}_3$ ,  $\text{CsPbI}_3$ , and  $\text{CH}_3\text{NH}_3\text{PbI}_3$  NCs (Reproduced with permission from ref 77. Copyright 2020 American Chemical Society):

1. Formation of metal-oleate:



2. Formation of perovskite and byproduct:



It should be noted that the ligands play a crucial role in the shape control of LHP NCs from nanocubes to nanoplatelets and nanowires,<sup>85</sup> and this has already been discussed in several review articles.<sup>8,29,76,86</sup> Herein, we limit our discussion to ligand binding on the surface of LHP NCs, interactions between LHP NCs with ligands that have different functional groups, and ligand-induced functionalities.

Many studies are still trying to elucidate the binding mode of the OAm/OA ligand pair to LHP NC surfaces, despite being



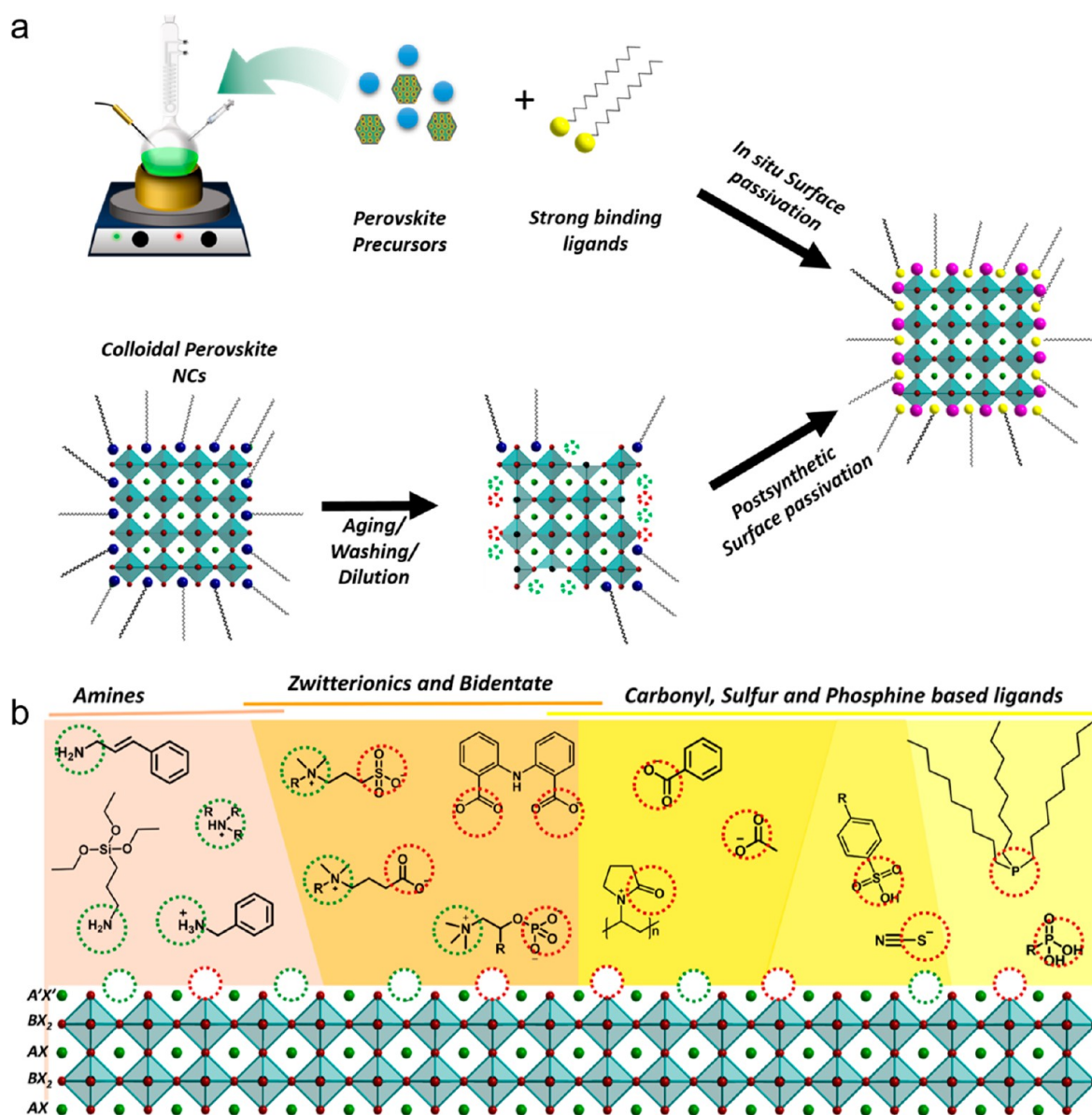


Figure 5. (a) Schematic illustration showing the synthesis of trap-free LHP NCs either by in situ passivation or postsynthetic surface passivation using strong binding ligands. While the in situ synthesis refers to the synthesis of NCs in the presence of strong binding ligands, postsynthetic surface passivation refers to the surface repair of the ligand-detached NCs obtained by aging, purification, or dilution. The surface is reconstructed by the addition of strong binding ligands, along with metal halide salts. (b) Summary of ligands employed in surface passivation with binding at A cation sites or X vacancies (also, see Table 1). The functional groups of the ligands are classified according to their binding site and are labeled with green or red dotted circles. It is likely that the green-labeled functional groups occupy A sites, while the red-labeled ones occupy halide vacancies. The A cations ( $\text{MA}^+$ ,  $\text{FA}^+$ ,  $\text{Cs}^+$ ), A cation vacancies, halides ( $\text{Cl}^-$ ,  $\text{Br}^-$ , or  $\text{I}^-$ ), halide vacancies, and lead atoms are labeled with solid green, dotted green, solid red, dotted red, and black, respectively.

widely used ligands, using various characterization techniques, with nuclear magnetic resonance spectroscopy (NMR) and X-ray photoelectron spectroscopy (XPS) as the most outstanding ones.<sup>35,51,53,87,88</sup> On the basis of the reported studies, there are several proposals regarding the binding nature of the OA/OAm ligand pair, as illustrated in Figure 4a.<sup>82</sup> For instance, De Roo et al.<sup>35</sup> first studied the OA/OAm ligand chemistry on the surface of  $\text{CsPbBr}_3$  NCs through NMR characterization. Through analysis of the difference in concentrations of OAm and OA in the  $^1\text{H}$  NMR spectra, they identified the presence of oleylammonium derived from the protonation of OAm [Figure 4b (left)]. In addition, the positive cross-peaks in nuclear Overhauser effect spectroscopy (NOESY-NMR) suggested

that the oleic acid and octadecene do not bind to the surface [Figure 4b (right)].<sup>35</sup> On the basis of the  $^1\text{H}$  NMR and NOESY-NMR studies, De Roo et al. proposed that the oleylammonium bromide acts as a ligand and binds to bromine atoms by electrostatic cation–anion interactions or through hydrogen bonds ( $\text{H}\cdots\text{Br}$ ), while the  $\text{Br}^-$  ions bind to the  $\text{Cs}^+$  or  $\text{Pb}^{2+}$  cations (Figure 4a-i).<sup>35</sup> Conversely, Ravi et al.,<sup>51</sup> analyzed the surface of  $\text{CsPbBr}_3$  NCs through  $^1\text{H}$  NMR and NOESY-NMR (Figure 4c) and proposed that the oleylammonium cations act as capping ligands by substituting some of the  $\text{Cs}^+$  cations on the surface, as well as by forming hydrogen bonds with neighboring  $\text{Br}^-$  atoms on the NC surface. Despite the low energy required for the replacement of Cs with

oleylammonium cations, the hydrogen bonds with neighboring  $\text{Br}^-$  ions stabilize the NCs.<sup>51</sup> In addition, the study suggests that the oleate ions do not bind to the surface; however, they neutralize the charge on the surface by the formation of equilibrium with the oleylammonium ligands (Figure 4a-ii). Theoretical studies by ten Brinck et al. further suggested that the oleylammonium cations act as capping ligands substituting 50% of the A cations on the surface of LHP NCs.<sup>89</sup> Contrary to previous reports, it was proposed that oleate molecules occupy the halide vacancies on the surface (Figure 4a-iii). Another possible mechanism is that both the oleate and oleylammonium ions interact with the  $\text{CsPbBr}_3$  NCs surface through  $\text{Cs}^+$  and  $\text{Br}^-$  ions, respectively, as proposed by Brutchey et al. (Figure 4a-iv).<sup>88</sup> However, yet another mechanism was determined by a recent study through  $^1\text{H}$  and  $^{133}\text{Cs}$  NMR spectroscopy, where oleylammonium substituted the  $\text{Cs}^+$  vacancies, and the oleate ions interacted with the rest of the  $\text{Cs}^+$  ions (Figure 4a-v).<sup>87</sup>

Despite several proposed ligand-binding mechanisms, the substitution of A cations and halide ions with oleylammonium and oleate ligands, respectively, has been widely accepted and used to explain many experimental studies. In addition, it is well studied that these ligands (OA/OAm) weakly bind to LHP NCs and that their interactions with NC surfaces are highly dynamic. Thus, the ligands are easily detached from the NC surface during a wash with polar antisolvents or by aging. The ligand detachment leads to the formation of vacancies at the A site and X sites, which thus results in spectral shift and a drastic reduction of PLQY.<sup>8,50</sup> In particular, iodide atoms were found to expel from the NC surface upon contact with polar solvents.<sup>50</sup> It is well understood and accepted that the exploration of and control over the ligand chemistry of LHP NCs are essential to enhance long-term colloidal stability against polar solvents, heat, and light. Therefore, over the years, a large number of studies have been focused on exploring different types of ligands for the effective passivation of LHP NC surfaces, with the aim of improving the colloidal stability and PLQY and imparting new properties and functionalities.

## ■ IN SITU AND POSTSYNTHETIC SURFACE PASSIVATION

Considering the ease of ligand detachment, which is accompanied by a decrease in the PLQY and stability of OAm/OA-capped LHP NCs, it is crucial to explore different capping ligands either by direct synthesis (in situ) or postsynthetic surface passivation treatments (Figure 5a).<sup>8</sup> The first approach that was considered to improve the PLQY of the purified OAm/OA-capped LHP NCs was to add excess OAm and OA to passivate the surface traps.<sup>8,35,77</sup> Such postsynthetic surface treatments have been greatly exploited using different ligands (see Ligand Exchange section), as well as halide salts, and have been reviewed.<sup>8,20,39,76,86,90</sup> For instance, several reports demonstrate that in situ (during synthesis) incorporation of certain additives, such as metal halides [e.g.,  $\text{ZnBr}_2$ ,  $\text{FeBr}_3$ ,  $\text{SnX}_4$  ( $\text{X} = \text{Cl}, \text{Br}, \text{I}$ )], alkali metals, alkaline earth metal salts, or thiocyanate, improve the PLQY, as well as colloidal stability.<sup>91–98</sup> Among all, the metal halide (e.g.  $\text{PbBr}_2$ ,  $\text{ZnBr}_2$ ,  $\text{CuBr}_2$ ,  $\text{InBr}_3$ ,  $\text{AgBr}$ , etc.) salts have been widely used to manipulate the defects and optical properties of perovskite NCs.<sup>64,99–101</sup> However, the position of the added metal cations in the host NC lattice is still unclear. In the case of

postsynthetic treatment, the added metal halides repair the surface by filling halide vacancies on the surface of LHP NCs. Nevertheless, the dopant-enhanced optical and structural stabilities of LHP NCs have often been studied by PL and XRD.<sup>99–102</sup> One proposed hypothesis for the dopant-enhanced stability of LHP NCs is because of the formation of a (110) surface with lead-halide-enriched  $\text{CsPbX}_3$  NCs.<sup>102</sup>

Another method to overcome the instability arising from the acid–base equilibrium of ligands is to carry out the synthesis in the absence of OAm or OA. For instance, upon the absence of OA, primary amines (L-type ligands) yield stable LHP NCs with near-unity PLQY, as demonstrated by Zhong and co-workers.<sup>103</sup> However, a new synthetic approach was developed using oleic acid as the capping ligand and quaternary alkylammonium halides as precursors, which allowed purified colloidal perovskites to be obtained with higher stability.<sup>104</sup> In particular, a ligand of special interest is didodecyl dimethylammonium bromide ( $\text{DDA}^+ \text{Br}^-$ ), which has been shown to be effective in the enhancement of stability and PLQY by restoring the surface of  $\text{CsPbBr}_3$  through postsynthetic treatment with a mixture of  $\text{PbBr}_2 + \text{DDABr}$ .<sup>52</sup> The main advantage of this type of ligand is that it is pH-independent, unlike octylammonium bromide. In addition, the DDAB-capped LHP NCs have great promise for LED fabrication because of their shorter alkyl chain length compared with OAm/OA. The large chain length of the OAm/OA pair can hinder the charge transport, and thus, only an EQE of 0.12% was observed in early research.<sup>25</sup> Consequently, a two-step ligand exchange process was developed, which involves an intermediate OAm desorption step followed by treatment with halide-ion-pair ligands (short-chain alkyl halides), to result in highly stable  $\text{CsPbX}_3$  perovskite NCs with an increased charge transport.<sup>105</sup> In connection with improved stability and PLQY, a wide range of ligands have been tested by improving the ligand–NC surface interaction strength. The ligands can be classified into a few types on the basis of the functional group that binds to the NC surface and are illustrated in Figure 5b. In the following sections, we discuss some of the widely explored ligand types for effective surface passivation of LHP NCs either by direct in situ synthesis or postsynthetic ligand exchange (Table 1).

**Phosphorus-Based Ligands.** The functional group in ligand chemistry plays an essential role in binding to the surface of NCs, with the acid–base theory being a predominant mechanism. In this regard, numerous studies involve alkyl phosphonic acids as capping ligands because of their high interaction ability with LHP NCs.<sup>106–110</sup> In fact, alkylphosphonate ligands were previously explored for the stabilization of classical colloidal QDs ( $\text{CdSe}$ ,  $\text{PbSe}$ ).<sup>111,112</sup> The  $\text{Cs}^+$  and  $\text{Pb}^{2+}$  ions of LHPs are hard and soft acids, respectively. Conversely, the OAm/OA ligands are hard Lewis bases, while the phosphine ligands are soft bases. Taking the acid–base theory into account, a higher affinity is expected for  $\text{Pb}^{2+}$  toward phosphine ligands than for  $\text{Pb}^{2+}$  toward OAm/OA.<sup>110,113</sup> For instance, trioctylphosphine oxide (TOPO) has been employed in conjunction with OAm/OA.<sup>114</sup> A strong coordination of the  $\text{P}=\text{O}$  group of TOPO to the NC surface was confirmed by Fourier transform infrared (FTIR) spectroscopy measurements, which appreciated a C–P stretching peak at  $1155 \text{ cm}^{-1}$  (a characteristic peak for TOPO) even after purification. A remarkable increase in stability was observed with TOPO as the photoluminescence was maintained after long exposures to ethanol.<sup>114</sup> In a subsequent study, Almeida



Table 1. Summary of Various Ligands Used to Improve the Stability and PLQY of LHP NCs through Strong Ligand–Surface Interactions

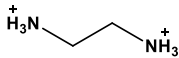
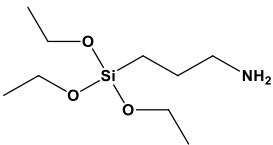
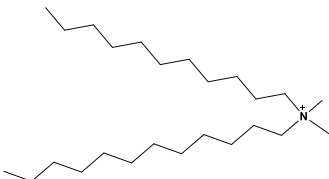
Ligands	NCs	Stability and luminescence	Ref.
<b>Amines and ammonium salts</b>			
Octanoic acid (OctAc)/octylamine (OctAm) with OA/OAm.	CsPbI <sub>3</sub>	PL intensity ≈80% of its initial value for 180 days.	181
n-octanoic acid (OTAC), oleylamine (OAm), and (3-aminopropyl)triethoxysilane (APTES).	CsPbI <sub>3</sub>	Maintenance of the cubic phase α-CsPbI <sub>3</sub> at room temperature for 40 days.	182
 Ethylenediammonium (EDA <sup>2+</sup> )	CsPbI <sub>3</sub>	>85% PCE (Power conversion efficiency) after 30 days PCE.	183,184
 3-aminopropyltriethoxysilane (APTES)	CsPbI <sub>3</sub>	Maintenance of the photoluminescence in water for more than 2 h. Mixed with Oleylamine and HI reaches a PLQY of 84 %.	185
3-aminopropyltriethoxysilane (APTES)	CsPbBr <sub>3</sub>	Near unity PLQY, long-term storage, polar solvent resistance, and high energy UV exposure.	165
 N,N-dimethyl-N-undecyldodecan-1-aminium	CsPbI <sub>3</sub>	Quantum yield higher than 80% for at least 60 days.	186

Table 1. continued

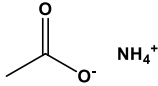
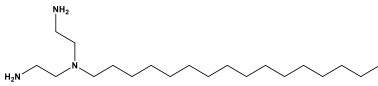
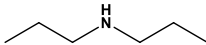
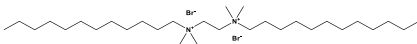
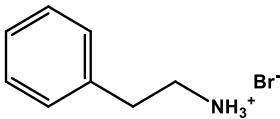
Ligands	NCs	Stability and luminescence	Ref.
<b>Amines and ammonium salts</b>			
 <p>Ammonium acetate</p>	CsPbI <sub>3</sub>	EQE of 10.6% and a maximum brightness of 981 cd m <sup>-2</sup> .	187
 <p>N'-(2-aminoethyl)-N'-hexadecylethane-1,2-diamine (AHDA)</p>	CsPbI <sub>3</sub>	CsPbI <sub>3</sub> Stable after 15 purification cycles with the maintenance of 60% PLQY.	188
 <p>di-n-propylamine</p>	CsPbI <sub>3</sub>	PCE ~ 15% for based solar cells.	189
 <p>N1,N2-didodecyl-N1,N1,N2,N2-tetramethylethane-1,2-diaminium bromide</p>	CsPbBr <sub>3</sub>	PLQY 92.3% and superior colloidal stability under intense purification for up to ten cycles.	
 <p>Phenethylammonium bromide</p>	CsPbBr <sub>3</sub>	PLQY over 80% and electroluminescence efficiency of 2%	190

Table 1. continued

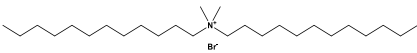
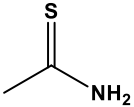
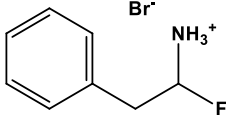
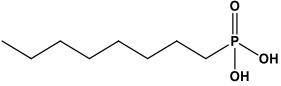
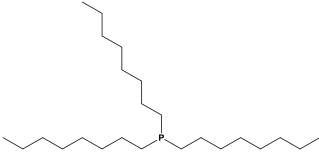
Ligands	NCs	Stability and luminescence	Ref.
<b>Amines and ammonium salts</b>			
 <p>di-dodecyl dimethyl ammonium bromide</p>	CsPbBr <sub>3</sub>	High EQE (1.9% for the blue, and 3.0% for the green).	191,192
 <p>Thioacetamide and Oleylamine</p>	CsPbBr <sub>3</sub>	90% PLQY and increase of stability and PLQY retention in time	193
 <p>Fluorophenethyl ammonium bromide</p>	CsPbBr <sub>3</sub>	95.79% PLQY and 76% of the initial PL intensity was maintained after 21 days under air exposure.	194
<b>Phosphines and phosphonic acids</b>			
 <p>Octylphosphonic acid</p>	CsPbI <sub>3</sub>	50% of their original PL QY after 15 days in air.	195
 <p>Trioctylphosphine</p>	CsPbI <sub>3</sub>	PLQY remain 30% after 1 month.	113,196



Table 1. continued

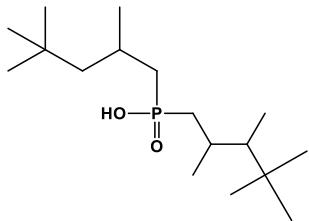
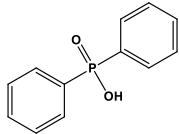
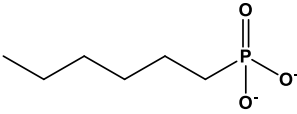
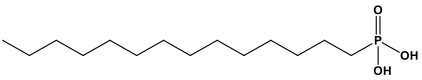
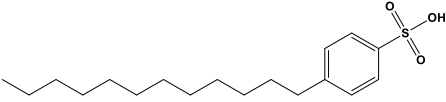
Ligands	NCs	Stability and luminescence	Ref.
<b>Phosphines and phosphonic acids</b>			
	CsPbI <sub>3</sub>	Preservation of photoluminescence after 20 days of storage under ambient conditions.	197
Bis-(2,2,4-trimethylpentyl) phosphonic acid			
	CsPbI <sub>3</sub>	Only a 40% emission get lost after 6 days.	198
Diphenylphosphinic acid			
	CsPbBr <sub>3</sub>	Thin films present PLQY of 40% with emission peak at 450 nm in solid state, which is preserved after one month.	107
Hexylphosphonate			
	CsPbBr <sub>3</sub>	95% PLQY and high stability.	106
Tetradecylphosphonic acid			
<b>Organosulfur compounds</b>			
	CsPbI <sub>3</sub>	Preservation of ~90% of the initial PL intensity after 36 h storage in ambient air.	199
4-dodecylbenzenesulfonic acid			

Table 1. continued

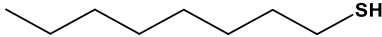
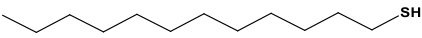
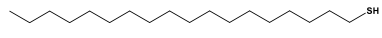
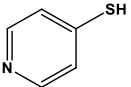
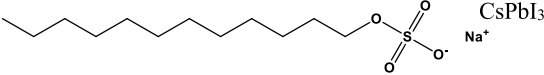
Ligands	NCs	Stability and luminescence	Ref.
<b>Organosulfur compounds</b>			
	CsPbI <sub>3</sub>	Improved stability under UV irradiation for 4 days.	200
1-octanethiol			
	CsPbI <sub>3</sub>	Conservation of 46% photoluminescence over 120 h under UV light.	200
1-dodecanethiol			
	CsPbBr <sub>3</sub>	PLQY reaches 90–99%, and can remain for over 25 days.	124
	CsPbI <sub>3</sub>	High PLQY (93%) and preservation of 80% after 10 days.	201
1-octadecanethiol			
	CsPbI <sub>3</sub>	PCE ~60% after 30 days.	202
p-mercaptopyridine			
	CsPbI <sub>3</sub>	Conservation of 80% of the original PL intensity after 30 days.	203
Sodium dodecyl sulfate			

Table 1. continued

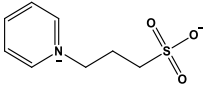
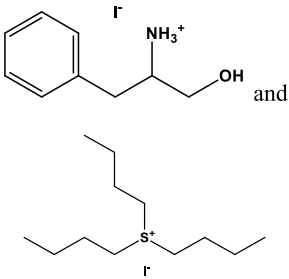

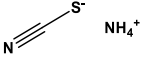
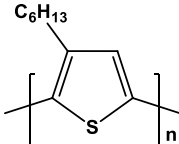
Ligands	NCs	Stability and luminescence	Ref.
<b>Organosulfur compounds</b>			
	CsPbI <sub>3</sub>	>85% after 30 days PCE.	151
3-(1-Pyridinio)-1-propanesulfonate			
	CsPbI <sub>3</sub>	75% PLQY for 72 h.	204
1-hydroxy-3-phenylpropan-2-aminium iodide (HPAI) and tributylsulfonium Iodide (TBSI)			
	CsPbI <sub>3</sub>	Preservation of 92% PL intensity after 7 days.	205
Sulfur oleylamine			
	CsPbI <sub>3</sub>	Maximum luminance of 823 cd m <sup>-2</sup> .	93
Ammonium thiocyanate			
	CsPbI <sub>3</sub>	Increase in the responsivity after 10 h and in the dark current and photocurrent for 3 hours under humid conditions.	206
Ammonium thiocyanate			



Table 1. continued

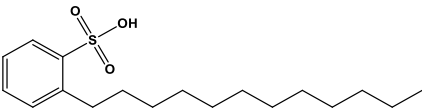
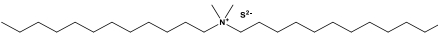
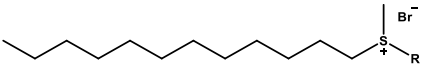
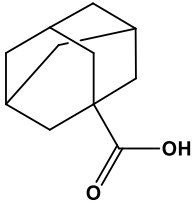
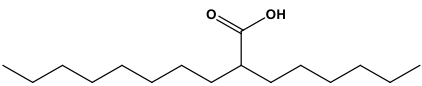
Ligands	NCs	Stability and luminescence	Ref.
<b>Organosulfur compounds</b>			
Poly(3-hexylthiophene)			
	CsPbBr <sub>3</sub>	PLQY above 90%, stable emission peaks, good long-term storage stability, and robust high-energy irradiation stability, even after five washes.	122
Dodecyl benzene sulfonic acid			
	CsPbBr <sub>3</sub>	Photostability under continuous pulsed laser excitation in ambient conditions for 34 h.	127
Didodecyl dimethylammonium sulfide (DDA <sup>+</sup> S <sup>2-</sup> )			
	CsPbBr <sub>3</sub> / MAPbBr <sub>3</sub>	High ambient stability with PLQYs over 90% after 2 months.	207
Dodecylmethylsulfide			
<b>Carboxylic acids and benzoyl halides</b>			
		PLQY of 83% (and 88% after 1 week of storage despite some loss in yield)	208
adamantlyl-1-carboxylic acid			
	CsPbBr <sub>3</sub>	Improved stability, longer lifetime, stronger PL intensity and smoother thin morphology.	209
2-hexyldecanoic acid			

Table 1. continued

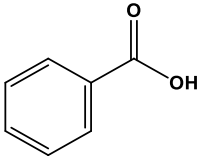
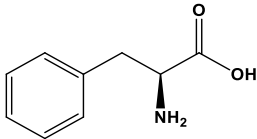
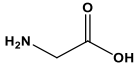
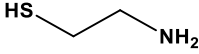
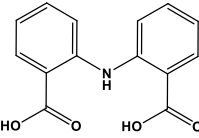
Ligands	NCs	Stability and luminescence	Ref.
<b>Carboxylic acids and benzoyl halides</b>			
	CsPbBr <sub>3</sub>	Photoluminescence increase by 1.5-fold with benzoic acid post-treatment Retention of ~65% of initial PL intensity even after one year	210
Benzoic acid			
<b>Bidentate and multidentate</b>			
	CsPbI <sub>3</sub>	90% PCE after 160 hours.	211
<i>L</i> -phenylalanine			
	CsPbI <sub>3</sub>	Preservation of 87% of the original PCE after 10 days.	212
Glycine			
	CsPbI <sub>3</sub>	Maintenance of 95% of the initial intensity after immersion in water for 60 min or under UV irradiation for 120 min.	213
2-Aminoethanethiol			
	CsPbI <sub>3</sub>	2.26% EQE and near-unity PLQY values with a good stability.	144
2,2'-iminodibenzoic acid (IDA)			

Table 1. continued


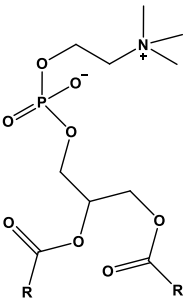
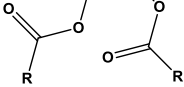
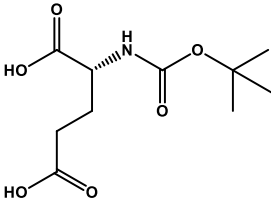
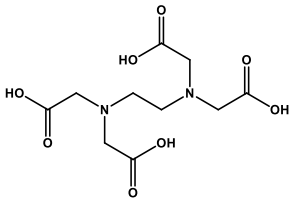
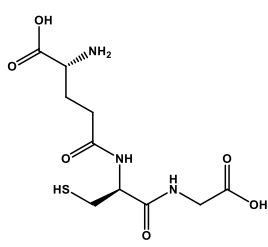
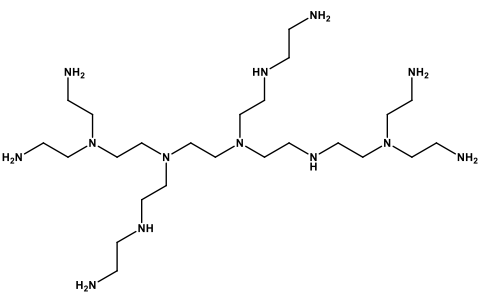
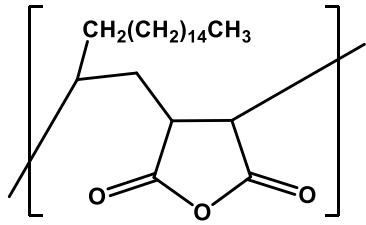
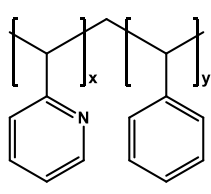
Ligands	NCs	Stability and luminescence	Ref.
<b>Bidentate and multidentate</b>			
 <p>Polyethylenimine</p>	CsPbBr <sub>3</sub>	EQE of 12.3%.	217
 <p>Lecithin</p>	CsPbBr <sub>3</sub>	Stable after intense purification for more than 1 month.	146
 <p>Lecithin</p>	CsPbI <sub>3</sub>	PLQY close to unit table for 6 months of storage in air.	218
 <p>Boc-D-Glutamic acid</p>	CsPbBr <sub>3</sub>	PLQY close to near-unity, superior colloidal stability, improving stability against thermal treatment and UV irradiation.	219
 <p>Ethylenediaminetetraacetic acid (EDTA)</p>	CsPbI <sub>3</sub>	PLQY of CsPbI <sub>3</sub> NCs increased from 72.9% to 94.3%. Stability enhancement in polar environment, maintaining strong fluorescence in ethanol for 1 month. High luminescence of 584 cd m <sup>-2</sup> and EQE of 8.15% improving the device performance.	220
	MAPbI <sub>2</sub> Br	Stable red electroluminescence LEDs with an EQE at 620 nm greater than 20%.	163



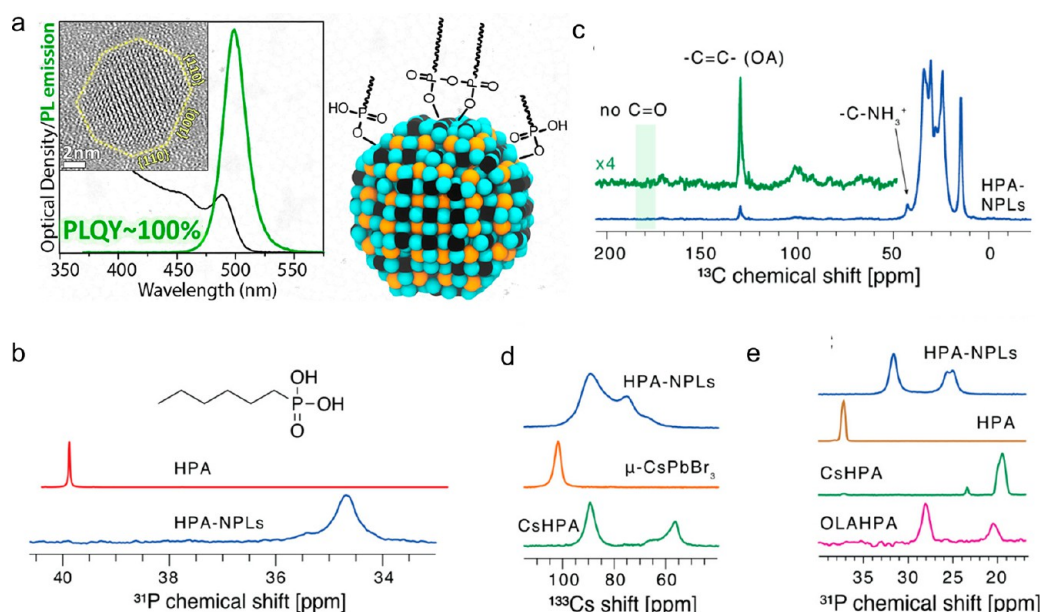
Table 1. continued

Ligands	NCs	Stability and luminescence	Ref.
<b>Bidentate and multidentate</b>			
 <p>Glutathione (GSH)</p>			
	CsPbBr <sub>3</sub>	Stability enhancement together with an improvement of the carrier transport.	162
 <p>Polyethylenimine</p>			
	CsPbX <sub>3</sub>	Increase in the PLQY and optical stability of CsPbX <sub>3</sub> NCs under illumination at ambient conditions.	221
 <p>poly(maleicanhydride-alt-1-octadecene)</p>			
	CsPbBr <sub>3</sub>	Enhanced stability in both the colloidal and thin films.	159
 <p>Polystyrene-block-poly-2-vinylpyridine</p>			

et al. employed TOPO and OA as capping ligands in the amine-free synthesis of CsPbX<sub>3</sub> NCs.<sup>115</sup> It was determined through <sup>1</sup>H NMR studies that the TOPO was not present on the NC surface, which is covered by only oleate ligands. However, the <sup>31</sup>P NMR studies showed the interaction of the protonated TOPO with the PbBr<sub>2</sub> precursor,<sup>116</sup> which resulted in competition with OA.<sup>115</sup> Thus, the protonation of the TOPO caused by the acidic environment tunes the reactivity of the PbX<sub>2</sub> to control the size of the nanocrystals. Furthermore, <sup>31</sup>P NMR and XPS studies by Li et al. show that phosphine ligands of different types [trioctylphosphine (TOP), diphenyl-

phosphine (DPP), and tributylphosphine (TBP)] can bind to a LHP NC surface to improve its tolerance to ethanol, water, and UV light.<sup>110</sup> The <sup>31</sup>P NMR of TOP was unaltered in the presence of cesium oleate, while a downfield shift was observed with the addition of PbBr<sub>2</sub>, which suggests its interaction with the Pb<sup>2+</sup> atoms.<sup>110</sup> In addition, X-ray photoelectron spectroscopy (XPS) showed a peak at 132 eV that corresponds to P 2p<sup>3</sup>, thereby establishing the existence of TOP on the CsPbBr<sub>3</sub> NC surface.<sup>110</sup>

Similarly, a new synthetic approach was reported involving alkyl phosphonic acids as surfactants for obtaining colloidal

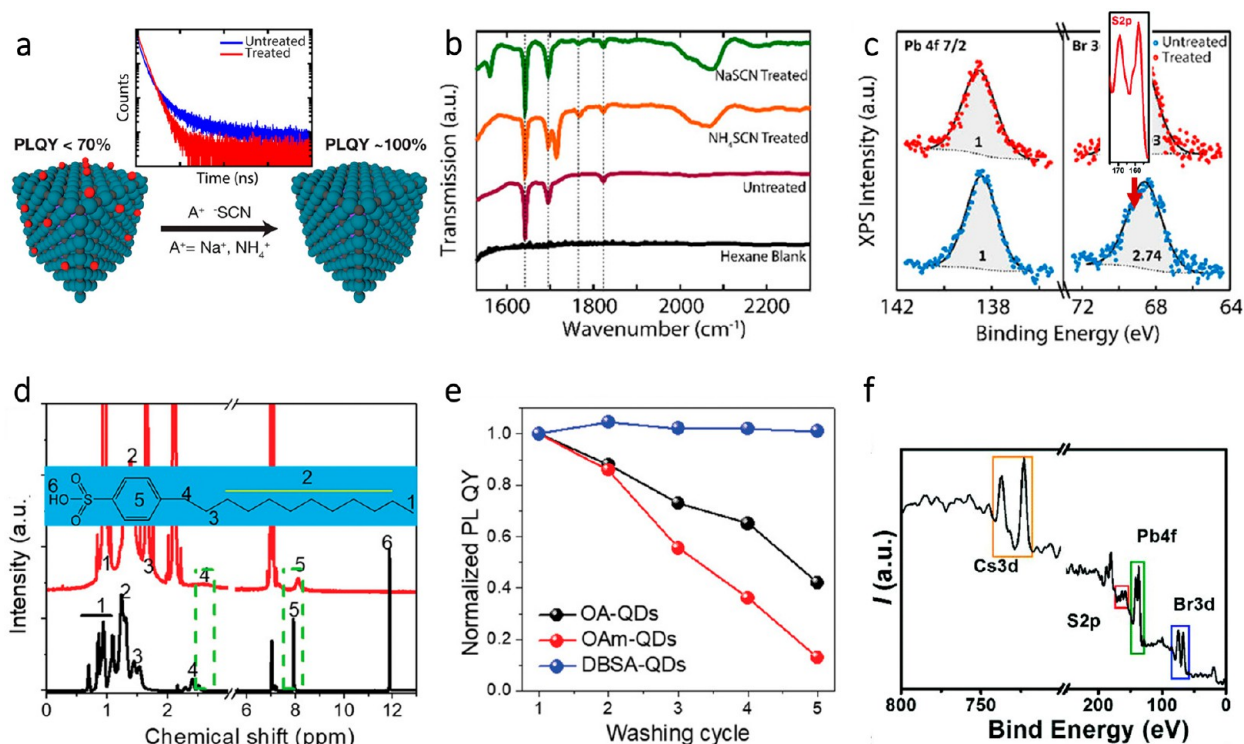


**Figure 6.** (a) Scheme of alkylphosphonic-acid-capped CsPbBr<sub>3</sub> octahedron-shaped NCs and their absorption and PL spectra. The strong binding of ligands to the NC surface results in 100% PLQY. Reproduced with permission from ref 106. Copyright 2019 American Chemical Society. (b) Liquid-state <sup>31</sup>P NMR spectra of hexylphosphonic acid (HPA) and HPA-capped CsPbBr<sub>3</sub> nanoplatelets in toluene-*d*<sub>8</sub>. (c) <sup>1</sup>H–<sup>13</sup>C cross-polarization (CP) spectrum of HPA-capped CsPbBr<sub>3</sub> nanoplatelets. (d) <sup>133</sup>Cs MAS NMR spectra of HPA-capped CsPbBr<sub>3</sub> nanoplatelets (NPLs). OLAHPA, oleylammonium *n*-hexylphosphonate; CsHPA, cesium *n*-hexylphosphonate. (e) <sup>1</sup>H–<sup>31</sup>P cross-polarization magic-angle spinning (CP MAS) NMR spectra of HPA-capped CsPbBr<sub>3</sub> nanoplatelets. Reproduced with permission from ref 107. Copyright 2020 American Chemical Society.

CsPbBr<sub>3</sub> NCs with octahedral shape, high colloidal stability, and near-unity PLQY (Figure 6a).<sup>106</sup> The surface of tetradecyl phosphonic acid (TDPA)-capped CsPbBr<sub>3</sub> NCs were analyzed by XPS, FTIR, and STEM-EDS, and these measurements indicated the presence of TDPA at the surface. In particular, the XPS analysis revealed the Cs/Pb/Br/P molar ratio of 1/1.06/2.19/0.77, which indicates that the alkyl phosphonates replaced most of the bromides on the surface.<sup>106</sup> Interestingly, the NCs capped with TDPA ligands exhibit a truncated octahedron shape covered by Pb-terminated facets because of a strong binding affinity of the phosphonate to Pb<sup>2+</sup> ions. These NCs exhibit near-unity PLQY without postsynthetic treatment, and the optical properties remain unaltered after dilution, thereby suggesting these ligands strongly passivate the NC surface. Furthermore, <sup>31</sup>P NMR studies were performed for a more exhaustive study of the binding mode of phosphonic acids.<sup>112,117</sup> The parent OAm/OA ligands can also be replaced by octylphosphonic acid ligands through postsynthetic surface treatment, and the 2D solid-state <sup>31</sup>P–<sup>1</sup>H NMR suggests that these ligands preferentially bind via the negatively charged P–O<sup>−</sup> termination, which leaves the P=O and P–OH groups free to form interligand hydrogen bonds.<sup>118</sup> The phosphonate ligands also strongly passivate the NC surface, which results in a well-purified colloidal CsPbBr<sub>3</sub> NC solution with a PLQY over 3 times higher than that of untreated NCs.<sup>118</sup> In another report, Zhang et al. showed the advantage of using oleyl phosphonic acid (OLPA) over linear chain alkyl phosphonic acids because their higher solubility in apolar solvents enables the synthesis of LHP NCs at lower temperatures, which offers size tunability.<sup>109</sup> They were able to synthesize CsPbBr<sub>3</sub> NCs with sizes down to 5 nm, thereby showing quantum confinement effects. The NCs were found to be passivated with hydrogen phosphonates, phosphonic acid anhydrides, and phosphonates species, and thus, they exhibited excellent

colloidal stability. It is worth mentioning that the perovskite NCs were treated with trimethylchlorosilane (TMS-Cl) and the corresponding products were analyzed via <sup>31</sup>P NMR to study the binding modes of the OLPA molecules. The TMS-Cl, generally as halides or chalcogenides, reacts with phosphonate species of the colloidal NCs, which yields the TMS-substituted compounds that can be analyzed by <sup>31</sup>P NMR.

Despite the numerous studies that have explored the use of phosphonic acids as capping ligands for CsPbBr<sub>3</sub> nanocubes,<sup>106,108–110</sup> the use of these ligands for nanoplatelets (NPLs) has been rarely reported. A passivation strategy employing hexyl phosphonate (HPA) as a capping ligand allowed the synthesis of blue-emitting CsPbBr<sub>3</sub> NPLs with remarkable PLQY.<sup>107</sup> The NMR measurements on liquid samples showed a shift, along with a broadening, in the signal when comparing free HPA (40.1 ppm) and HPA-capped NPLs (34.7 ppm), thereby indicating that the ligands interact with the NPLs (Figure 6b). Furthermore, the solid-state magic-angle spinning (MAS) NMR measurements suggested the presence of residual OAm ligands on the surface. They were identified using <sup>1</sup>H–<sup>13</sup>C cross-polarization (CP) MAS NMR because of a strong deshielding of the carbon, which is directly bonded to the –NH<sub>3</sub><sup>+</sup> group (shifted to higher ppm values) (Figure 6c).<sup>107</sup> Additionally, the solid-state <sup>1</sup>H–<sup>31</sup>P CP MAS NMR revealed four peaks (31.6, 29.8, 25.7, and 24.9 ppm) that do not correspond to free hexylphosphonate acid, cesium phosphonate (19.5 and 23.4 ppm), or oleylammonium phosphonate (20.4 and 28.0 ppm), thereby leading to the conclusion that they indicate different binding modes of hexylphosphonate acid on the nanoplatelet surface (Figure 6d).<sup>107</sup> In addition, <sup>133</sup>Cs MAS NMR experiments revealed the structure of the HPA-NPLs (Figure 6e). Furthermore, the broad peaks existed between 60 and 100 ppm, which were



**Figure 7.** (a) Surface passivation of CsPbBr<sub>3</sub> NCs with thiocyanate to achieve 100% PLQY. The PL decay kinetics transform from multiexponential to a monoexponential decay, which suggests the removal of traps and thus leads to single energy level emitters. (b) FTIR transmission spectra for untreated (violet line), NH<sub>4</sub>SCN-treated (orange line), NaSCN-treated aged NCs (green line), and hexanes (black line) over the IR region of interest. The passivation with NaSCN results in a peak at 1560 cm<sup>-1</sup> that corresponds to the C=O stretching of sodium oleate, while passivation with NH<sub>4</sub>SCN results in a peak at 1712 cm<sup>-1</sup> that corresponds to the C=O stretching of oleic acid. It is likely that the counterion (Na, NH<sub>4</sub>) interacts with oleate species of the colloidal solution, while the thiocyanate binds to the lead of NCs. (c) XPS spectra of the Pb 4f<sub>7/2</sub> and Br 3d regions for the untreated and treated NCs. The results suggest that the thiocyanate removes excess lead atoms from the surface, thus leading to the removal of traps. Reproduced with permission from ref 121. Copyright 2017 American Chemical Society. (d) Passivation of CsPbBr<sub>3</sub> NCs with benzenesulfonic acid: <sup>1</sup>H NMR full spectra of pure dodecylbenzenesulfonic acid (DBSA) and DBSA-capped NCs after three purification cycles. The chemical shift and broadening of the benzene-ring-related hydrogen peaks suggest the strong binding of DBSA to the NC surface. (e) Comparison of normalized PLQY of colloidal CsPbBr<sub>3</sub> NCs obtained with different capping ligands. The DBSA-capped NCs exhibit greater stability after three washing cycles. Reproduced with permission from ref 122. Copyright 2019 Wiley-VCH GmbH. (f) Surface passivation of CsPbBr<sub>3</sub> NCs with thiols: XPS of octanethiol-treated CsPbBr<sub>3</sub> NCs. The peaks at 158 and 169 eV correspond to the Pb–S bond in the treated sample and suggest that the thiol molecules are adsorbed on the surface. Reproduced with permission from ref 123. Copyright 2017 Royal Society of Chemistry.

shifted to lower frequencies with respect to bulk microcrystalline CsPbBr<sub>3</sub> (101.7 ppm), and the absence of the impurity cesium hexyl phosphonate phase (CsHPA) revealed that the broad resonances corresponded to the HPA-NPL. These broad NMR resonances are likely due to the local disorder caused by the anisotropic shape that characterizes semiconductor NCs.<sup>119,120</sup>

**Sulfur-Based Ligands.** The ligands with sulfur-based functional groups, such as sulfonic acids, thiolates, or thioethers, were also explored toward enhancing the stability and luminescence enhancement because of their strong interaction with Pb<sup>2+</sup> ions.<sup>122,124</sup> In this regard, Koscher et al. first reported the use of thiocyanate salt (ammonium or sodium) to passivate uncoordinated lead atoms for improving the quantum yield for fresh and old samples and maintaining colloidal stability of CsPbBr<sub>3</sub> NCs (Figure 7a).<sup>121</sup> Despite expected lead–thiocyanate bond formation, the XPS results revealed that the thiocyanate did not bind to the NC surface because there were no peaks corresponding to sulfur.<sup>121</sup> It was proposed that the thiocyanate passivation removes the excess lead atoms from the surface, which is consistent with the Pb/Br ratio of 1:3 and the absence of a sulfur peak in the XPS

(Figure 7c).<sup>121</sup> Later, several studies explored thiocyanates as passivating agents to obtain highly luminescent CsPbX<sub>3</sub> NCs.<sup>93,121,125</sup> A few studies reported the formation of thiocyanate–Pb bonds after the surface passivation. After the treatment with thiocyanate, a broad peak around 2060 cm<sup>-1</sup> could be seen in the FTIR spectra (Figure 7b), which corresponds to the C≡N bond linked to the sulfur-coordinated lead atom and may undergo a slight shift depending on which group it is bonded to (NH<sub>4</sub><sup>+</sup> or Na<sup>+</sup>).<sup>126</sup> The treatment with sodium thiocyanate (NaSCN) resulted in a distinctive peak at 1560 cm<sup>-1</sup> that was attributed to the C=O stretching of sodium oleate. In contrast, the passivation with NH<sub>4</sub>SCN resulted in a peak at 1712 cm<sup>-1</sup> related to the C=O stretching of oleic acid. Therefore, it seems that the Na<sup>+</sup> ion interacts with the oleic acid, while the thiocyanate interacts with the Pb<sup>2+</sup> atoms. Another type of sulfur containing ligand, for example, is didodecylmethylammonium sulfide (DDA<sup>+</sup>S<sup>2-</sup>), which is analogous to didodecylmethylammonium bromide (DDAB), and has shown an effective postsynthetic surface passivation of CsPbBr<sub>3</sub> NCs in enhancing their PLQY and stability against air and light.<sup>127</sup> Despite the crucial role of sulfur in the passivation of the NC



surface, the binding mode of  $\text{DDA}^+\text{S}^{2-}$  to the NC surface was unclear. Interestingly, the  $\text{DDA}^+\text{S}^{2-}$  ligands, along with OA, self-assembles  $\text{CsPbBr}_3$  nanocubes into nanowires through halide vacancies.<sup>128</sup> Similarly, benzenesulfonic acid ligands were also used in an attempt to increase the stability, luminescence, and electronic coupling in NC films.<sup>129</sup> The low PLQYs of LHP NCs are often attributed to the presence of halide vacancies that result in uncoordinated Pb atoms,<sup>8,64,74,130</sup> and these lead-rich surfaces show a remarkable trapping effect<sup>131</sup> because of the orbital composition of the conduction band<sup>16,89,132</sup> being counterproductive for their luminescence efficiency. Nevertheless, the strong ionic sulfonates can tightly bind to the  $\text{Pb}^{2+}$  ions, thereby eliminating the exciton trapping probability.<sup>129</sup> The  $\text{CsPbBr}_3$  NCs prepared using dodecylbenzenesulfonic acid (DBSA) exhibited PLQY up to 90%, which was retained for more than five months of storage, thereby showing a remarkable enhancement of stability (Figure 7e).<sup>129</sup> Furthermore, the chemical shift and broadening of the  $^1\text{H}$  NMR signal for the hydrogen peaks of the benzene indicate the strong coordination of DBSA to the surface of the NCs (Figure 7d). XPS studies further confirmed the presence of the sulfonate groups together with their binding mode, which showed the expected S 2p and O 1s XPS results. In addition, diffusion-ordered spectroscopy (DOSY), Fourier transform infrared (FTIR), and thermogravimetric (TG) measurements confirmed the stronger interaction of DBSA ligands firmly binding to the uncoordinated  $\text{Pb}^{2+}$  ions on the surface of NCs through sulfonate head groups.<sup>129</sup> In other words, the sulfonate groups fill the halide vacancies.

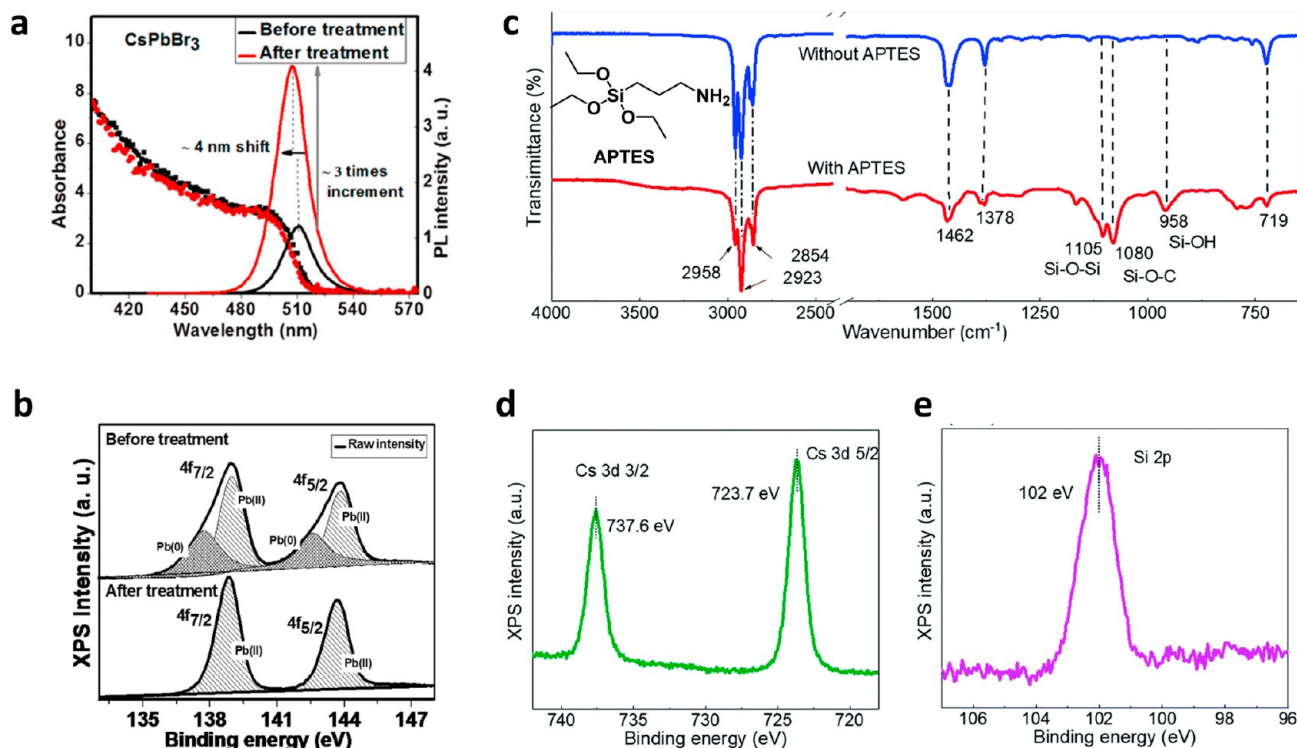
Alternatively, alkyl thiols ( $\text{R-S-H}$ ) are an excellent class of ligands for NCs. They have the strong tendency to form sulfur–metal bonds and, thus, they can confer excellent stability to NCs.<sup>133–136</sup> Alkyl thiols have been extensively used for the capping of colloidal gold,<sup>137</sup> silver<sup>138,139</sup> NCs, and classical QDs.<sup>133–136</sup> The use of thiol ligands have been extended to LHP NCs as they have the potential to bind to the surfaces through the formation of S–Pb bonds.<sup>123</sup> In this context, postsynthetic ligand exchange has been used to substitute the OAm/OA ligands with octanethiol, which leads to an increase in luminescence, stability, and conductivity.<sup>123</sup> The surface binding of thiol molecules was confirmed by XPS, in which two peaks at 158 and 169 eV related to the Pb–S bond were detected after the treatment with thiol (Figure 7f).<sup>123</sup>

On the contrary, dithiols together with OAm can cause a decrease in the luminescence intensity because of the transformation from  $\text{CsPbBr}_3$  NCs to  $\text{Cs}_4\text{PbBr}_6$  NCs.<sup>140</sup> This transformation also occurs with an excess of OAm, but it is reinforced in the presence 1,3-propanedithiol (PDT) and can be explained according to the hard–soft acid–base theory. The ability of dithiols to bind strongly to  $\text{PbBr}_2$  results in the dissolution of  $\text{CsPbBr}_3$  NCs with the consequent transformation into  $\text{Cs}_4\text{PbBr}_6$  NCs. Further studies have indicated the presence of thiol signals in XPS (bound thiolate and unbounded thiol)<sup>141</sup> and FTIR ( $800\text{ cm}^{-1}$  sulfur–metal bonds),<sup>142</sup> which are characteristics for sulfur, thereby proving that the dithiols are acting as capping ligands that display increased stability and better size distribution for  $\text{Cs}_4\text{PbBr}_6$  NCs. In a subsequent study, Uddin et al. compared the effectiveness of various ligands, such as dodecanethiol (DDT), trioctylphosphine oxide (TOPO) and tri-*n*-octylphosphine (TOP), ammonium thiocyanate ( $\text{NH}_4\text{SCN}$ ), tetradecyldimethyl (3-sulfopropyl)ammonium hydroxide inner salt (sulfo-

betaine), and sodium dodecyl sulfate (SDS), to improve photoluminescence and its mechanistic exploration.<sup>124</sup> A greater increase in luminescence and long-term stability were observed for DDT, which showed additional long-term stability. However, we believe further studies are required to rationalize the differences in the stability of LHP NCs with different ligands. It was proposed that the DDT protonates the oleic acid ions, thereby leading to the formation of thiolates and thioethers that then bind to undercoordinated Pb atoms at the  $\text{CsPbBr}_3$  NC surfaces to result in near-unity PLQY.<sup>124</sup> In conclusion, the strong interaction of alkyl phosphonic acids, sulfonates, and thiolates toward  $\text{Pb}^{2+}$  ions leads to high affinity to the LHP NC surface and, thus, results in improved PLQY and chemical stability.

**Bidentate and Multidentate Ligands.** Bidentate ligands, i.e., having two functional groups that can bind to NCs, are of special interest<sup>37,143–152</sup> because of their ability to improve the stability of NCs through the chelate effect.<sup>153</sup> The bidentate ligands show great promise for efficient surface passivation and photoluminescence enhancement. Importantly, the bidentate-capped NCs retain their PL efficiency after several cycles of washing. To address the issues associated with ligand detachment, Krieg et al. proposed the use of long-chain zwitterionic molecules (sulfobetaines, phosphocholines,  $\gamma$ -amino acids, etc.) as capping ligands for  $\text{CsPbX}_3$  NCs, and these ligands showed a remarkable increase in durability and stability.<sup>37</sup> The presence of an anionic and a cationic group on the same molecule prevents them from being neutralized by a Bronsted acid–base equilibrium, and their binding to the NC surface is kinetically stabilized by the chelate effect.<sup>144,153</sup> The NMR spectra confirmed that the zwitterionic ligands are the only species present on the NC surface.<sup>37</sup> In addition, DFT studies suggest that the dimethylammonium group of the zwitterionic ligand can be accommodated at the cation site of the surface despite its bulkiness. Furthermore, the ligand binding energies (ca. 40–45 kcal/mol) suggest high affinity of the ionic species for the surface, without significant energetic difference between the conventional and the zwitterionic passivation, thereby supporting the theory that they are stabilized because of the chelating effect.<sup>37</sup> Interestingly, the number of carbons present in the sulfobetaine ligand has a substantial effect on the synthesis: four carbons are favored for iodine perovskites, likely because of the greater anion cation distance, while three carbons are preferred for chlorine and bromine perovskites.<sup>37</sup> Subsequent studies have shown the effectiveness of employing soy lecithin, a phospholipid, as a capping agent that confers high stability because it maximizes the repulsion between nanocrystals due to its brushlike structure to prevent aggregation.<sup>146</sup> The efficient ligand binding mode was confirmed by  $^1\text{H}$  and  $^{31}\text{P}$  NMR spectroscopy of lecithin-capped NCs that showed a line broadening compared with the spectra of lecithin and decomposed NCs. This was attributed to an increase in the ligand's rotational correlation time resulting from the association with the NCs. In addition, DOSY data showed an increase in the diffusion coefficient of the ligands upon association with the NCs that is in agreement with the values previously reported for zwitterions.<sup>37</sup> Further studies analyzed the effectiveness of various zwitterionic polymers for improving the stability and PLQY of NCs, where the parent ligands were replaced with zwitterionic polymers.<sup>147</sup>

The long-chain ligands such as OAm/OA hinder the charge carrier transport in LHP NC films because of their insulating



**Figure 8.** (a) Absorption and PL spectra of CsPbBr<sub>3</sub> NCs before and after the treatment with tetrafluoroborate salts. The PLQY increases by 3 times after the treatment. (b) XPS of Pb 4f<sub>7/2</sub> and 4f<sub>5/2</sub> before and after treatment. The spectra are calibrated with respect to the C 1s peak (at 285.35 eV). Quantitative XPS indicate that the Br/Pb ratio increases from 3.8 to 4 after the surface treatment, which suggests the removal of Pb from the NC surface. However, no signature of fluorine was observed. Panels (a) and (b) are reproduced with permission from ref 164. Copyright 2018 American Chemical Society (c) Synthesis of CsPbBr<sub>3</sub> nanoplatelets with (3-aminopropyl)triethoxysilane (APTES) ligands: FTIR spectra of the samples with and without APTES. The vibration of Si–O–C at 1080 cm<sup>-1</sup> indicates that the APTES ligands bind to the NC surface. XPS spectra of the (d) Cs 3d and (e) Si 2p regions for APTES-NPLs. Panels (c–e) are reproduced with permission from ref 165. Copyright 2021 Royal Society of Chemistry.

nature.<sup>144</sup> In general, the shorter the ligands are, the better the charge carrier transport is. However, the NCs exhibit relatively less colloidal stability with short-chain ligands. Therefore, short-chain bidentate ligands, for example, 2,2'-iminodibenzoic acid (IDA), were explored by replacing the original ligands through postsynthetic ligand exchange.<sup>154</sup> XPS and IR spectroscopy analysis suggest that IDA molecules bind to CsPbI<sub>3</sub> NCs through their carboxyl groups. The strong interaction between the bidentate ligand and the PbI<sub>2</sub> surface atoms through the two carboxyl groups leads to reduced surface traps and, thus, an increase in photoluminescence, stability, and charge transport.<sup>144</sup> Successively, another dicarboxylic acid, succinic acid, and OAm were used for the synthesis of colloidal MAPbBr<sub>3</sub> perovskites.<sup>150</sup> The presence of two carboxyl groups enabled binding to two exposed Pb atoms on the NC surface<sup>144</sup> and showed an improvement in environmental stability.<sup>150</sup>

Recent studies reported the surface passivation of LHP NCs with phthalimide,<sup>148</sup> thereby showing a large increase in environmental and photostability. XPS studies revealed a lower Br/Pb ratio after the passivation in contrast to the lead-rich surface prior to treatment, which is detrimental to their optical properties.<sup>35</sup> Another important class of bidentate ligands are amino acids with at least an amine and a carboxylic acid group on them that are naturally available. For example, L-cysteine, an amino acid, has been employed in a reprecipitation method to passivate MAPbBr<sub>3</sub> NCs, thereby resulting in highly stable and luminescent supercrystals (self-assembled nanocubes).<sup>155</sup> The

FTIR spectra suggest a strong interaction of L-cysteine (L-cys) as the stretching mode of C=O (1635 cm<sup>-1</sup>) with respect to free L-cys (1577 cm<sup>-1</sup>) changes upon binding.<sup>156</sup> Furthermore, the absence of the S–H vibrational peak in the spectrum of L-cys-capped NCs indicates the formation of a coordination bond between the sulfhydryl group and the Pb<sup>2+</sup> atoms.<sup>155</sup> Bidentate ligands are also used for the stabilization of perovskite solar cells. One example involves 2-mercaptopyridine (2-MP) for the passivation of CH<sub>3</sub>NH<sub>3</sub>PbI<sub>3</sub> films, in which the presence of the sulfhydryl group adjacent to the nitrogen favors the interaction with the Pb<sup>2+</sup> atoms on the surface by chelating effect.<sup>145</sup> In comparison with monodentate analogues, such as pyridine (Py)<sup>157,158</sup> and *p*-toluenethiol (PTT),<sup>158</sup> 2-MP displayed a high anchoring strength, and a CH<sub>3</sub>NH<sub>3</sub>PbI<sub>3</sub>-based planar n–i–p structured solar cell with the addition of 2-MP exhibited an increase in power conversion efficiency from 18.35% to 20.28%, along with a substantial increase in stability against moisture and other environmental factors.<sup>145</sup>

As the studies suggest that the increase in binding moieties of ligands leads to an enhanced stability and PLQY of LHP NCs, various multidentate ligands have been exploited.<sup>159,160</sup> For example, multidentate block copolymer (P2VP) was used to obtain a micelle shell on the surface of CsPbBr<sub>3</sub> NCs.<sup>159</sup> The pyridine functional groups of the block copolymer show affinity for the PbBr<sub>2</sub> precursor and, thus, increase its solubility and serve as a template for the growth and nucleation of the NCs in the polymer shell.<sup>161</sup> In addition, the polymer shell



protects the surfaces of the NCs to significantly improve their stability against polar solvents. Another multidentate ligand of interest is polyethylenimine, which serves as a template for the assembly of CsPbBr<sub>3</sub> perovskite nanoplatelets and passivates the bromine vacancies, thus improving colloidal stability.<sup>162</sup> Furthermore, the short-chain length of the polyethylenimine allows for carrier hopping and tunneling between adjacent NPLs, thus favoring charge transport. Alternatively, multidentate ligands L-glutathione and ethylenediaminetetraacetic acid (EDTA) were used to obtain stable red-emitting mixed halide LHP NCs that exhibit red electroluminescence (620 nm) with an EQE higher than 20%.<sup>163</sup> Moreover, ligand–ligand interactions of the multidentate molecules result in a ligand shell on the nanocrystal surface, while the multidentate ligand interactions with the surface remarkably suppress the surface defects.

**Tetrafluoroborates and Silane Ligands.** In addition to the above-discussed ligand types, various other inorganic ligands, such as tetrafluoroborates and silanes, have also been explored to enhance the optical and chemical stability of LHP NCs. It was demonstrated that the postsynthetic surface treatment with tetrafluoroborate salts significantly enhances the photoluminescence of CsPbX<sub>3</sub> NCs (Figure 8a).<sup>164</sup> Quantitative XPS analysis (Figure 8b) revealed that the removal of some of the surface lead atoms acts as traps for the charge carrier and, thus, results in enhancement of the PLQY.<sup>121,166</sup> It was proposed that the BF<sub>4</sub><sup>−</sup> ions have access only to limited places on the NC surface and do not remove all surface capping ligands.<sup>164</sup> However, in another study, the FTIR spectra of the NCs showed a broad peak around 1080 cm<sup>−1</sup> corresponding to the B–F stretching of BF<sub>4</sub><sup>−</sup> bound to lead, thereby suggesting the presence of BF<sub>4</sub><sup>−</sup> on the surface of NCs.<sup>167</sup>

Conversely, silane-based ligands have often been used for silica shell coating on colloidal NCs.<sup>168–173</sup> Because the colloidal perovskites are vulnerable to water, silane ligands were extensively used to protect the surface of LHP NCs. The use of silane ligands often leads to the formation of a protective shell on the NC surfaces. For instance, alkyltrichlorosilanes (R-SiCl<sub>3</sub>) can be used as Cl-sources for an anion exchange with CsPbBr<sub>3</sub> NCs that result in CsPbCl<sub>3</sub> NCs coated with siloxane shells. The CsPbCl<sub>3</sub> NCs show improved long-term stability against water and increased PLQY.<sup>174</sup> In particular, dodecyltrichlorosilane (DTS) forms a hydrophobic layer around the NCs upon reaction with carboxyl groups or water molecules, which leads to the formation of silols that coordinate with the surface lead atoms. The shift of the Si–O–Si antisymmetric stretching modes (970–1200 cm<sup>−1</sup>) in the FTIR spectra suggests that the Si–O–Si groups coordinate to the NC surfaces with the disappearance of the Si–Cl bands (562 and 585 cm<sup>−1</sup>) that were present in pure DTS. The displacement of OAm by DTS can be supported by the absence of the N–H bending mode peaks (1644 cm<sup>−1</sup>) in the Raman spectra of DTS NCs. However, FTIR and Raman data show that a fraction of carboxylates remain bound to the surface after DTS anion exchange because of the fact that the carboxylate–ligand-related shoulder peaks remain present at 1435 and 1420 cm<sup>−1</sup>.<sup>175</sup> These studies suggest that the silane ligands exhibit higher binding affinity than amines.<sup>35,176</sup>

The two most extensively used silanes for SiO<sub>2</sub> shell coating on NCs are 3-aminopropyltriethoxysilane (APTES) and tetramethoxysilane (TMOS).<sup>165,168,177,178</sup> These have also been used to passivate (in situ, as well as postsynthetic)

CsPbBr<sub>3</sub> NCs, which has significantly improved stability against environmental factors, long-term storage, and polar solvents because of the formation of a cross-linking SiO<sub>2</sub> matrix by hydrolysis of the silyl ether groups.<sup>165,177</sup> The hydrolysis reaction can take place in the presence of water or with a slight addition of a base. The FTIR spectra show the characteristic peaks at 2923 and 2854 cm<sup>−1</sup>, which can be assigned to the C–H vibrations of OAm and APTES, respectively (Figure 8c).<sup>179</sup> The presence of the vibration of Si–O–C at 1080 cm<sup>−1</sup> implies that the APTES was functionalized to the NC surface.<sup>180</sup> The binding energies corresponding to Cs 3d suggest the presence of only one type of Cs<sup>+</sup> in APTES-nanoplatelets (Figure 8d). The Si 2p signal at 102 eV in the XPS spectra further confirms the existence of APTES on the surface (Figure 8e). The vibration bands of Si–O–Si (1105 cm<sup>−1</sup>) and Si–OH (958 cm<sup>−1</sup>) result from the hydrolysis of APTES. In addition, the Si/O atomic ratio (1:2) reveals the formation of a SiO<sub>2</sub> coating on the surface by hydrolytic condensation of the APTES.<sup>165</sup>

As summarized above, the chemistry of ligands and their interactions with LHP NC surfaces play an important role in the optical and electronic properties, as well as the chemical stability, and thus, are crucial for corresponding optoelectronic devices. Consequently, many studies are still being focused on optimizing the surfaces and ligands of LHP NCs to maximize their properties, as discussed in later sections.

## ■ LIGAND EXCHANGE

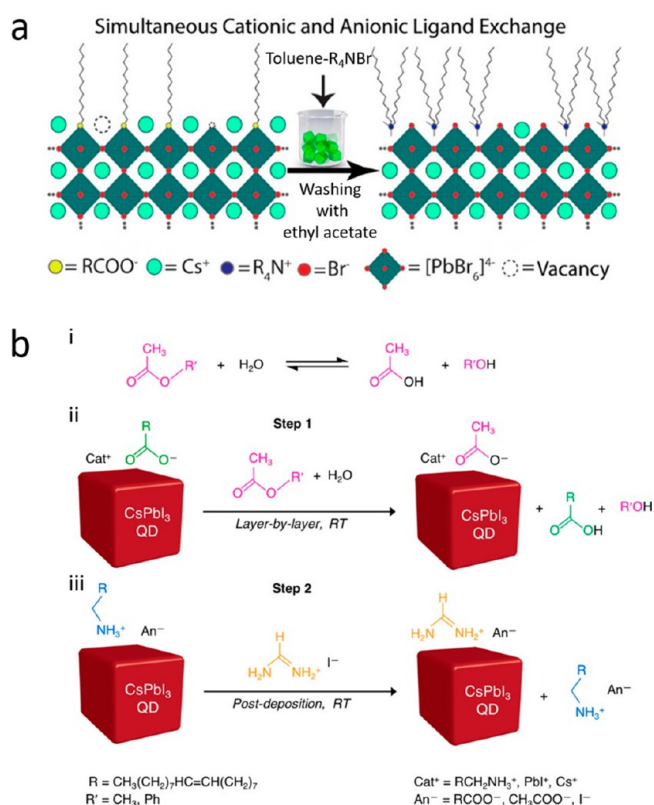
Postsynthetic ligand exchange is an inevitable process for many colloidal NC systems to improve their stability, dispersibility, and to impart desired properties and functions. It enables the surface functionalization of NCs with desired molecules that are not possible to use as ligands during synthesis and is often used to tailor the properties of NCs in accordance with the desired applications. In addition, this strategy is critical for the phase transfer of NCs from aqueous to organic solvents and vice versa with the use of respective ligands. Therefore, ligand exchange on colloidal NCs is a foundation for their applications. Over the years, ligand exchange has been implemented on a wide range of colloidal NC systems, including metals and classical QDs. The ligand exchange in LHP NCs is relatively less explored than in classical NC systems. Moreover, the exchange mechanism and the surface chemistry of the NCs after the ligand exchange are yet to be fully explored. As discussed above, the soft ionic nature of perovskites make the ligands more dynamic on the NC surface and often leads to their degradation of phase transformation.<sup>50,78,222–224</sup> The interaction strength between the

The interaction strength between the NC surface and the foreign molecules often drives the ligand exchange process, and the interactions can be either covalent or electrostatic.

NC surface and the foreign molecules often drives the ligand exchange process, and the interactions can be either covalent or electrostatic.

Currently, researchers are screening different ligands to replace the typical amine and acid ligands used in the colloidal LHP synthesis to improve the stability of NCs with strong

binding ligands and to improve the conductivity of corresponding NC films and, thus, their performance in optoelectronic devices by reducing the chain length of the ligands.<sup>76,86,192,225</sup> In this regard, Pan et al.<sup>192</sup> demonstrated the replacement of native long-chain oleylamine (OAm) and oleic acid (OA) ligands with a relatively short ligand, didodecyl dimethylammonium bromide (DDAB), through ligand exchange. The ligand exchange has been carried out by sequential addition of OA and DDAB ligand to the purified LHP NCs in toluene. It was found that the addition of OA is critical for the desorption of native OAm from the NC surface through protonation; otherwise, it leads to the degradation of NCs. Importantly, the DDAB ligands facilitate the charge carrier transport in LHP NC films and, thus, enables the fabrication of efficient LEDs.<sup>191,192,226,227</sup> Several other studies have also found that quaternary alkylammonium halides ( $R_4NX$ ) dramatically improve the stability and PLQY of NCs after postsynthetic ligand exchange through efficient passivation of surface traps (A and X sites).<sup>47,228</sup> The  $R_4NX$  molecules can simultaneously exchange both anionic (typically carboxylates that occupy X sites) and cationic (A site) ligands from the surface of LHP NCs (Figure 9a).<sup>47</sup> Furthermore, it was found that the  $R_4NBr$  molecules can replace the native ligands of  $CsPbBr_3$  NCs without the assistance of excess OA ligands; however, excess  $R_4NBr$  molecules can lead to the degradation of LHP NCs.<sup>47,229</sup> The proton-free  $R_4NX$ -ligand-capped NCs are more stable than primary ammonium-halide-protected NCs. In particular, the  $R_4NX$  molecules with two long alkyl chains and two methyl groups impart the NCs with excellent colloidal stability and high PLQY even after washing with polar solvents. However, the study by Quarta et al.<sup>230</sup> suggests that primary amines can also be used for the effective replacement of the native oleate or oleylammonium ligands from  $CsPbBr_3$  NCs and passivate the NC surfaces to achieve near-unity PLQY. However, excess addition of amines leads to etching of  $PbX_2$  from the surfaces of the NCs and even their degradation. Although the ligand exchange enables the replacement of native ligands with amines of different carbon lengths, the poor colloidal stability of ligand-capped LHP NCs limits their applications. For instance, Ye et al.<sup>225</sup> found that the replacement of a short–long-chain with long-chain acid–base pair (OAm and OA) drastically improves the colloidal stability and the device performance of the corresponding LEDs. Besides, various other exchanging ligands, including thiols,<sup>123,200,231,232</sup> thionyl halides,<sup>233</sup> phosphonic acids,<sup>49,118,234</sup> phenethylammonium ( $PEA^+$ ),<sup>235</sup> cinnamate acid,<sup>236</sup> chiral molecules,<sup>237</sup> and zwitterionic molecules (including bi- and multidentate ligands), such as iminodibenzoic acid,<sup>154</sup> ethylenediaminetetraacetic acid (EDTA)–glutathione (GSH),<sup>163,214</sup> trithiocarbonate (TTC),<sup>238</sup> heterocyclic aromatic carboxylates,<sup>143</sup> and zwitterionic polymers,<sup>147,152,239</sup> have been potentially exploited to replace native ligands of LHP NCs. In addition, neutral ligands, such as carboxylic acid, sulfonic acid, and phosphonic acids, can replace the alkylammonium cations, as well as etch the surface, of LHP NCs.<sup>49</sup> The higher the acidity of the ligands, the higher the etching; therefore, ligands such as dodecylbenzenesulfonic acid can cause complete degradation.<sup>49</sup> Most of these studies have aimed at improving the stability, PLQY, and performance in LEDs through surface passivation of A and X site vacancies. Among all, significant attention has been paid to replacing native ligands with zwitterion molecules and polymers that have more than one binding site for enhanced ligand–surface



**Figure 9.** (a) Schematic illustration showing the simultaneous cationic (A site) and anionic (X site) ligand exchange on oleate capped- $CsPbBr_3$  NCs with quaternary ammonium ligands. The ligand exchange is carried out by dispersing crude LHP NCs in toluene solution containing  $R_4NBr$  and then washing with ethyl acetate solution. Reprinted with permission from ref 47. Copyright 2019 American Chemical Society. (b) Hydrolysis of an ester to carboxylic acid and alcohol in the presence of atmospheric moisture (i); carboxylate ligand exchange on  $CsPbI_3$  NCs, both in thin films and in colloidal solutions (ii); and alkyl ammonium cation exchange on  $CsPbI_3$  NCs in thin films (iii). Reproduced with permission from ref 240. Copyright 2018 American Chemical Society.

interactions. Furthermore, the purification of colloidal NCs by the addition of an antisolvent, usually methyl acetate (MeOAc), is an important postprocessing step for device applications. Interestingly, the washing step results in ligand exchange because of the atmospheric moisture-induced hydrolysis of the antisolvent, MeOAc, into acetic acid, which then replaces the native oleate ligands of LHP NCs (Figure 9b).<sup>240</sup> In addition, the native oleylammonium ligands that remain on NCs are replaceable with small molecular cations, like formamidinium, by treating them with respective molecular halides, for instance, formamidinium halide (Figure 9b-iii).<sup>240</sup> The replacement with small molecular cations has only been demonstrated on NCs deposited on a substrate. It is still challenging to obtain stable colloidal LHP NCs with short-chain or small molecular ligands.

## ■ LIGAND-INDUCED STRUCTURAL TRANSFORMATIONS

The ligands not only improve the optical properties and chemical stability but also induce phase transformations in  $CsPbX_3$  NCs depending on the ligand type and concentration. Early studies on LHP NCs demonstrated the ligand-induced



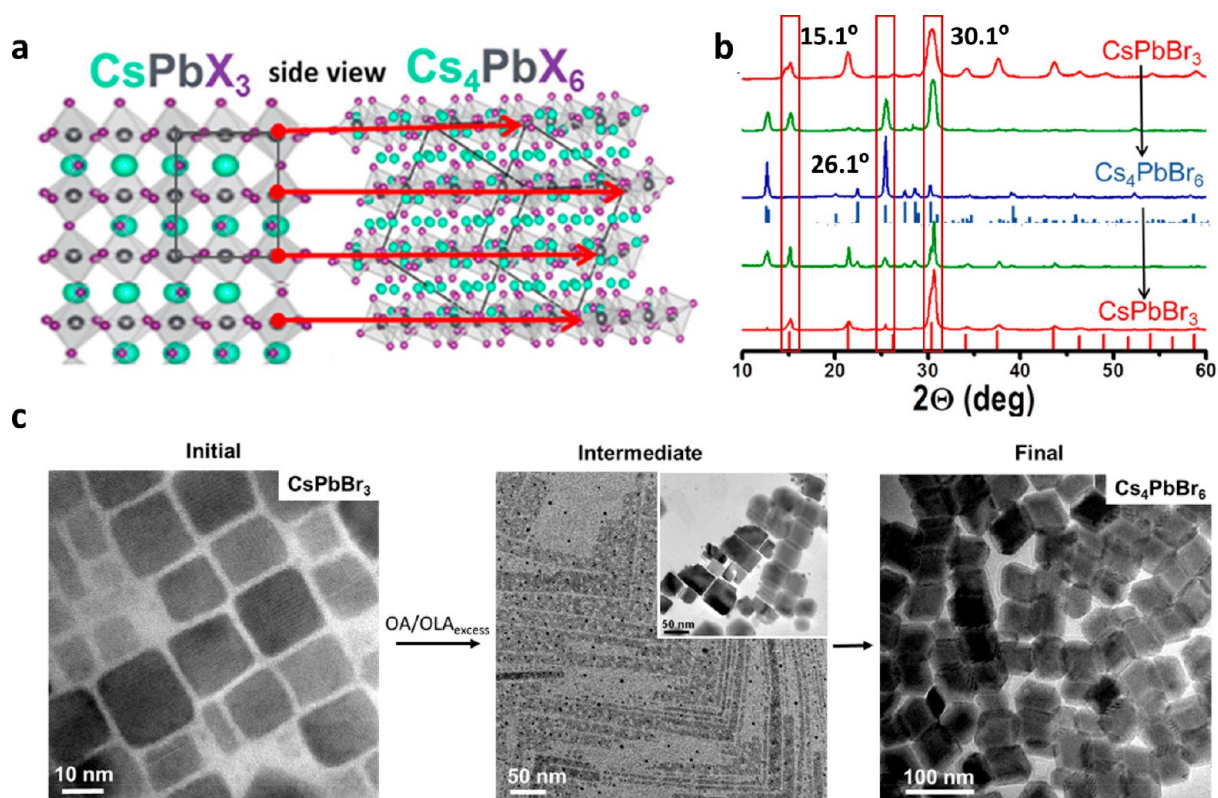


Figure 10. (a) Illustration of ligand passivation-induced structural and compositional change of  $\text{CsPbX}_3$  into rhombohedral  $\text{Cs}_4\text{PbX}_6$  NCs. (b) XRD pattern of the transformation of  $\text{CsPbBr}_3$  to  $\text{Cs}_4\text{PbBr}_6$  NCs, along with the intermediates (green). (c) TEM images of the  $\text{CsPbBr}_3$  NCs and the intermediate product in the transformation into  $\text{Cs}_4\text{PbBr}_6$  NCs. Reprinted with permission from ref 241. Copyright 2018 American Chemical Society.

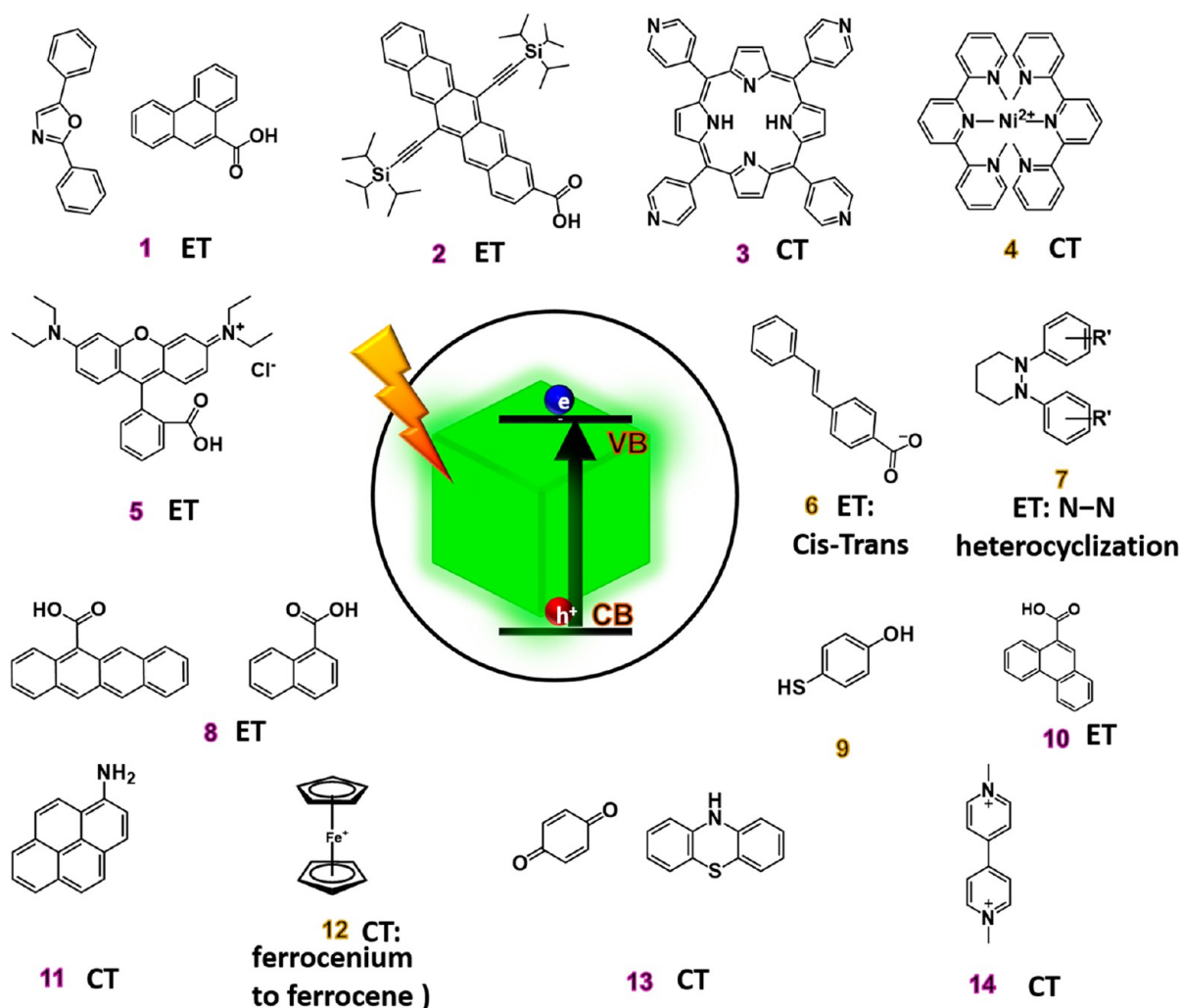
transformation of bulk 3D perovskites into 2D NPLs by ultrasonication.<sup>242</sup> The ligands either exfoliate 3D perovskites or dissolve into precursors and then recrystallize into 2D NPLs.<sup>8</sup> One of the most commonly observed phase transformations is the cubic  $\text{CsPbX}_3$  to the rhombohedral  $\text{Cs}_4\text{PbX}_6$  phase (Figure 10a),<sup>241,243,244</sup> which is induced by a change of the surface ligand and recrystallization process.<sup>241</sup> The transformation is reversible and is controllable by varying the ratio of OAm to OA-capping molecules or intercalating  $\text{PbX}_2$ .<sup>241,243</sup> The size uniformity and the chemical stability of the derived  $\text{Cs}_4\text{PbX}_6$  NCs was enhanced by the addition of alkyl thiols.<sup>140</sup> This transformation of the cubic  $\text{CsPbBr}_3$  phase to the rhombohedral  $\text{Cs}_4\text{PbBr}_6$  phase could be followed by XRD. The suppression of the dispersion peaks at  $15.1^\circ$  and  $30.1^\circ$ , together with the appearance of a new peak at  $26.1^\circ$ , corroborate the loss of the pristine phase with the following transition to  $\text{Cs}_4\text{PbBr}_6$  NCs, as can be seen in Figure 10b.<sup>241</sup> This has been supported by TEM images where it was possible to observe the gradual decomposition into lamellar structures, sheets, platelets, and amorphous material, as well as conversion to homogeneous-sized  $\text{Cs}_4\text{PbBr}_6$  NCs (Figure 10c).<sup>241</sup> Another transformation, 3D  $\text{CsPbBr}_3$  NCs to 2D  $\text{CsPb}_2\text{Br}_5$  nanosheets, was demonstrated by excess addition of  $\text{PbBr}_2$  ( $\text{CsPbBr}_3 + \text{PbBr}_2 = \text{CsPb}_2\text{Br}_5$ ) or an environment triggering the formation of  $\text{PbBr}_3^-$  complexes.<sup>245,246</sup> The latter transformation starts with a ligand (dodecyl dimethylammonium bromide) exchange step and concurrently forms  $[\text{PbBr}_3]^-$  complexes. Then, the  $[\text{PbBr}_3]^-$  complexes react with  $\text{Cs}^+$  to result in the formation of  $\text{CsPb}_2\text{Br}_5$ .<sup>246</sup> In another work, Fanizza et al. demonstrated the transformation of  $\text{CsPbBr}_3$

NCs into 1D tetragonal nanowires or 0D rhombohedral  $\text{Cs}_4\text{PbBr}_6$ , depending on the addition of either oleyl amine or OA.<sup>247</sup> The structural transformations are often analyzed by GIWAXS and XRD, along with optical characterization.<sup>8,247</sup>

## IMPARTING OF NEW FUNCTIONALITIES BY LIGANDS

Ligand exchange not only improves the stability and PLQY of LHP NCs through strong binding but also imparts new properties and functions using specific ligands of interest.<sup>8,248–252</sup> In addition, functional ligands allow the possibility of modulating the properties of LHP NCs by introducing new features.<sup>8</sup> Consequently, numerous studies have emerged demonstrating the possibility of inducing new functionalities to LHP NCs through surface functionalization (or surface adsorption) of different molecules of interest either by direct synthesis or through postsynthetic treatments. Examples of new features include chirality, photocatalysis through energy/charge transfer to nearby molecules,<sup>8,248–252</sup> and Stokes-shifted emission through exciton-to-ligand energy transfer.

**Photoexcited Charge Transfer to Surface-Anchored Molecules.** Because they have emerged as excellent semiconductor materials for visible light absorption and efficient charge carrier generation and transport, LHP NCs have started to receive significant attention for photocatalytic applications through the efficient extraction of photogenerated charge carriers.<sup>8,266–273</sup> The charge carriers of LHP NCs are generally extracted using specific ligands or small molecules that interact with their surfaces through electrostatic interactions. A good alignment of energy levels (HOMO and LUMO) of the

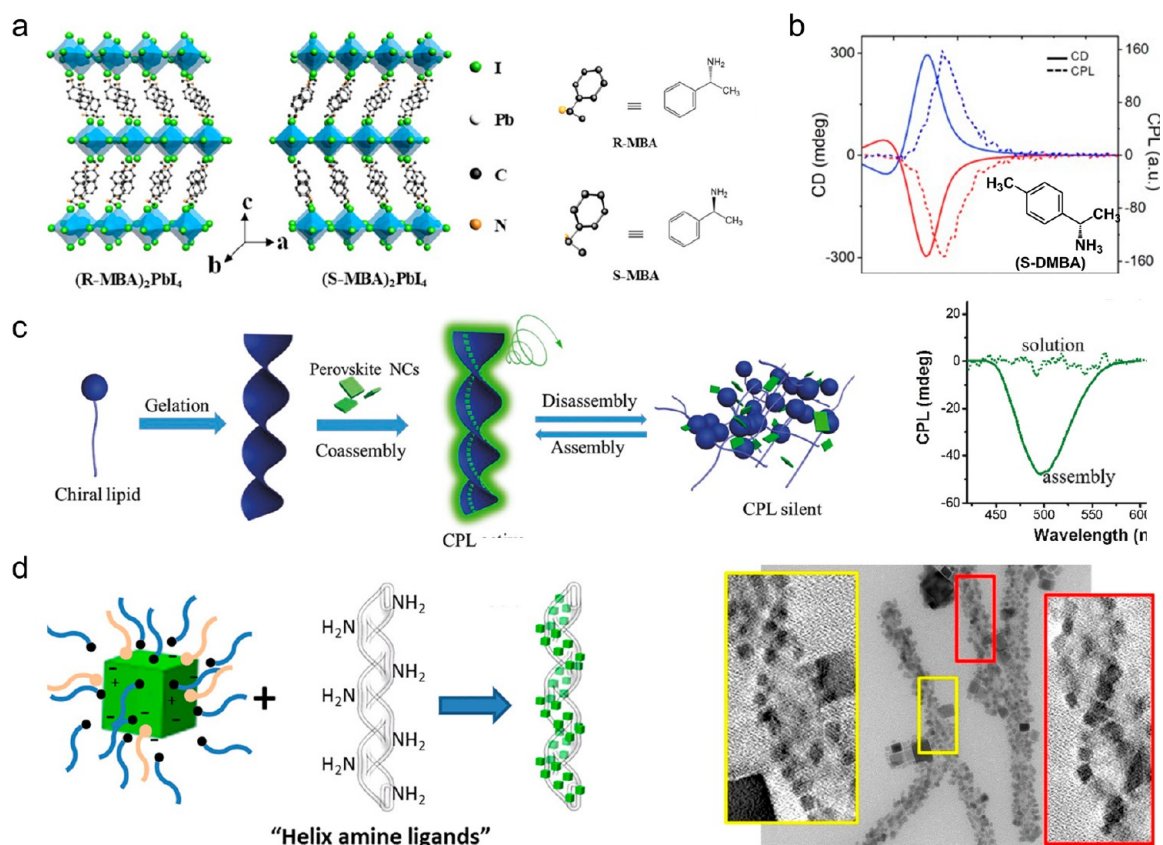


**Figure 11.** Summary of some of the ligands (molecules interacting with the surface of NCs) employed for energy/charge transfer from LHP NCs to ligands and for photocatalysis and chemical reactions. ET, energy transfer; CT, charge (electron or hole) transfer. It should be noted that the energy transfer is also mediated by charge transfer. The molecules are adapted from various references: (1) ref 253, (2) ref 252, (3) ref 254, (4) ref 255, (5) refs 256 and 257, (6) ref 250, (7) ref 258, (8) ref 259, (9) ref 260, (10) ref 261, (11) ref 262, (12) ref 263, (13) ref 264, and (14) ref 265.

molecules and perovskite NCs is also important for the favorable charge transfer across the interface.<sup>266,274</sup> A variety of molecules have been exploited for the efficient extraction of the photoexcited charge carriers (electron and hole) from LHP NCs (Figure 11). The extracted charge carriers have also been used to drive photoredox organic chemical reactions<sup>238,250,270,272,275–279</sup> or CO<sub>2</sub> reduction on the surface of LHP NCs on the basis of charge or energy transfer from LHP NCs to nearby molecules (Figure 11).<sup>8,266,268,269</sup> For example, Jin et al.<sup>238</sup> demonstrated the polymerization of trithiocarbonate (TTC) ligand on the surface of CsPbBr<sub>3</sub> NCs upon photoexcitation, which leads to the formation of core–shell-type CsPbBr<sub>3</sub>–polymer NCs that exhibit improved stability in air, water, and UV light illumination. The charge transfer from perovskite NCs to surface-bound TTC ligands drives the polymerization reaction. Similarly, the photoexcited CsPbBr<sub>3</sub> NCs also catalyze *cis*–*trans* isomerization and intermolecular cycloaddition reactions in the molecules anchored to the surface of NCs.<sup>250,280</sup> The molecules are often coupled to LHP NCs with either carboxylate, amine (or ammonium), or thiol functional groups to test the photocatalytic reactions.<sup>248,250,262,277,280–285</sup> For instance, Lin et al.<sup>280</sup> demon-

strated triplet energy transfer (TET) from LHP NCs to surface-bound carboxylate-linked polycyclic aromatic hydrocarbon acceptors for diastereomeric *syn*-selective 2 + 2 cycloadditions. In this case, the LHP NCs act as templates to carry out intermolecular cycloaddition reactions by anchoring the molecules on NCs with close proximity using carboxylic or amine functional groups. Different research groups have explored the triplet sensitization via TET transfer in LHP NC–organic molecular systems.<sup>248,250,270,278,280,281,283</sup>

In most cases, the sensitizers with carboxylate or amine groups are used to attach to the surface of LHP NCs because the energy transfer is highly dependent on the distance between the donor (LHP NC) and acceptor (e.g., triplet emitters). In this regard, 1-pyrenecarboxylic acid (PCA) molecules (triplet acceptors) were anchored onto the CsPbBr<sub>3</sub> NC surface through the carboxyl group, and it was found that the TET occurs only for quantum confinement NCs.<sup>283</sup> The linear correlation of TET rate with carrier probability density at the surface of NCs suggests the Dexter-type TET mechanism.<sup>283,258</sup> In the case of surface-bound Rhodamine B (RhB), the quenching of LHP NC emissions, along with a subsequent increase in fluorescence of chromophores, suggests



**Figure 12.** Strategies to induce chirality in LHPs. (a) Chiral ligand [(R)/(S)-MBA]-induced chiral 2D Ruddlesden–Popper-layered thin films of [(S)-MBA]<sub>2</sub>PbI<sub>4</sub> and [(R)-MBA]<sub>2</sub>PbI<sub>4</sub>. Reproduced with permission from ref 289. Copyright 2019 American Chemical Society. (b) Left, CD and CPL spectra of DMBA-capped chiral perovskite NCs; right, CPL spectra of individual NCs and chiral assemblies. Reproduced with permission from ref 290. Copyright 2022 Wiley-VCH GmbH. (c) Schematic illustration of the chiral gel-induced assembly of CsPbBr<sub>3</sub> NCs into chiral assemblies. Reproduced with permission from ref 291. Copyright 2018 Wiley-VCH. (d) Left, scheme of the ligand-exchange grafting method to obtain chiral assemblies; right, TEM images of nanohelices@perovskite NCs. Reproduced with permission from ref 292. Copyright 2020 American Chemical Society.

the singlet energy transfer mechanism.<sup>257</sup> Interestingly, it was found that the energy transfer mechanism (Förster or Dexter) depends on the bandgap of the LHP NCs with respect to that of RhB. The rate constants suggest a Förster energy transfer for CsPbBr<sub>3</sub>–RhB assemblies, while CsPb(Br<sub>1-x</sub>Cl<sub>x</sub>)<sub>3</sub>–RhB assemblies favor the Dexter-type mechanism.<sup>257</sup> In a recent study, Martin et al.<sup>258</sup> reported a photocatalytic transformation of surface-anchored diamine to N–N heterocyclization reaction through a sequential electron transfer from transition-metal-doped LHP NCs. The surface-bound diamine requires two simultaneous photo-oxidation events for each reaction cycle. However, the separation of reaction products from NC catalysts is important for their further utilization.

Alternatively, a few studies have demonstrated the energy/electron transfer from LHP NCs to nonbinding molecules without having carboxylic, amine, or thiol groups.<sup>250,255,263,264,270,272,274,278,279</sup> The photoexcited energy of LHP NCs can either directly transfer to free molecules in solution<sup>255,263,264,270,272,279</sup> or via the molecules attached on the NC surface.<sup>250</sup> In these cases, the free molecules dynamically interact with the surfaces of the NCs and, thus, lead to an energy/electron transfer. This process has been explored to carry out triplet sensitization, organic reactions, and CO<sub>2</sub> reduction. For instance, Yuan et al.<sup>279</sup> reported photocatalytic oxidative dimerization of  $\alpha$ -aryl ketonitriles using CsPbBr<sub>3</sub> perovskite NCs, in which the reactant

molecules dynamically attach to the surfaces of NCs. In general, such photocatalytic C–C coupling reactions proceed through a radical-mediated reaction pathway.<sup>272,279</sup> Furthermore, the photoexcited charge carriers of CsPbBr<sub>3</sub> NCs have also been used to catalyze organic reactions with C–N and C–O bond formations from nonbinding reactant molecules.<sup>270</sup> Interestingly, small molecules that have either sulfur or oxygen or nitrogen atoms can efficiently extract the photoexcited electrons or holes from LHP NCs.<sup>264,286,287</sup> It is most likely that these atoms facilitate the adsorption of the molecules on the surface of LHP NCs. However, in-depth studies are needed to understand the interactions of different molecules on the surface of LHP NCs. Nevertheless, the native ligands (typically OAm and OA) strongly influence the excited-state interactions of LHP NCs with charge acceptor molecules. DuBose et al.<sup>274</sup> investigated the influence of the surface ligands of CsPbBr<sub>3</sub> NCs on the excited-state interactions with methyl viologen (MV<sup>2+</sup>) for three different ligands: typical OAm/OA pair, PbSO<sub>4</sub>–oleate, and DDAB. It was found that despite the relatively weak complexation of MV<sup>2+</sup> with the DDAB ligand environment, it exhibits the highest electron transfer efficiency of 73%.<sup>274</sup> Thus, it is important to note that the combination of the three factors, namely, surface binding strength, interfacial electron transfer rate, and stabilization of the charge transfer product, dictates the photocatalytic efficiency. In some cases, the ligands facilitate the charge transfer process by



**Table 2. Summary of Various Chiral LHP NCs Obtained Using Chiral Ligands in the Literature and Their Dissymmetry Factors, along with CD Signals<sup>a</sup>**

composition	CD signal intensity in mdeg	$g_{CD}$	$g_{lum}$	absorbance (wavelength range, nm)	ref
[( <i>R</i> )-2-octylamine] FAPbBr <sub>3</sub>			$6.8 \times 10^{-2}$	528–490	310
[( <i>S</i> )-MBA: Br]FAPbBr <sub>3</sub>			$1.18 \times 10^{-2}$	500–540	310
[( <i>R</i> )/( <i>S</i> )-PEA]MAPbBr <sub>3</sub>	100	$\sim 1.7 \times 10^{-3}$	$4.0 \times 10^{-3}$	$\sim 450$	311
[( <i>R</i> )- $\beta$ -MPEA]CsPbBr <sub>3</sub> NCs	–9	$\sim 0.15 \times 10^{-3}$		390	237
[( <i>S</i> )- $\alpha$ -PEA: I] CsPbBr <sub>3</sub> NCs	120	$\sim 2.6 \times 10^{-3}$		475	237
[( <i>S</i> )-MBA] CsPbBr <sub>3</sub> NCs		$\sim 5 \times 10^{-5}$		405	318
[( <i>S</i> )- $\alpha$ -octylamine] CsPbBr <sub>3</sub> NCs	5	$\sim 2.4 \times 10^{-4}$	$-1.0 \times 10^{-3}$	$\sim 508$	316
( <i>S</i> )- $\alpha$ -PEA-MAPbBr <sub>3</sub> NCs	3.5			$\sim 440$	325
<i>N,N'</i> -bis(octadecyl)-L-glutamic diamide (LGA <sub>m</sub> ) CsPbX <sub>3</sub>			$3 \times 10^{-3}$	410–585	291
CsPbBr <sub>3</sub> NCs–(L/R)-silica nanohelices	–230	$\sim 6.4 \times 10^{-3}$	$6.9 \times 10^{-3}$	368	292
( <i>R</i> )-DACH-CsPb(I/Br) <sub>3</sub> NCs	–240	$\sim 1.5 \times 10^{-3}$		247	319
[( <i>R</i> )-PEA]MAPbBr <sub>3</sub> NPLs	–10			432	312
[( <i>S</i> )-PEA]CsPbBr <sub>3</sub> NCs	35	$\sim 0.002$		474	317
( <i>S</i> )-MPEA NSs	60	$\sim 3.7 \times 10^{-3}$		399	315
[( <i>S</i> )-DMBA]MAPbBr <sub>3</sub> NPLs	300	$\sim 8.4 \times 10^{-3}$		430	290

<sup>a</sup>Note: The CD signal intensity also depends on the concentration, so it can't be compared in different literature. NSs, nanosheets; NPLs, nanoplatelets.

channeling the flow of charges to free molecules. The excited electrons/energy first transfer to surface-bound chromophores, which then transfer to acceptors in bulk solution.<sup>250,278</sup> This approach has been applied to achieve up-conversion emission through triplet sensitization,<sup>278</sup> as well as for *cis*–*trans* isomerization stilbene molecules and ring-closing organic reactions.<sup>250</sup> Furthermore, the energy transfer from LHP NCs to nearby emitters exhibits large Stokes-shifted emission, and this concept has been used for the realization of scintillators for  $\alpha$  particles and X-rays because they emit stable radioluminescence upon excitation.<sup>288</sup>

**Induced Chirality through Surface Ligands.** Recently, low-dimensional chiral perovskites have received significant research attention because of their interesting properties and technological applications, such as circular dichroism (CD), circularly polarized photoluminescence (CPL), nonlinear optical effects, 3D display, ferroelectricity, and spintronics, which has attracted the interest of numerous research studies.<sup>293–295</sup> The chirality in LHP NCs is generally induced through chiral ligands or through self-assembly into helical architectures using chiral templates.<sup>8,296,297</sup> The chiral ligands on LHP NCs allow access to chiroptical properties that cannot be achieved by achiral perovskites with a centrosymmetric structure. In 2003, Billing et al.<sup>298</sup> demonstrated the use of chiral molecules [methylbenzyl ammonium (MBA)] to crystallize organic–inorganic hybrid 1D [(*S*)-C<sub>6</sub>H<sub>5</sub>C<sub>2</sub>H<sub>4</sub>NH<sub>3</sub>]-[PbBr<sub>3</sub>] perovskites. However, it took until 2017 to study the chiroptical properties of 2D-layered [(*S*)-MBA]<sub>2</sub>PbI<sub>4</sub> and [(*R*)-MBA]<sub>2</sub>PbI<sub>4</sub> perovskites. The CD spectra of [(*S*)/(*R*)-MBA]<sub>2</sub>PbI<sub>4</sub>-layered perovskites exhibit oppositely signed peaks at their excitonic absorption, while the (*S*)/(*R*)-MBA alone does not show any CD signal at these wavelengths. After this work, numerous studies have been reported on the preparation of chiral LHPs by the incorporation of chiral organic cations such as (*S*)/(*R*)-MBA into the framework of layered iodide perovskites (Figure 12a),<sup>299–302</sup> in addition to the possibility of modulating the CD signal from 495 to 474 nm by varying the bandgap through control of the ratio of iodide and bromide.<sup>303</sup> The use of other chiral aromatic ligands such as (*S*)/(*R*)-1-(2-naphthyl)ethylamine [(*S*)/(*R*)-NEA] is also

effective in inducing chirality because of the interligand  $\pi$ -stacking interactions, which is also observed for (*S*)/(*R*)-MBA.<sup>303–306</sup> The versatility of this strategy has also been extended to obtain lead-free chiral perovskite thin films with considerable polarization anisotropy.<sup>307–309</sup>

Subsequently, the concept has been extended to obtain chiral LHP NCs that exhibit CPL.<sup>237,310–314</sup> Chiral LHP NCs have received increasing attention, and a number of reports have been published over the years (Table 2). In particular, numerous studies have been carried out inducing chirality in perovskite nanoplatelets (NPLs).<sup>312,313</sup> This is because the NPLs exhibit a higher surface-to-volume ratio that leads to a higher ligand density and, thus, they show a relatively high degree of chirality. Chiral perovskite NPLs or nanosheets can be prepared by a typical ligand-assisted reprecipitation approach using a mixture of chiral ligands [e.g. (*S*)/(*R*)-MBA-Br or methylphenethylammonium bromide (*S*)-MPEABr] with long chain ligands that help to stabilize the NPLs.<sup>312,315</sup> The CD spectra of NPLs exactly overlap with their extinction spectra that are controllable by the thickness. However, thickness-tunable colloidal chiral LHP NPLs have not yet been obtained. It is most likely that the degree of chirality reduces with increasing NPL thickness because of reduced chiral ligand density on the surface with respect to volume. Importantly, the ratio of chiral to achiral ligands plays an important role in the colloidal stability and the degree of chirality because of the competitive binding of the ligands. In general, reduced amounts of achiral ligands improve chirality; however, it affects the stability of NCs. By optimizing the amount of achiral and chiral ligands, Yan and co-workers<sup>315</sup> achieved a dissymmetry factor ( $g$ -factor) of  $6.5 \times 10^{-3}$  for 2D hybrid perovskite nanosheets. Very recently, Hubley et al.<sup>313</sup> demonstrated dissymmetry factors up to  $g_{lum} = 4.3 \times 10^{-3}$  and  $g_{abs} = 8.4 \times 10^{-3}$  for hybrid LHP NPLs synthesized by optimizing the mixture of chiral and achiral ligands. They found that too high or too low of a molar fraction of chiral to achiral ligands results in a decrease in the chiroptical signals because of the formation of polydisperse thicknesses and different ligand binding orientations. Moreover, small structural variations in chiral ligands significantly affect the

magnitude and sign of the CD signals, and the study found that dimethylbenzylammonium chiral ligands, along with achiral octylammonium ligands, were found to be efficient in yielding chiral NPLs with relatively high  $g$ -factors (Figure 12b).<sup>313</sup>

In addition, several attempts were made in inducing the chirality in bulklike LHP nanocubes using chiral ligands.<sup>237,310,316</sup> In this regard, Kim et al.<sup>310</sup> proposed both ligand-controlled synthesis and postsynthetic ligand exchange to obtain chiral FAPbBr<sub>3</sub> NCs using the short chiral ligands (*R*)-2-octylamine and (*S*)/(*R*)-MBA-Br. The anchoring of (*R*)-2-octylamine to FAPbBr<sub>3</sub> NCs results in chiral perovskite NCs that emit CPL with a relatively high luminescence dissymmetry ( $g_{\text{lum}}$ ) factor of  $6.8 \times 10^{-2}$ . However, the chiral FAPbBr<sub>3</sub> NCs obtained by postligand exchange with (*S*)/(*R*)-MBA-Br molecules exhibit a  $g_{\text{lum}}$  of  $\pm 1.18 \times 10^{-2}$ . The postsynthetic ligand exchange strategy has also been extended to obtain chiral quantum-confined LHP NCs with intense signals in circular dichroism using a variety of chiral ligands.<sup>317</sup> Despite significant progress in chiral LHP NCs, the origin of chirality is still not well understood. Luther and co-workers proposed that the chiral ligands anchored on the surface of LHP NCs induce centro-asymmetric distortion in the surface of the perovskite lattice, thereby leading to a chiroptical response.<sup>318</sup> In addition, it is noteworthy to mention the induced chirality in LHP NCs by self-assembly<sup>291,319,320</sup> or through the surface functionalization of achiral perovskites on chiral helical fibers (Figure 12c,d), where the surface chemistry plays an important role.<sup>292,320,321</sup> However, the  $g$ -factors reported for LHP NCs are considerably lower than reported for chiral plasmonic NCs. We refer the reader to the previous reviews for extensive information on chiral perovskite thin films and nanocrystals.<sup>296,322–324</sup>

## SUMMARY AND OUTLOOK

Over the last 8 years, LHP NCs have emerged at the forefront of colloidal semiconductor nanomaterials for various applications because of their interesting optical and optoelectronic properties. The rapid developments in the field regarding their preparation with controlled dimensions and composition have led to a greater understanding of their properties. They have already shown great promise as efficient light sources for LEDs, lasers, and single photon emission. In addition, they are gaining interest as light-harvesting materials for photocatalysis, as well as NC-based solar cells with improved long-term stability. Despite significant progress in the field, the poor stability of LHPs and their vulnerability toward antisolvent-induced purification is a major obstacle to advancing their applications. The aging of the colloidal NC solution or purification process often leads to the detachment of ligands because of weak ionic ligand–surface interactions. The ligand detachment leads to the formation of surface traps and, thus, significant reduction in PLQY. The surface traps can be passivated and, thus, can recover the photoluminescence by passivation with ligands that bind strongly to the NC surface.

Therefore, the type of ligands and their interaction with NC surfaces play a crucial role in the stability and PL efficiency of LHP NCs. This review discusses different ligands used for the stability of LHP NCs through in situ synthesis or postsynthetic surface passivation. Such ligands as alkyl quaternary ammonium cations, phosphine oxides, alkyl sulfonyl, thiols, and bidentate (zwitterionic) ligands have been exploited, and their interactions with NC surfaces have been discussed in this review. In particular, alkyl quaternary ammonium and

zwitterionic ligands have been proven to be excellent stabilizers of perovskite NCs toward long-term stability and maintaining high PLQY after purification. The ligands not only improve the stability but also induce new properties and functions in LHP NCs, depending on their type. For instance, chiral ligands induce chirality in LHP NCs either by intrinsic structural change or through self-assembly into chiral architectures. Different chiral ligands used to obtain colloidal LHP NCs through different synthesis strategies are discussed and rationalized in this review. In addition, the use of special ligands leads to photoexcited charge/electron transfer from perovskite NCs to nearby molecules that interact with NC surfaces. Such LHP NC–molecular systems have been explored for enhanced photocatalysis and chemical reactions, which are also discussed in this review.

Multidentate ligands that interact with several binding sites of the NC surface can be promising for strong surface passivation and high density of surface coverage.

Despite great progress in exploiting different ligands, there are still several outstanding challenges to be addressed for a better understanding of their interaction with the surface of LHP NCs. It is somewhat clear that the cationic ligands occupy the A cation sites, while the anionic ligands occupy the halide positions on the surface of NCs. However, different studies have proposed different kinds of ligand binding modes to the NC surface. Therefore, advanced characterization methods are needed for an atomic-level understanding of the surface chemistry of LHP NCs. In addition, new types of ligands are needed to be explored for further improvement in the stability of NCs. Especially, multidentate ligands that interact with several binding sites of the NC surface can be promising for strong surface passivation and high density of surface coverage. The ligands reported so far need to be rationalized in order to design new ligands on the basis of the current understanding of the ligand–NC interactions. Special attention needs to be focused on the design of ligands (e.g., conjugated multidentate ligands) that bind to NC surfaces strongly, as well as improve the interparticle charge transport in NC films. Furthermore, despite increasing attention in the preparation of chiral LHP NCs using chiral ligands, they exhibit poor stability and low dissymmetric factors. We think it would be interesting to explore chiral multidentate and polymer ligands in order to improve the long-term stability and dissymmetry factor of chiral LHP NCs. In addition, it is important to understand the chiral ligand structure and dissymmetric factor of the resulting colloidal NCs in order to design better ligands that induce strong chirality. Finally, there is a plenty of room for enhanced energy/charge transfer for enhanced light harvesting and driving chemical reactions by rationalizing the NC–molecular interactions and through the design of new molecules. We believe this review not only provides insights into ligands that improve colloidal stability but also guides the researcher to design new ligands for inducing new functions for LHP NCs.

## AUTHOR INFORMATION

### Corresponding Author

Lakshminarayana Polavarapu – CINBIO, Universidade de Vigo, Materials Chemistry and Physics Group, Department of Physical Chemistry, Campus Universitario Lagoas Marcosende, 36310 Vigo, Spain; [orcid.org/0000-0002-9040-5719](https://orcid.org/0000-0002-9040-5719); Email: [lakshmi@uvigo.es](mailto:lakshmi@uvigo.es)

### Authors

Nadesh Fiuza-Maneiro – CINBIO, Universidade de Vigo, Materials Chemistry and Physics Group, Department of Physical Chemistry, Campus Universitario Lagoas Marcosende, 36310 Vigo, Spain

Kun Sun – Lehrstuhl für Funktionelle Materialien, Physik-Department, Technische Universität München, 85748 Garching, Germany; [orcid.org/0000-0001-8960-0798](https://orcid.org/0000-0001-8960-0798)

Iago López-Fernández – CINBIO, Universidade de Vigo, Materials Chemistry and Physics Group, Department of Physical Chemistry, Campus Universitario Lagoas Marcosende, 36310 Vigo, Spain; [orcid.org/0000-0002-9920-6169](https://orcid.org/0000-0002-9920-6169)

Sergio Gómez-Graña – CINBIO, Universidade de Vigo, Materials Chemistry and Physics Group, Department of Physical Chemistry, Campus Universitario Lagoas Marcosende, 36310 Vigo, Spain; [orcid.org/0000-0002-7736-051X](https://orcid.org/0000-0002-7736-051X)

Peter Müller-Buschbaum – Lehrstuhl für Funktionelle Materialien, Physik-Department, Technische Universität München, 85748 Garching, Germany; Heinz Maier-Leibnitz Zentrum (MLZ), Technische Universität München, 85748 Garching, Germany; [orcid.org/0000-0002-9566-6088](https://orcid.org/0000-0002-9566-6088)

Complete contact information is available at:

<https://pubs.acs.org/10.1021/acseenergylett.2c02363>

### Notes

The authors declare no competing financial interest.

### Biographies

Nadesh Fiuza-Maneiro received her Master's Degree in Chemical Research and Industrial Chemistry from the University of Vigo in 2021. Currently, she is a Ph.D. candidate in the Materials Chemistry and Physics group. Her research interests are focused on the size and shape-controlled synthesis of chiral perovskites and the study of their self-assembly and optical properties.

Kun Sun is presently a Ph.D. student at the School of Natural Sciences, Technical University of Munich, under the supervision of Professor Peter Müller-Buschbaum. His current research is related to the growth of perovskite films and the degradation mechanisms of perovskite solar cells.

Iago López-Fernández obtained his Master's Degree from the University of Vigo and the University of Santiago. Currently, he is a Ph.D. student in the Materials Chemistry and Physics group, and his research is focused on the synthesis and modulation of doped perovskite nanoparticles for their use in LEDs, solar cells, and infrared detectors.

Sergio Gómez-Graña obtained his Ph.D. in Chemistry at the University of Vigo (2013). He is currently an assistant professor at the Department of Physical Chemistry of the University of Vigo. His current interest includes the synthesis and assembly of nanoparticles and their applications in sensing and catalysis.

Peter Müller-Buschbaum is full professor and the Chair of Functional Materials at the Technical University of Munich,

Germany. Moreover, he is the scientific director of the Munich neutron source FRM II and the Heinz Maier Leibnitz Zentrum MLZ. His research interests cover polymer and hybrid materials for energy and sensing applications.

Lakshminarayana Polavarapu is the Principal Investigator of the Materials Chemistry and Physics research group at the Centro de Investigaciones Biomedicas (CINBIO) and Ramón y Cajal fellow at the department of Physical Chemistry, University of Vigo. His research interests include shape-controlled synthesis and optical spectroscopy of plasmonic and semiconductor colloidal nanocrystals (<https://cinbio.es/en/MCPG>).

## ACKNOWLEDGMENTS

L.P. acknowledges the support from the Spanish Ministerio de Ciencia e Innovación through the Ramón y Cajal grant (RYC2018-026103-I) and the Spanish State Research Agency (Grant No. PID2020-117371RA-I00), as well as the grant from the Xunta de Galicia (ED431F2021/05). K.S. acknowledges the financial support from China Scholarship Council (CSC), and P.M.-B. acknowledges support from Deutsche Forschungsgemeinschaft (DFG, German Research Foundation) under Germany's Excellence Strategy – EXC 2089/1–390776260 (e-conversion). The authors acknowledge the Universidade de Vigo/CISUG for open access funding.

## REFERENCES

- (1) Brus, L. Electronic wave functions in semiconductor clusters: experiment and theory. *J. Phys. Chem.* **1986**, *90*, 2555.
- (2) Talapin, D. V.; Mekis, I.; Götzinger, S.; Kornowski, A.; Benson, O.; Weller, H. CdSe/CdS/ZnS and CdSe/ZnSe/ZnS Core–Shell–Shell Nanocrystals. *J. Phys. Chem. B* **2004**, *108*, 18826.
- (3) Alivisatos, A. P. Perspectives on the Physical Chemistry of Semiconductor Nanocrystals. *J. Phys. Chem.* **1996**, *100*, 13226.
- (4) Alivisatos, A. P. Semiconductor Clusters, Nanocrystals, and Quantum Dots. *Science* **1996**, *271*, 933.
- (5) Murray, C. B.; Norris, D. J.; Bawendi, M. G. Synthesis and characterization of nearly monodisperse CdE (E = sulfur, selenium, tellurium) semiconductor nanocrystallites. *J. Am. Chem. Soc.* **1993**, *115*, 8706.
- (6) Talapin, D. V.; Lee, J.-S.; Kovalenko, M. V.; Shevchenko, E. V. Prospects of Colloidal Nanocrystals for Electronic and Optoelectronic Applications. *Chem. Rev.* **2010**, *110*, 389.
- (7) Astruc, D. Introduction: Nanoparticles in Catalysis. *Chem. Rev.* **2020**, *120*, 461.
- (8) Dey, A.; Ye, J.; De, A.; Debroye, E.; Ha, S. K.; Bladt, E.; Kshirsagar, A. S.; Wang, Z.; Yin, J.; Wang, Y.; Quan, L. N.; Yan, F.; Gao, M.; Li, X.; Shamsi, J.; Debnath, T.; Cao, M.; Scheel, M. A.; Kumar, S.; Steele, J. A.; Gerhard, M.; Chouhan, L.; Xu, K.; Wu, X.-g.; Li, Y.; Zhang, Y.; Dutta, A.; Han, C.; Vincon, I.; Rogach, A. L.; Nag, A.; Samanta, A.; Korgel, B. A.; Shih, C.-J.; Gamelin, D. R.; Son, D. H.; Zeng, H.; Zhong, H.; Sun, H.; Demir, H. V.; Scheblykin, I. G.; Mora-Seró, I.; Stolarczyk, J. K.; Zhang, J. Z.; Feldmann, J.; Hofkens, J.; Luther, J. M.; Pérez-Prieto, J.; Li, L.; Manna, L.; Bodnarchuk, M. I.; Kovalenko, M. V.; Roeloffs, M. B. J.; Pradhan, N.; Mohammed, O. F.; Bakr, O. M.; Yang, P.; Müller-Buschbaum, P.; Kamat, P. V.; Bao, Q.; Zhang, Q.; Krahne, R.; Galian, R. E.; Stranks, S. D.; Bals, S.; Biju, V.; Tisdale, W. A.; Yan, Y.; Hoye, R. L. Z.; Polavarapu, L. State of the Art and Prospects for Halide Perovskite Nanocrystals. *ACS Nano* **2021**, *15*, 10775.
- (9) Burda, C.; Chen, X.; Narayanan, R.; El-Sayed, M. A. Chemistry and Properties of Nanocrystals of Different Shapes. *Chem. Rev.* **2005**, *105*, 1025.
- (10) Kagan, C. R.; Lifshitz, E.; Sargent, E. H.; Talapin, D. V. Building devices from colloidal quantum dots. *Science* **2016**, *353*, aac5523.



- (11) Lee, T. W.; Im, S. H.; Kim, Y. H.; Cho, H. *Perovskite nanocrystalline particles and optoelectronic device using same*. US 10193088 B2, 2019.
- (12) Peng, X.; Manna, L.; Yang, W.; Wickham, J.; Scher, E.; Kadavanich, A.; Alivisatos, A. P. Shape control of CdSe nanocrystals. *Nature* **2000**, *404*, 59.
- (13) Ramasamy, P.; Kim, N.; Kang, Y.-S.; Ramirez, O.; Lee, J.-S. Tunable, Bright, and Narrow-Band Luminescence from Colloidal Indium Phosphide Quantum Dots. *Chem. Mater.* **2017**, *29*, 6893.
- (14) Tessier, M. D.; Dupont, D.; De Nolf, K.; De Roo, J.; Hens, Z. Economic and Size-Tunable Synthesis of InP/ZnE (E = S, Se) Colloidal Quantum Dots. *Chem. Mater.* **2015**, *27*, 4893.
- (15) Kershaw, S. V.; Susha, A. S.; Rogach, A. L. Narrow bandgap colloidal metal chalcogenide quantum dots: synthetic methods, heterostructures, assemblies, electronic and infrared optical properties. *Chem. Soc. Rev.* **2013**, *42*, 3033.
- (16) Manser, J. S.; Christians, J. A.; Kamat, P. V. Intriguing optoelectronic properties of metal halide perovskites. *Chem. Rev.* **2016**, *116*, 12956.
- (17) Shamsi, J.; Urban, A. S.; Imran, M.; De Trizio, L.; Manna, L. Metal Halide Perovskite Nanocrystals: Synthesis, Post-Synthesis Modifications, and Their Optical Properties. *Chem. Rev.* **2019**, *119*, 3296.
- (18) Akkerman, Q. A.; Rainò, G.; Kovalenko, M. V.; Manna, L. Genesis, challenges and opportunities for colloidal lead halide perovskite nanocrystals. *Nat. Mater.* **2018**, *17*, 394.
- (19) Kovalenko, M. V.; Protesescu, L.; Bodnarchuk, M. I. Properties and potential optoelectronic applications of lead halide perovskite nanocrystals. *Science* **2017**, *358*, 745.
- (20) Ye, J.; Byrnavand, M. M.; Martinez, C. O.; Hoye, R. L. Z.; Saliba, M.; Polavarapu, L. Defect Passivation in Lead-Halide Perovskite Nanocrystals and Thin Films: Toward Efficient LEDs and Solar Cells. *Angew. Chem., Int. Ed.* **2021**, *60*, 21636.
- (21) Schmidt, L. C.; Pertegás, A.; González-Carrero, S.; Malinkiewicz, O.; Agouram, S.; Mínguez Espallargas, G.; Bolink, H. J.; Galian, R. E.; Pérez-Prieto, J. Nontemplate Synthesis of CH<sub>3</sub>NH<sub>3</sub>PbBr<sub>3</sub> Perovskite Nanoparticles. *J. Am. Chem. Soc.* **2014**, *136*, 850.
- (22) Zhang, F.; Zhong, H.; Chen, C.; Wu, X.-G.; Hu, X.; Huang, H.; Han, J.; Zou, B.; Dong, Y. Brightly Luminescent and Color-Tunable Colloidal CH<sub>3</sub>NH<sub>3</sub>PbX<sub>3</sub> (X = Br, I, Cl) Quantum Dots: Potential Alternatives for Display Technology. *ACS Nano* **2015**, *9*, 4533.
- (23) Protesescu, L.; Yakunin, S.; Bodnarchuk, M. I.; Krieg, F.; Caputo, R.; Hendon, C. H.; Yang, R. X.; Walsh, A.; Kovalenko, M. V. Nanocrystals of Cesium Lead Halide Perovskites (CsPbX<sub>3</sub>, X = Cl, Br, and I): Novel Optoelectronic Materials Showing Bright Emission with Wide Color Gamut. *Nano Lett.* **2015**, *15*, 3692.
- (24) Tong, Y.; Bladt, E.; Aygüer, M. F.; Manzi, A.; Milowska, K. Z.; Hintermayr, V. A.; Docampo, P.; Bals, S.; Urban, A. S.; Polavarapu, L.; Feldmann, J. Highly Luminescent Cesium Lead Halide Perovskite Nanocrystals with Tunable Composition and Thickness by Ultrasonication. *Angew. Chem., Int. Ed.* **2016**, *55*, 13887.
- (25) Song, J.; Li, J.; Li, X.; Xu, L.; Dong, Y.; Zeng, H. Quantum dot light-emitting diodes based on inorganic perovskite cesium lead halides (CsPbX<sub>3</sub>). *Adv. Mater.* **2015**, *27*, 7162.
- (26) Huang, H.; Bodnarchuk, M. I.; Kershaw, S. V.; Kovalenko, M. V.; Rogach, A. L. Lead Halide Perovskite Nanocrystals in the Research Spotlight: Stability and Defect Tolerance. *ACS Energy Lett.* **2017**, *2*, 2071.
- (27) Byrnavand, M. M.; Otero-Martínez, C.; Ye, J.; Zuo, W.; Manna, L.; Saliba, M.; Hoye, R. L. Z.; Polavarapu, L. Recent Progress in Mixed A-Site Cation Halide Perovskite Thin-Films and Nanocrystals for Solar Cells and Light-Emitting Diodes. *Adv. Opt. Mater.* **2022**, *10*, 2200423.
- (28) Li, X.; Wu, Y.; Zhang, S.; Cai, B.; Gu, Y.; Song, J.; Zeng, H. CsPbX<sub>3</sub> Quantum Dots for Lighting and Displays: Room-Temperature Synthesis, Photoluminescence Superiorities, Underlying Origins and White Light-Emitting Diodes. *Adv. Funct. Mater.* **2016**, *26*, 2435.
- (29) Otero-Martínez, C.; Ye, J.; Sung, J.; Pastoriza-Santos, I.; Pérez-Juste, J.; Xia, Z.; Rao, A.; Hoye, R. L. Z.; Polavarapu, L. Colloidal Metal-Halide Perovskite Nanoplatelets: Thickness-Controlled Synthesis, Properties, and Application in Light-Emitting Diodes. *Adv. Mater.* **2022**, *34*, 2107105.
- (30) Han, T.-H.; Jang, K. Y.; Dong, Y.; Friend, R. H.; Sargent, E. H.; Lee, T.-W. A roadmap for the commercialization of perovskite light emitters. *Nat. Rev. Mater.* **2022**, *7*, 757.
- (31) Tyagi, P.; Arveson, S. M.; Tisdale, W. A. Colloidal Organohalide Perovskite Nanoplatelets Exhibiting Quantum Confinement. *J. Phys. Chem. Lett.* **2015**, *6*, 1911.
- (32) Sichert, J. A.; Tong, Y.; Mutz, N.; Vollmer, M.; Fischer, S.; Milowska, K. Z.; García Cortadella, R.; Nickel, B.; Cardenas-Daw, C.; Stolarczyk, J. K.; Urban, A. S.; Feldmann, J. Quantum Size Effect in Organometal Halide Perovskite Nanoplatelets. *Nano Lett.* **2015**, *15*, 6521.
- (33) Swarnkar, A.; Marshall, A. R.; Sanehira, E. M.; Chernomordik, B. D.; Moore, D. T.; Christians, J. A.; Chakrabarti, T.; Luther, J. M. Quantum dot-induced phase stabilization of  $\alpha$ -CsPbI<sub>3</sub> perovskite for high-efficiency photovoltaics. *Science* **2016**, *354*, 92.
- (34) Hao, M.; Bai, Y.; Zeiske, S.; Ren, L.; Liu, J.; Yuan, Y.; Zarrabi, N.; Cheng, N.; Ghasemi, M.; Chen, P.; Lyu, M.; He, D.; Yun, J.-H.; Du, Y.; Wang, Y.; Ding, S.; Armin, A.; Meredith, P.; Liu, G.; Cheng, H.-M.; Wang, L. Ligand-assisted cation-exchange engineering for high-efficiency colloidal Cs<sub>1-x</sub>FA<sub>x</sub>PbI<sub>3</sub> quantum dot solar cells with reduced phase segregation. *Nat. Energy* **2020**, *5*, 79.
- (35) De Roo, J.; Ibáñez, M.; Geiregat, P.; Nedelcu, G.; Walravens, W.; Maes, J.; Martins, J. C.; Van Driessche, I.; Kovalenko, M. V.; Hens, Z. Highly Dynamic Ligand Binding and Light Absorption Coefficient of Cesium Lead Bromide Perovskite Nanocrystals. *ACS Nano* **2016**, *10*, 2071.
- (36) Yang, D.; Li, X.; Zeng, H. Surface Chemistry of All Inorganic Halide Perovskite Nanocrystals: Passivation Mechanism and Stability. *Adv. Mater. Interfaces* **2018**, *5*, 1701662.
- (37) Krieg, F.; Ochsenbein, S. T.; Yakunin, S.; Ten Brinck, S.; Aellen, P.; Suess, A.; Clerc, B.; Guggisberg, D.; Nazarenko, O.; Shynkarenko, Y.; Kumar, S.; Shih, C. J.; Infante, I.; Kovalenko, M. V. Colloidal CsPbX<sub>3</sub> (X = Cl, Br, I) Nanocrystals 2.0: Zwitterionic Capping Ligands for Improved Durability and Stability. *ACS Energy Lett.* **2018**, *3*, 641.
- (38) Bodnarchuk, M. I.; Boehme, S. C.; Ten Brinck, S.; Bernasconi, C.; Shynkarenko, Y.; Krieg, F.; Widmer, R.; Aeschlimann, B.; Gunther, D.; Kovalenko, M. V.; Infante, I. Rationalizing and Controlling the Surface Structure and Electronic Passivation of Cesium Lead Halide Nanocrystals. *ACS Energy Lett.* **2019**, *4*, 63.
- (39) Seth, S.; Ahmed, T.; De, A.; Samanta, A. Tackling the Defects, Stability, and Photoluminescence of CsPbX<sub>3</sub> Perovskite Nanocrystals. *ACS Energy Lett.* **2019**, *4*, 1610.
- (40) Xue, J.; Wang, R.; Yang, Y. The surface of halide perovskites from nano to bulk. *Nat. Rev. Mater.* **2020**, *5*, 809.
- (41) Boles, M. A.; Ling, D.; Hyeon, T.; Talapin, D. V. The Surface Science of Nanocrystals. *Nat. Mater.* **2016**, *15*, 141.
- (42) Deringer, V. L.; Dronskowski, R. From Atomistic Surface Chemistry to Nanocrystals of Functional Chalcogenides. *Angew. Chem., Int. Ed.* **2015**, *54*, 15334.
- (43) Rainò, G.; Becker, M. A.; Bodnarchuk, M. I.; Mahrt, R. F.; Kovalenko, M. V.; Stöferle, T. Superfluorescence From Lead Halide Perovskite Quantum Dot Superlattices. *Nature* **2018**, *563*, 671.
- (44) Tong, Y.; Yao, E.-P.; Manzi, A.; Bladt, E.; Wang, K.; Döblinger, M.; Bals, S.; Müller-Buschbaum, P.; Urban, A. S.; Polavarapu, L.; Feldmann, J. Spontaneous Self-Assembly of Perovskite Nanocrystals into Electronically Coupled Supercrystals: Toward Filling the Green Gap. *Adv. Mater.* **2018**, *30*, 1801117.
- (45) Chen, Y.; Smock, S. R.; Flintgruber, A. H.; Perras, F. A.; Brutchey, R. L.; Rossini, A. J. Surface Termination of CsPbBr<sub>3</sub> Perovskite Quantum Dots Determined by Solid-State NMR Spectroscopy. *J. Am. Chem. Soc.* **2020**, *142*, 6117.

- (46) Smock, S. R.; Chen, Y.; Rossini, A. J.; Brutchey, R. L. The Surface Chemistry and Structure of Colloidal Lead Halide Perovskite Nanocrystals. *Acc. Chem. Res.* **2021**, *54*, 707.
- (47) Imran, M.; Ijaz, P.; Goldoni, L.; Maggioni, D.; Petralanda, U.; Prato, M.; Almeida, G.; Infante, I.; Manna, L. Simultaneous Cationic and Anionic Ligand Exchange For Colloidally Stable CsPbBr<sub>3</sub> Nanocrystals. *ACS Energy Lett.* **2019**, *4*, 819.
- (48) Imran, M.; Ijaz, P.; Baranov, D.; Goldoni, L.; Petralanda, U.; Akkerman, Q.; Abdelhady, A. L.; Prato, M.; Bianchini, P.; Infante, I.; Manna, L. Shape-Pure, Nearly Monodispersed CsPbBr<sub>3</sub> Nanocubes Prepared Using Secondary Aliphatic Amines. *Nano Lett.* **2018**, *18*, 7822.
- (49) Zaccaria, F.; Zhang, B.; Goldoni, L.; Imran, M.; Zito, J.; van Beek, B.; Lauciello, S.; De Trizio, L.; Manna, L.; Infante, I. The Reactivity of CsPbBr<sub>3</sub> Nanocrystals toward Acid/Base Ligands. *ACS Nano* **2022**, *16*, 1444.
- (50) Ye, J.; Li, Z.; Kubicki, D. J.; Zhang, Y.; Dai, L.; Otero-Martínez, C.; Reus, M. A.; Arul, R.; Dudipala, K. R.; Andaji-Garmaroudi, Z.; Huang, Y.-T.; Li, Z.; Chen, Z.; Müller-Buschbaum, P.; Yip, H.-L.; Stranks, S. D.; Grey, C. P.; Baumberg, J. J.; Greenham, N. C.; Polavarapu, L.; Rao, A.; Hoyer, R. L. Z. Elucidating the Role of Antisolvents on the Surface Chemistry and Optoelectronic Properties of CsPbBr<sub>3-x</sub>I<sub>3-x</sub> Perovskite Nanocrystals. *J. Am. Chem. Soc.* **2022**, *144*, 12102.
- (51) Ravi, V. K.; Santra, P. K.; Joshi, N.; Chugh, J.; Singh, S. K.; Rensmo, H.; Ghosh, P.; Nag, A. Origin of the Substitution Mechanism for the Binding of Organic Ligands on the Surface of CsPbBr<sub>3</sub> Perovskite Nanocubes. *J. Phys. Chem. Lett.* **2017**, *8*, 4988.
- (52) Bodnarchuk, M. I.; Boehme, S. C.; Ten Brinck, S.; Bernasconi, C.; Shynkarenko, Y.; Krieg, F.; Widmer, R.; Aeschlimann, B.; Gunther, D.; Kovalenko, M. V.; Infante, I. Rationalizing and Controlling the Surface Structure and Electronic Passivation of Cesium Lead Halide Nanocrystals. *ACS Energy Lett.* **2019**, *4*, 63.
- (53) Chen, Y.; Smock, S. R.; Flintgruber, A. H.; Perras, F. A.; Brutchey, R. L.; Rossini, A. J. Surface Termination of CsPbBr<sub>3</sub> Perovskite Quantum Dots Determined by Solid-State NMR Spectroscopy. *J. Am. Chem. Soc.* **2020**, *142*, 6117.
- (54) Karmakar, A.; Dodd, M. S.; Zhang, X.; Oakley, M. S.; Klobukowski, M.; Michaelis, V. K. Mechanochemical synthesis of 0D and 3D cesium lead mixed halide perovskites. *Chem. Commun.* **2019**, *55*, 5079.
- (55) Rosales, B. A.; Men, L.; Cady, S. D.; Hanrahan, M. P.; Rossini, A. J.; Vela, J. Persistent dopants and phase segregation in organolead mixed-halide perovskites. *Chem. Mater.* **2016**, *28*, 6848.
- (56) Hanrahan, M. P.; Men, L.; Rosales, B. A.; Vela, J.; Rossini, A. J. Sensitivity-enhanced 207Pb solid-state NMR spectroscopy for the rapid, non-destructive characterization of organolead halide perovskites. *Chem. Mater.* **2018**, *30*, 7005.
- (57) Bertolotti, F.; Nedelcu, G.; Vivani, A.; Cervellino, A.; Masciocchi, N.; Guagliardi, A.; Kovalenko, M. V. Crystal Structure, Morphology, and Surface Termination of Cyan-Emissive, Six-Monolayers-Thick CsPbBr<sub>3</sub> Nanoplatelets from X-ray Total Scattering. *ACS Nano* **2019**, *13*, 14294.
- (58) Toso, S.; Baranov, D.; Giannini, C.; Manna, L. Structure and Surface Passivation of Ultrathin Cesium Lead Halide Nanoplatelets Revealed by Multilayer Diffraction. *ACS Nano* **2021**, *15*, 20341.
- (59) Zhou, Y.; Sternlicht, H.; Padture, N. P. Transmission electron microscopy of halide perovskite materials and devices. *Joule* **2019**, *3*, 641.
- (60) Ran, J.; Dyck, O.; Wang, X.; Yang, B.; Geohegan, D. B.; Xiao, K. Electron-Beam-Related Studies of Halide Perovskites: Challenges and Opportunities. *Adv. Energy Mater.* **2020**, *10*, 1903191.
- (61) Dang, Z.; Shamsi, J.; Palazon, F.; Imran, M.; Akkerman, Q. A.; Park, S.; Bertoni, G.; Prato, M.; Brescia, R.; Manna, L. In situ Transmission Electron Microscopy Study of Electron Beam-Induced Transformations in Colloidal Cesium Lead Halide Perovskite Nanocrystals. *ACS Nano* **2017**, *11*, 2124.
- (62) Schlipf, J.; Müller-Buschbaum, P. Structure of organometal halide perovskite films as determined with grazing-incidence x-ray scattering methods. *Adv. Energy Mater.* **2017**, *7*, 1700131.
- (63) du Fossé, I.; Mulder, J. T.; Almeida, G.; Spruit, A. G. M.; Infante, I.; Grozema, F. C.; Houtepen, A. J. Limits of Defect Tolerance in Perovskite Nanocrystals: Effect of Local Electrostatic Potential on Trap States. *J. Am. Chem. Soc.* **2022**, *144*, 11059.
- (64) Bohn, B. J.; Tong, Y.; Gramlich, M.; Lai, M. L.; Döblinger, M.; Wang, K.; Hoyer, R. L. Z.; Müller-Buschbaum, P.; Stranks, S. D.; Urban, A. S.; Polavarapu, L.; Feldmann, J. Boosting Tunable Blue Luminescence of Halide Perovskite Nanoplatelets through Post-synthetic Surface Trap Repair. *Nano Lett.* **2018**, *18*, 5231.
- (65) Meggiolaro, D.; Mosconi, E.; De Angelis, F. Formation of Surface Defects Dominates Ion Migration in Lead-Halide Perovskites. *ACS Energy Lett.* **2019**, *4*, 779.
- (66) ten Brinck, S.; Zaccaria, F.; Infante, I. Defects in Lead Halide Perovskite Nanocrystals: Analogies and (Many) Differences with the Bulk. *ACS Energy Lett.* **2019**, *4*, 2739.
- (67) Swarnkar, A.; Ravi, V. K.; Nag, A. Beyond Colloidal Cesium Lead Halide Perovskite Nanocrystals: Analogous Metal Halides and Doping. *ACS Energy Lett.* **2017**, *2*, 1089.
- (68) Shen, X.; Zhang, Y.; Kershaw, S. V.; Li, T.; Wang, C.; Zhang, X.; Wang, W.; Li, D.; Wang, Y.; Lu, M.; Zhang, L.; Sun, C.; Zhao, D.; Qin, G.; Bai, X.; Yu, W. W.; Rogach, A. L. Zn-Alloyed CsPbI<sub>3</sub> Nanocrystals for Highly Efficient Perovskite Light-Emitting Devices. *Nano Lett.* **2019**, *19*, 1552.
- (69) Brandt, R. E.; Stevanović, V.; Ginley, D. S.; Buonassisi, T. Identifying defect-tolerant semiconductors with high minority-carrier lifetimes: beyond hybrid lead halide perovskites. *MRS Commun.* **2015**, *5*, 265.
- (70) Brandt, R. E.; Poindexter, J. R.; Gorai, P.; Kurchin, R. C.; Hoyer, R. L.; Nienhaus, L.; Wilson, M. W.; Polizzotti, J. A.; Sereika, R.; Zaltauskas, R.; et al. Searching for “defect-tolerant” Photovoltaic Materials: Combined Theoretical and Experimental Screening. *Chem. Mater.* **2017**, *29*, 4667.
- (71) Li, Y.; Zhang, C.; Zhang, X.; Huang, D.; Shen, Q.; Cheng, Y.; Huang, W. Intrinsic point defects in inorganic perovskite CsPbI<sub>3</sub> from first-principles prediction. *Appl. Phys. Lett.* **2017**, *111*, 162106.
- (72) Kim, J.; Chung, C.-H.; Hong, K.-H. Understanding of the formation of shallow level defects from the intrinsic defects of lead trihalide perovskites. *Phys. Chem. Chem. Phys.* **2016**, *18*, 27143.
- (73) Buin, A.; Comin, R.; Xu, J.; Ip, A. H.; Sargent, E. H. Halide-Dependent Electronic Structure of Organolead Perovskite Materials. *Chem. Mater.* **2015**, *27*, 4405.
- (74) Nenon, D. P.; Pressler, K.; Kang, J.; Koscher, B. A.; Olshansky, J. H.; Osowiecki, W. T.; Koc, M. A.; Wang, L.-W.; Alivisatos, A. P. Design Principles for Trap-Free CsPbX<sub>3</sub> Nanocrystals: Enumerating and Eliminating Surface Halide Vacancies with Softer Lewis Bases. *J. Am. Chem. Soc.* **2018**, *140*, 17760.
- (75) Otero-Martínez, C.; García-Lojo, D.; Pastoriza-Santos, I.; Pérez-Juste, J.; Polavarapu, L. Dimensionality Control of Inorganic and Hybrid Perovskite Nanocrystals by Reaction Temperature: From No-Confinement to 3D and 1D Quantum Confinement. *Angew. Chem., Int. Ed.* **2021**, *60*, 26677.
- (76) Hills-Kimball, K.; Yang, H.; Cai, T.; Wang, J.; Chen, O. Recent Advances in Ligand Design and Engineering in Lead Halide Perovskite Nanocrystals. *Adv. Sci.* **2021**, *8*, 2100214.
- (77) Zhang, Y.; Siegler, T. D.; Thomas, C. J.; Abney, M. K.; Shah, T.; De Gorostiza, A.; Greene, R. M.; Korgel, B. A. A “Tips and Tricks” Practical Guide to the Synthesis of Metal Halide Perovskite Nanocrystals. *Chem. Mater.* **2020**, *32*, 5410.
- (78) Otero-Martínez, C.; Fiuza-Maneiro, N.; Polavarapu, L. Enhancing the Intrinsic and Extrinsic Stability of Halide Perovskite Nanocrystals for Efficient and Durable Optoelectronics. *ACS Appl. Mater. Interfaces* **2022**, *14*, 34291.
- (79) Haydous, F.; Gardner, J. M.; Cappel, U. B. The impact of ligands on the synthesis and application of metal halide perovskite nanocrystals. *J. Mater. Chem. A* **2021**, *9*, 23419.



- (80) Park, J.; Jang, H. M.; Kim, S.; Jo, S. H.; Lee, T.-W. Electroluminescence of Perovskite Nanocrystals with Ligand Engineering. *Trends Chem.* **2020**, *2*, 837.
- (81) Sun, W.; Yun, R.; Liu, Y.; Zhang, X.; Yuan, M.; Zhang, L.; Li, X. Ligands in Lead Halide Perovskite Nanocrystals: From Synthesis to Optoelectronic Applications. *Small* **2022**, 2205950.
- (82) Mourdikoudis, S.; Menelaou, M.; Fiuzza-Maneiro, N.; Zheng, G.; Wei, S.; Pérez-Juste, J.; Polavarapu, L.; Sofer, Z. Oleic acid/oleylamine ligand pair: a versatile combination in the synthesis of colloidal nanoparticles. *Nanoscale Horiz.* **2022**, *7*, 941.
- (83) Almeida, G.; Goldoni, L.; Akkerman, Q.; Dang, Z.; Khan, A. H.; Marras, S.; Moreels, I.; Manna, L. Role of Acid–Base Equilibria in the Size, Shape, and Phase Control of Cesium Lead Bromide Nanocrystals. *ACS Nano* **2018**, *12*, 1704.
- (84) Huang, H.; Li, Y.; Tong, Y.; Yao, E.-P.; Feil, M. W.; Richter, A. F.; Döblinger, M.; Rogach, A. L.; Feldmann, J.; Polavarapu, L. Spontaneous Crystallization of Perovskite Nanocrystals in Nonpolar Organic Solvents: A Versatile Approach for their Shape-Controlled Synthesis. *Angew. Chem., Int. Ed.* **2019**, *58*, 16558.
- (85) Sun, S.; Yuan, D.; Xu, Y.; Wang, A.; Deng, Z. Ligand-Mediated Synthesis of Shape-Controlled Cesium Lead Halide Perovskite Nanocrystals via Reprecipitation Process at Room Temperature. *ACS Nano* **2016**, *10*, 3648.
- (86) Bai, Y.; Hao, M.; Ding, S.; Chen, P.; Wang, L. Surface Chemistry Engineering of Perovskite Quantum Dots: Strategies, Applications, and Perspectives. *Adv. Mater.* **2022**, *34*, 2105958.
- (87) Smock, S. R.; Chen, Y.; Rossini, A. J.; Brutchey, R. L. The Surface Chemistry and Structure of Colloidal Lead Halide Perovskite Nanocrystals. *Acc. Chem. Res.* **2021**, *54*, 707.
- (88) Smock, S. R.; Williams, T. J.; Brutchey, R. L. Quantifying the Thermodynamics of Ligand Binding to CsPbBr<sub>3</sub> Quantum Dots. *Angew. Chem., Int. Ed.* **2018**, *57*, 11711.
- (89) ten Brinck, S.; Infante, I. Surface Termination, Morphology, and Bright Photoluminescence of Cesium Lead Halide Perovskite Nanocrystals. *ACS Energy Lett.* **2016**, *1*, 1266.
- (90) Kim, Y.-H.; Kim, S.; Kakekhani, A.; Park, J.; Park, J.; Lee, Y.-H.; Xu, H.; Nagane, S.; Wexler, R. B.; Kim, D.-H.; Jo, S. H.; Martínez-Sarti, L.; Tan, P.; Sadhanala, A.; Park, G.-S.; Kim, Y.-W.; Hu, B.; Bolink, H. J.; Yoo, S.; Friend, R. H.; Rappe, A. M.; Lee, T.-W. Comprehensive defect suppression in perovskite nanocrystals for high-efficiency light-emitting diodes. *Nat. Photonics* **2021**, *15*, 148.
- (91) Yoo, D.; Woo, J. Y.; Kim, Y.; Kim, S. W.; Wei, S.-H.; Jeong, S.; Kim, Y.-H. Origin of the Stability and Transition from Anionic to Cationic Surface Ligand Passivation of All-Inorganic Cesium Lead Halide Perovskite Nanocrystals. *J. Phys. Chem. Lett.* **2020**, *11*, 652.
- (92) Yang, F.; Chen, H.; Zhang, R.; Liu, X.; Zhang, W.; Zhang, J.; Gao, F.; Wang, L. Efficient and Spectrally Stable Blue Perovskite Light-Emitting Diodes Based on Potassium Passivated Nanocrystals. **2020**, *30*, 1908760.
- (93) Lu, M.; Guo, J.; Lu, P.; Zhang, L.; Zhang, Y.; Dai, Q.; Hu, Y.; Colvin, V. L.; Yu, W. W. Ammonium Thiocyanate-Passivated CsPbI<sub>3</sub> Perovskite Nanocrystals for Efficient Red Light-Emitting Diodes. *J. Phys. Chem. C* **2019**, *123*, 22787.
- (94) Woo, J. Y.; Kim, Y.; Bae, J.; Kim, T. G.; Kim, J. W.; Lee, D. C.; Jeong, S. Highly Stable Cesium Lead Halide Perovskite Nanocrystals through in Situ Lead Halide Inorganic Passivation. *Chem. Mater.* **2017**, *29*, 7088.
- (95) Chen, J.-K.; Ma, J.-P.; Guo, S.-Q.; Chen, Y.-M.; Zhao, Q.; Zhang, B.-B.; Li, Z.-Y.; Zhou, Y.; Hou, J.; Kuroiwa, Y.; Moriyoshi, C.; Bakr, O. M.; Zhang, J.; Sun, H.-T. High-Efficiency Violet-Emitting All-Inorganic Perovskite Nanocrystals Enabled by Alkaline-Earth Metal Passivation. *Chem. Mater.* **2019**, *31*, 3974.
- (96) Xiao, X.; Li, Y.; Xie, R.-J. Blue-emitting and Self-assembled Thinner Perovskite CsPbBr<sub>3</sub> Nanoplates: Synthesis and Formation Mechanism. *Nanoscale* **2020**, *12*, 9231.
- (97) Yang, J.-N.; Song, Y.; Yao, J.-S.; Wang, K.-H.; Wang, J.-J.; Zhu, B.-S.; Yao, M.-M.; Rahman, S. U.; Lan, Y.-F.; Fan, F.-J.; Yao, H.-B. Potassium Bromide Surface Passivation on CsPbI<sub>3-x</sub>Br<sub>x</sub> Nanocrystals for Efficient and Stable Pure Red Perovskite Light-Emitting Diodes. *J. Am. Chem. Soc.* **2020**, *142*, 2956.
- (98) Bonato, L. G.; Moral, R. F.; Nagamine, G.; Alo, A.; Germino, J. C.; da Silva, D. S.; Almeida, D. B.; Zagonel, L. F.; Galembeck, F.; Padilha, L. A.; et al. Revealing the Role of Tin (IV) Halides in the Anisotropic Growth of CsPbX<sub>3</sub> Perovskite Nanoplates. *Angew. Chem., Int. Ed.* **2020**, *59*, 11501.
- (99) Li, F.; Liu, Y.; Wang, H.; Zhan, Q.; Liu, Q.; Xia, Z. Postsynthetic surface trap removal of CsPbX<sub>3</sub> (X = Cl, Br, or I) quantum dots via a ZnX<sub>2</sub>/hexane solution toward an enhanced luminescence quantum yield. *Chem. Mater.* **2018**, *30*, 8546.
- (100) Di Stasio, F.; Christodoulou, S.; Huo, N.; Konstantatos, G. Near-unity photoluminescence quantum yield in CsPbBr<sub>3</sub> nanocrystal solid-state films via postsynthesis treatment with lead bromide. *Chem. Mater.* **2017**, *29*, 7663.
- (101) Li, H.; Qian, Y.; Xing, X.; Zhu, J.; Huang, X.; Jing, Q.; Zhang, W.; Zhang, C.; Lu, Z. Enhancing luminescence and photostability of CsPbBr<sub>3</sub> nanocrystals via surface passivation with silver complex. *J. Phys. Chem. C* **2018**, *122*, 12994.
- (102) Woo, J. Y.; Kim, Y.; Bae, J.; Kim, T. G.; Kim, J. W.; Lee, D. C.; Jeong, S. Highly stable cesium lead halide perovskite nanocrystals through in situ lead halide inorganic passivation. *Chem. Mater.* **2017**, *29*, 7088.
- (103) Zhong, Q.; Cao, M.; Xu, Y.; Li, P.; Zhang, Y.; Hu, H.; Yang, D.; Xu, Y.; Wang, L.; Li, Y.; Zhang, X.; Zhang, Q. L-Type Ligand-Assisted Acid-Free Synthesis of CsPbBr<sub>3</sub> Nanocrystals with Near-Unity Photoluminescence Quantum Yield and High Stability. *Nano Lett.* **2019**, *19*, 4151.
- (104) Yassitepe, E.; Yang, Z.; Voznyy, O.; Kim, Y.; Walters, G.; Castañeda, J. A.; Kanjanaboos, P.; Yuan, M.; Gong, X.; Fan, F.; Pan, J.; Hoogland, S.; Comin, R.; Bakr, O. M.; Padilha, L. A.; Nogueira, A. F.; Sargent, E. H. Amine-Free Synthesis of Cesium Lead Halide Perovskite Quantum Dots for Efficient Light-Emitting Diodes. *Adv. Funct. Mater.* **2016**, *26*, 8757.
- (105) Pan, J.; Quan, L. N.; Zhao, Y.; Peng, W.; Murali, B.; Sarmah, S. P.; Yuan, M.; Sinatra, L.; Alyami, N. M.; Liu, J.; Yassitepe, E.; Yang, Z.; Voznyy, O.; Comin, R.; Hedhili, M. N.; Mohammed, O. F.; Lu, Z. H.; Kim, D. H.; Sargent, E. H.; Bakr, O. M. Highly Efficient Perovskite-Quantum-Dot Light-Emitting Diodes by Surface Engineering. *Adv. Mater.* **2016**, *28*, 8718.
- (106) Zhang, B.; Goldoni, L.; Zito, J.; Dang, Z.; Almeida, G.; Zaccaria, F.; de Wit, J.; Infante, I.; De Trizio, L.; Manna, L. Alkyl Phosphonic Acids Deliver CsPbBr<sub>3</sub> Nanocrystals with High Photoluminescence Quantum Yield and Truncated Octahedron Shape. *Chem. Mater.* **2019**, *31*, 9140.
- (107) Shamsi, J.; Kubicki, D.; Anaya, M.; Liu, Y.; Ji, K.; Frohna, K.; Grey, C. P.; Friend, R. H.; Stranks, S. D. Stable Hexylphosphonate-Capped Blue-Emitting Quantum-Confined CsPbBr<sub>3</sub> Nanoplatelets. *ACS Energy Lett.* **2020**, *5*, 1900.
- (108) Tan, Y.; Zou, Y.; Wu, L.; Huang, Q.; Yang, D.; Chen, M.; Ban, M.; Wu, C.; Wu, T.; Bai, S.; Song, T.; Zhang, Q.; Sun, B. Highly Luminescent and Stable Perovskite Nanocrystals with Octylphosphonic Acid as a Ligand for Efficient Light-Emitting Diodes. *ACS Appl. Mater. Interfaces* **2018**, *10*, 3784.
- (109) Zhang, B.; Goldoni, L.; Lambroschini, C.; Moni, L.; Imran, M.; Pianetti, A.; Pinchetti, V.; Brovelli, S.; De Trizio, L.; Manna, L. Stable and Size Tunable CsPbBr<sub>3</sub> Nanocrystals Synthesized with Oleylphosphonic Acid. *Nano Lett.* **2020**, *20*, 8847.
- (110) Li, Y.; Wang, X.; Xue, W.; Wang, W.; Zhu, W.; Zhao, L. Highly Luminescent and Stable CsPbBr<sub>3</sub> Perovskite Quantum Dots Modified by Phosphine Ligands. *Nano Res.* **2019**, *12*, 785.
- (111) Woo, J. Y.; Lee, S.; Lee, S.; Kim, W. D.; Lee, K.; Kim, K.; An, H. J.; Lee, D. C.; Jeong, S. Air-stable PbSe Nanocrystals Passivated by Phosphonic Acids. *J. Am. Chem. Soc.* **2016**, *138*, 876.
- (112) Owen, J. S.; Park, J.; Trudeau, P.-E.; Alivisatos, A. P. Reaction chemistry and ligand exchange at cadmium–selenide nanocrystal surfaces. *J. Am. Chem. Soc.* **2008**, *130*, 12279.
- (113) Liu, F.; Zhang, Y.; Ding, C.; Kobayashi, S.; Izuishi, T.; Nakazawa, N.; Toyoda, T.; Ohta, T.; Hayase, S.; Minemoto, T.;

- Yoshino, K.; Dai, S.; Shen, Q. Highly Luminescent Phase-Stable CsPbI<sub>3</sub> Perovskite Quantum Dots Achieving Near 100% Absolute Photoluminescence Quantum Yield. *ACS Nano* **2017**, *11*, 10373.
- (114) Wu, L.; Zhong, Q.; Yang, D.; Chen, M.; Hu, H.; Pan, Q.; Liu, H.; Cao, M.; Xu, Y.; Sun, B.; et al. Improving the Stability and Size Tunability of Cesium Lead Halide Perovskite Nanocrystals Using Trioctylphosphine Oxide as the Capping Ligand. *Langmuir* **2017**, *33*, 12689.
- (115) Almeida, G.; Ashton, O. J.; Goldoni, L.; Maggioni, D.; Petralanda, U.; Mishra, N.; Akkerman, Q. A.; Infante, I.; Snaith, H. J.; Manna, L. The Phosphine Oxide Route toward Lead Halide Perovskite Nanocrystals. *J. Am. Chem. Soc.* **2018**, *140*, 14878.
- (116) Zeldin, M.; Mehta, P.; Vernon, W. D. J. I. C. Phosphorus-<sup>31</sup>NMR of Triphenylphosphine Oxide Complexes with Compounds of Silicon, Germanium, and Tin. *Inorg. Chem.* **1979**, *18*, 463.
- (117) Gomes, R.; Hassinen, A.; Szczygiel, A.; Zhao, Q.; Vantomme, A.; Martins, J. C.; Hens, Z. Binding of phosphonic acids to CdSe quantum dots: a solution NMR study. *J. Phys. Chem. Lett.* **2011**, *2*, 145.
- (118) Brown, A. A.; Hooper, T. J.; Veldhuis, S. A.; Chin, X. Y.; Bruno, A.; Vashishtha, P.; Tey, J. N.; Jiang, L.; Damodaran, B.; Pu, S. H.; et al. Self-assembly of a Robust Hydrogen-bonded Octylphosphonate Network on Cesium Lead Bromide Perovskite Nanocrystals for Light-Emitting Diodes. *Nanoscale* **2019**, *11*, 12370.
- (119) Cadars, S.; Smith, B.; Epping, J.; Acharya, S.; Belman, N.; Golan, Y.; Chmelka, B. Atomic Positional versus Electronic order in Semiconducting ZnSe Nanoparticles. *Phys. Rev. Lett.* **2009**, *103*, 136802.
- (120) Piveteau, L.; Ong, T.-C.; Rossini, A. J.; Emsley, L.; Coperet, C.; Kovalenko, M. Structure of colloidal quantum dots from dynamic nuclear polarization surface enhanced NMR spectroscopy. *J. Am. Chem. Soc.* **2015**, *137*, 13964.
- (121) Koscher, B. A.; Swabeck, J. K.; Bronstein, N. D.; Alivisatos, A. P. Essentially Trap-Free CsPbBr<sub>3</sub> Colloidal Nanocrystals by Postsynthetic Thiocyanate Surface Treatment. *J. Am. Chem. Soc.* **2017**, *139*, 6566.
- (122) Yang, D.; Li, X.; Zhou, W.; Zhang, S.; Meng, C.; Wu, Y.; Wang, Y.; Zeng, H. CsPbBr<sub>3</sub> Quantum Dots 2.0: Benzenesulfonic Acid Equivalent Ligand Awakens Complete Purification. *Adv. Mater.* **2019**, *31*, e1900767.
- (123) Ruan, L.; Shen, W.; Wang, A.; Zhou, Q.; Zhang, H.; Deng, Z. Stable and conductive lead halide perovskites facilitated by X-type ligands. *Nanoscale* **2017**, *9*, 7252.
- (124) Uddin, M. A.; Mobley, J. K.; Masud, A. A.; Liu, T.; Calabro, R. L.; Kim, D.-Y.; Richards, C. I.; Graham, K. R. Mechanistic Exploration of Dodecanethiol-Treated Colloidal CsPbBr<sub>3</sub> Nanocrystals with Photoluminescence Quantum Yields Reaching Near 100%. *J. Phys. Chem. C* **2019**, *123*, 18103.
- (125) Cai, T.; Li, F.; Jiang, Y.; Liu, X.; Xia, X.; Wang, X.; Peng, J.; Wang, L.; Daoud, W. A. In situ Inclusion of Thiocyanate for Highly Luminescent and Stable CH<sub>3</sub>NH<sub>3</sub>PbBr<sub>3</sub> Perovskite Nanocrystals. *Nanoscale* **2019**, *11*, 1319.
- (126) Fafarman, A. T.; Koh, W.-k.; Diroll, B. T.; Kim, D. K.; Ko, D.-K.; Oh, S. J.; Ye, X.; Doan-Nguyen, V.; Crump, M. R.; Reifsnnyder, D. C.; et al. Thiocyanate-capped Nanocrystal Colloids: Vibrational Reporter of Surface Chemistry and Solution-based Route to Enhanced Coupling in Nanocrystal Solids. *J. Am. Chem. Soc.* **2011**, *133*, 15753.
- (127) Pan, J.; Sarmah, S. P.; Murali, B.; Dursun, I.; Peng, W.; Parida, M. R.; Liu, J.; Sinatra, L.; Alyami, N.; Zhao, C.; Alarousu, E.; Ng, T. K.; Ooi, B. S.; Bakr, O. M.; Mohammed, O. F. Air-Stable Surface-Passivated Perovskite Quantum Dots for Ultra-Robust, Single- and Two-Photon-Induced Amplified Spontaneous Emission. *J. Phys. Chem. Lett.* **2015**, *6*, 5027.
- (128) Pan, J.; Li, X.; Gong, X.; Yin, J.; Zhou, D.; Sinatra, L.; Huang, R.; Liu, J.; Chen, J.; Dursun, I.; El-Zohry, A. M.; Saidaminov, M. I.; Sun, H.-T.; Mohammed, O. F.; Ye, C.; Sargent, E. H.; Bakr, O. M. Halogen Vacancies Enable Ligand-Assisted Self-Assembly of Perovskite Quantum Dots into Nanowires. *Angew. Chem., Int. Ed.* **2019**, *58*, 16077.
- (129) Yang, D.; Li, X.; Zhou, W.; Zhang, S.; Meng, C.; Wu, Y.; Wang, Y.; Zeng, H. CsPbBr<sub>3</sub> Quantum Dots 2.0: Benzenesulfonic Acid Equivalent Ligand Awakens Complete Purification. *Adv. Mater.* **2019**, *31*, 1900767.
- (130) Kang, J.; Wang, L.-W. High defect tolerance in lead halide perovskite CsPbBr<sub>3</sub>. *J. Phys. Chem. Lett.* **2017**, *8*, 489.
- (131) Wu, Y.; Wei, C.; Li, X.; Li, Y.; Qiu, S.; Shen, W.; Cai, B.; Sun, Z.; Yang, D.; Deng, Z.; et al. In Situ Passivation of PbBr<sub>6</sub><sup>4-</sup> Octahedra Toward Blue Luminescent CsPbBr<sub>3</sub> Nanoplatelets with Near 100% Absolute Quantum Yield. *ACS Energy Lett.* **2018**, *3*, 2030.
- (132) Kim, Y.; Yassitepe, E.; Voznyy, O.; Comin, R.; Walters, G.; Gong, X.; Kanjanaboos, P.; Nogueira, A. F.; Sargent, E. H. Interfaces. Efficient luminescence from perovskite quantum dot solids. *ACS Appl. Mater. Interfaces* **2015**, *7*, 25007.
- (133) Biju, V. Chemical Modifications and Bioconjugate Reactions of Nanomaterials for Sensing, Imaging, Drug Delivery and Therapy. *Chem. Soc. Rev.* **2014**, *43*, 744.
- (134) Zhang, X.; Chen, Z.-K.; Loh, K. P. Coordination-assisted Assembly of 1-D Nanostructured Light-harvesting Antenna. *J. Am. Chem. Soc.* **2009**, *131*, 7210.
- (135) Coronado, E.; Galan-Mascaros, J.; Monrabal-Capilla; Garcia-Martinez, J.; Pardo-Ibanez, P. Bistable Spin-Crossover Nanoparticles Showing Magnetic Thermal Hysteresis near Room Temperature. *Adv. Mater.* **2007**, *19*, 1359.
- (136) Aldeek, F.; Balan, L.; Lambert, J.; Schneider, R. The Influence of Capping Thioalkyl Acid on the Growth and Photoluminescence Efficiency of CdTe and CdSe Quantum Dots. *Nanotechnology* **2008**, *19*, 475401.
- (137) Pei, Y.; Lin, S.; Su, J.; Liu, C. Structure prediction of Au<sub>44</sub> (SR)<sub>28</sub>: a chiral superatom cluster. *J. Am. Chem. Soc.* **2013**, *135*, 19060.
- (138) Krishnadas, K.; Ghosh, A.; Baksi, A.; Chakraborty, I.; Natarajan, G.; Pradeep, T. Intercluster Reactions between Au<sub>25</sub> (SR)<sub>18</sub> and Ag<sub>44</sub> (SR)<sub>30</sub>. *J. Am. Chem. Soc.* **2016**, *138*, 140.
- (139) Yang, H.; Wang, Y.; Huang, H.; Gell, L.; Lehtovaara, L.; Malola, S.; Häkkinen, H.; Zheng, N. All-thiol-stabilized Ag<sub>44</sub> and Au<sub>12</sub>Ag<sub>32</sub> Nanoparticles with Single-crystal Structures. *Nat. Commun.* **2013**, *4*, 2422.
- (140) Liu, Z.; Bekenstein, Y.; Ye, X.; Nguyen, S. C.; Swabeck, J.; Zhang, D.; Lee, S.-T.; Yang, P.; Ma, W.; Alivisatos, A. P. Ligand mediated transformation of cesium lead bromide perovskite nanocrystals to lead depleted Cs<sub>4</sub>PbBr<sub>6</sub> nanocrystals. *J. Am. Chem. Soc.* **2017**, *139*, 5309.
- (141) Cao, Y.; Stavrinadis, A.; Lasanta, T.; So, D.; Konstantatos, G. The Role of Surface Passivation for Efficient and Photostable PbS Quantum Dot Solar Cells. *Nat. Energy* **2016**, *1*, 16035.
- (142) Reznickova, A.; Kolska, Z.; Siegel, J.; Svorcik, V. Grafting of gold nanoparticles and nanorods on plasma-treated polymers by thiols. *J. Mater. Sci.* **2012**, *47*, 6297.
- (143) Malinoski, A.; Hu, G.; Wang, C. Strong Bidentate Coordination for Surface Passivation and Ligand-Shell Engineering of Lead Halide Perovskite Nanocrystals in the Strongly Quantum-Confinement Regime. *J. Phys. Chem. C* **2021**, *125*, 24521.
- (144) Pan, J.; Shang, Y.; Yin, J.; De Bastiani, M.; Peng, W.; Dursun, I.; Sinatra, L.; El-Zohry, A. M.; Hedhili, M. N.; Emwas, A.-H.; Mohammed, O. F.; Ning, Z.; Bakr, O. M. Bidentate Ligand-Passivated CsPbI<sub>3</sub> Perovskite Nanocrystals for Stable Near-Unity Photoluminescence Quantum Yield and Efficient Red Light-Emitting Diodes. *J. Am. Chem. Soc.* **2018**, *140*, 562.
- (145) Zhang, H.; Wu, Y.; Shen, C.; Li, E.; Yan, C.; Zhang, W.; Tian, H.; Han, L.; Zhu, W.-H. Efficient and Stable Chemical Passivation on Perovskite Surface via Bidentate Anchoring. *Adv. Energy Mater.* **2019**, *9*, 1803573.
- (146) Krieg, F.; Ong, Q. K.; Burian, M.; Raino, G.; Naumenko, D.; Amenitsch, H.; Suess, A.; Grotevent, M. J.; Krumeich, F.; Bodnarchuk, M. I.; Shorubalko, I.; Stellacci, F.; Kovalenko, M. V. Stable Ultraconcentrated and Ultradilute Colloids of CsPbX<sub>3</sub> (X = Cl,

- Br) Nanocrystals Using Natural Lecithin as a Capping Ligand. *J. Am. Chem. Soc.* **2019**, *141*, 19839.
- (147) Wang, S.; Du, L.; Jin, Z.; Xin, Y.; Mattoussi, H. Enhanced Stabilization and Easy Phase Transfer of CsPbBr<sub>3</sub> Perovskite Quantum Dots Promoted by High-Affinity Polyzwitterionic Ligands. *J. Am. Chem. Soc.* **2020**, *142*, 12669.
- (148) Dutt, V. G. V.; Akhil, S.; Mishra, N. Enhancement of Photoluminescence and the Stability of CsPbX<sub>3</sub> (X = Cl, Br, and I) Perovskite Nanocrystals with Phthalimide Passivation. *Nanoscale* **2021**, *13*, 14442.
- (149) Li, Y.; Cai, M.; Shen, M.; Cai, Y.; Xie, R.-J. Bidentate aliphatic quaternary ammonium ligand-stabilized CsPbBr<sub>3</sub> perovskite nanocrystals with high PLQY (92.3%) and superior stability. *J. Mater. Chem. C* **2022**, *10*, 8356.
- (150) Bansal, P.; Kar, P. Succinic acid-assisted Stability Enhancement of a Colloidal Organometal Halide Perovskite and its Application as a Fluorescent Keypad Lock. *N. J. Chem.* **2019**, *43*, 4599.
- (151) Wang, Q.; Zheng, X.; Deng, Y.; Zhao, J.; Chen, Z.; Huang, J. Stabilizing the  $\alpha$ -phase of CsPbI<sub>3</sub> perovskite by sulfobetaine zwitterions in one-step spin-coating films. *Joule* **2017**, *1*, 371.
- (152) Kim, H.; Hight-Huf, N.; Kang, J.-H.; Bisnoff, P.; Sundararajan, S.; Thompson, T.; Barnes, M.; Hayward, R. C.; Emrick, T. Polymer Zwitterions for Stabilization of CsPbBr<sub>3</sub> Perovskite Nanoparticles and Nanocomposite Films. *Angew. Chem., Int. Ed.* **2020**, *59*, 10802.
- (153) Schwarzenbach, v. G. Der chelateffekt. *Helv. Chim. Acta* **1952**, *35*, 2344.
- (154) Zhang, C.; Turyanska, L.; Cao, H.; Zhao, L.; Fay, M. W.; Temperton, R.; O'Shea, J.; Thomas, N. R.; Wang, K.; Luan, W.; Patanè, A. Hybrid light emitting diodes based on stable, high brightness all-inorganic CsPbI<sub>3</sub> perovskite nanocrystals and InGaN. *Nanoscale* **2019**, *11*, 13450.
- (155) Wang, S.; Zhou, L.; Huang, F.; Xin, Y.; Jin, P.; Ma, Q.; Pang, Q.; Chen, Y.; Zhang, J. Z. Hybrid Organic–inorganic Lead Bromide Perovskite Supercrystals Self-assembled with L-cysteine and their Good Luminescence Properties. *J. Mater. Chem. C* **2018**, *6*, 10994.
- (156) Luo, B.; Naghadeh, S. B.; Allen, A. L.; Li, X.; Zhang, J. Z. Peptide-Passivated Lead Halide Perovskite Nanocrystals Based on Synergistic Effect between Amino and Carboxylic Functional Groups. *Adv. Funct. Mater.* **2017**, *27*, 1604018.
- (157) Ahmed, G. H.; Yin, J.; Bose, R.; Sinatra, L.; Alarousu, E.; Yengel, E.; AlYami, N. M.; Saidaminov, M. I.; Zhang, Y.; Hedhili, M. N.; Bakr, O. M.; Brédas, J.-L.; Mohammed, O. F. Pyridine-Induced Dimensionality Change in Hybrid Perovskite Nanocrystals. *Chem. Mater.* **2017**, *29*, 4393.
- (158) Noel, N. K.; Abate, A.; Stranks, S. D.; Parrott, E. S.; Burlakov, V. M.; Goriely, A.; Snaith, H. J. Enhanced Photoluminescence and Solar Cell Performance via Lewis Base Passivation of Organic–Inorganic Lead Halide Perovskites. *ACS Nano* **2014**, *8*, 9815.
- (159) Hou, S.; Guo, Y.; Tang, Y.; Quan, Q. Synthesis and Stabilization of Colloidal Perovskite Nanocrystals by Multidentate Polymer Micelles. *ACS Appl. Mater. Interfaces* **2017**, *9*, 18417.
- (160) Wang, S.; Wang, W.; Donmez, S.; Xin, Y.; Mattoussi, H. Engineering Highly Fluorescent and Colloidally Stable Blue-Emitting CsPbBr<sub>3</sub> Nanoplatelets Using Polysalt/PbBr<sub>2</sub> Ligands. *Chem. Mater.* **2022**, *34*, 4924.
- (161) Förster, S.; Antonietti, M. Amphiphilic Block Copolymers in Structure-Controlled Nanomaterial Hybrids. *Adv. Mater.* **1998**, *10*, 195.
- (162) Yin, W.; Li, M.; Dong, W.; Luo, Z.; Li, Y.; Qian, J.; Zhang, J.; Zhang, W.; Zhang, Y.; Kershaw, S. V.; Zhang, X.; Zheng, W.; Rogach, A. L. Multidentate Ligand Polyethylenimine Enables Bright Color-Saturated Blue Light-Emitting Diodes Based on CsPbBr<sub>3</sub> Nanoplatelets. *ACS Energy Lett.* **2021**, *6*, 477.
- (163) Hassan, Y.; Park, J. H.; Crawford, M. L.; Sadhanala, A.; Lee, J.; Sadighian, J. C.; Mosconi, E.; Shivanna, R.; Radicchi, E.; Jeong, M.; Yang, C.; Choi, H.; Park, S. H.; Song, M. H.; De Angelis, F.; Wong, C. Y.; Friend, R. H.; Lee, B. R.; Snaith, H. J. Ligand-engineered bandgap stability in mixed-halide perovskite LEDs. *Nature* **2021**, *591*, 72.
- (164) Ahmed, T.; Seth, S.; Samanta, A. Boosting the Photoluminescence of CsPbX<sub>3</sub> (X = Cl, Br, I) Perovskite Nanocrystals Covering a Wide Wavelength Range by Postsynthetic Treatment with Tetrafluoroborate salts. *Chem. Mater.* **2018**, *30*, 3633.
- (165) Huang, H.; Zhao, W.; Yang, H.; Zhang, X.; Su, J.; Hu, K.; Nie, Z.; Li, Y.; Zhong, J. In situ synthesis of blue-emitting bromide-based perovskite nanoplatelets towards unity quantum efficiency and ultrahigh stability. *J. Mater. Chem. C* **2021**, *9*, 5535.
- (166) Zhang, W.; Pathak, S.; Sakai, N.; Stergiopoulos, T.; Nayak, P. K.; Noel, N. K.; Haghighirad, A. A.; Burlakov, V. M.; Dequillettes, D. W.; Sadhanala, A.; et al. Enhanced Optoelectronic Quality of Perovskite Thin Films with Hypophosphorous Acid for Planar Heterojunction Solar Cells. *Nat. Commun.* **2015**, *6*, 10030.
- (167) Nagane, S.; Bansode, U.; Game, O.; Chhatre, S.; Ogale, S. J. CH<sub>3</sub>NH<sub>3</sub>PbI<sub>(3-x)</sub>(BF<sub>4</sub>)<sub>x</sub>: molecular ion substituted hybrid perovskite. *Chem. Commun.* **2014**, *50*, 9741.
- (168) Guerrero-Martínez, A.; Pérez-Juste, J.; Liz-Marzán, L. M. Recent Progress on Silica Coating of Nanoparticles and Related Nanomaterials. *Adv. Mater.* **2010**, *22*, 1182.
- (169) Zhang, F.; Shi, Z.-F.; Ma, Z.-Z.; Li, Y.; Li, S.; Wu, D.; Xu, T.-T.; Li, X.-J.; Shan, C.-X.; Du, G.-T. Silica coating enhances the stability of inorganic perovskite nanocrystals for efficient and stable down-conversion in white light-emitting devices. *Nanoscale* **2018**, *10*, 20131.
- (170) Shi, W.; Zhang, X.; Matras-Postolek, K.; Yang, P. Mesoporous silica-coated CsPbX<sub>3</sub> nanocrystals with high stability and ion-exchange resistance for bright white-emitting displays. *ACS Appl. Nano Mater.* **2021**, *4*, 9391.
- (171) Zhu, L.; Wu, C.; Riaz, S.; Dai, J. Stable silica coated DDAB-CsPbX<sub>3</sub> quantum dots and their application for white light-emitting diodes. *J. Lumin.* **2021**, *233*, 117884.
- (172) Wang, W.; Li, J.; Ni, P.; Liu, B.; Chen, Q.; Lu, Y.; Wu, H.; Cao, B.; Liu, Z. Improved synthesis of perovskite CsPbX<sub>3</sub>@SiO<sub>2</sub> (X = Cl, Br, and I) quantum dots with enhanced stability and excellent optical properties. *ES Mater. Manuf.* **2019**, *4*, 66.
- (173) Gao, F.; Yang, W.; Liu, X.; Li, Y.; Liu, W.; Xu, H.; Liu, Y. Highly stable and luminescent silica-coated perovskite quantum dots at nanoscale-particle level via nonpolar solvent synthesis. *Chem. Eng. J.* **2021**, *407*, 128001.
- (174) Uddin, M. A.; Calabro, R. L.; Kim, D.-Y.; Graham, K. R. Halide exchange and surface modification of metal halide perovskite nanocrystals with alkyltrichlorosilanes. *Nanoscale* **2018**, *10*, 16919.
- (175) Kulbak, M.; Gupta, S.; Kedem, N.; Levine, I.; Bendikov, T.; Hodes, G.; Cahen, D. Cesium enhances long-term stability of lead bromide perovskite-based solar cells. *J. Phys. Chem. Lett.* **2016**, *7*, 167.
- (176) Pan, A.; He, B.; Fan, X.; Liu, Z.; Urban, J. J.; Alivisatos, A. P.; He, L.; Liu, Y. Insight into the ligand-mediated synthesis of colloidal CsPbBr<sub>3</sub> perovskite nanocrystals: the role of organic acid, base, and cesium precursors. *ACS Nano* **2016**, *10*, 7943.
- (177) Zhong, Q.; Cao, M.; Hu, H.; Yang, D.; Chen, M.; Li, P.; Wu, L.; Zhang, Q. One-Pot Synthesis of Highly Stable CsPbBr<sub>3</sub>@SiO<sub>2</sub> Core–Shell Nanoparticles. *ACS Nano* **2018**, *12*, 8579.
- (178) Zhou, Y.; Yu, Y.; Zhang, Y.; Liu, X.; Yang, H.; Liang, X.; Xia, W.; Xiang, W. Highly Photoluminescent CsPbBr<sub>3</sub>/CsPb<sub>2</sub>Br<sub>5</sub> NCs@TEOS Nanocomposite in Light-Emitting Diodes. *Inorg. Chem.* **2021**, *60*, 3814.
- (179) Meng, C.; Yang, D.; Wu, Y.; Zhang, X.; Zeng, H.; Li, X. J. Synthesis of single CsPbBr<sub>3</sub>@SiO<sub>2</sub> core–shell particles via surface activation. *J. Mater. Chem. C* **2020**, *8*, 17403.
- (180) Sun, C.; Zhang, Y.; Ruan, C.; Yin, C.; Wang, X.; Wang, Y.; Yu, W. W. Efficient and stable white LEDs with silica-coated inorganic perovskite quantum dots. *Adv. Mater.* **2016**, *28*, 10088.
- (181) Chen, K.; Zhong, Q.; Chen, W.; Sang, B.; Wang, Y.; Yang, T.; Liu, Y.; Zhang, Y.; Zhang, H. Short-Chain Ligand-Passivated Stable  $\alpha$ -CsPbI<sub>3</sub> Quantum Dot for All-Inorganic Perovskite Solar Cells. *Adv. Funct. Mater.* **2019**, *29*, 1900991.
- (182) Chen, X.; Chen, Y.; Huang, J.; Li, C.; Ni, Z.; Zhang, K.; Cao, M.; Yu, T.; Chen, Y.; He, X.; Li, Y. Phase Regulation and Surface Passivation of Stable  $\alpha$ -CsPbI<sub>3</sub> Nanocrystals with Dual-Mode



- Luminescence via Synergistic Effects of Ligands. *J. Phys. Chem. C* **2022**, *126*, 5233.
- (183) Zhang, T.; Dar, M. I.; Li, G.; Xu, F.; Guo, N.; Grätzel, M.; Zhao, Y. Bication lead iodide 2D perovskite component to stabilize inorganic  $\alpha$ -CsPbI<sub>3</sub> perovskite phase for high-efficiency solar cells. *Sci. Adv.* **2017**, *3*, e1700841.
- (184) Li, N.; Apergi, S.; Chan, C. C. S.; Jia, Y.; Xie, F.; Liang, Q.; Li, G.; Wong, K. S.; Brocks, G.; Tao, S.; Zhao, N. Diammonium mediated perovskite film formation for high-luminescence red perovskite light-emitting diodes. *Adv. Mater.* **2022**, *34*, 2202042.
- (185) He, K.; Shen, C.; Zhu, Y.; Chen, X.; Bi, Z.; Marimuthu, T.; Xu, G.; Xu, X. Stable Luminescent CsPbI<sub>3</sub> Quantum Dots Passivated by (3-Aminopropyl)triethoxysilane. *Langmuir* **2020**, *36*, 10210.
- (186) Huang, Y.; Luan, W.; Liu, M.; Turyanska, L. DDAB-assisted synthesis of iodine-rich CsPbI<sub>3</sub> perovskite nanocrystals with improved stability in multiple environments. *J. Mater. Chem. C* **2020**, *8*, 2381.
- (187) Zhu, Y.; Zhao, J.; Yang, G.; Xu, X.; Pan, G. Ammonium acetate passivated CsPbI<sub>3</sub> perovskite nanocrystals for efficient red light-emitting diodes. *Nanoscale* **2020**, *12*, 7712.
- (188) Zeng, Q.; Zhang, X.; Bing, Q.; Xiong, Y.; Yang, F.; Liu, H.; Liu, J.-y.; Zhang, H.; Zheng, W.; Rogach, A. L.; Yang, B. Surface Stabilization of Colloidal Perovskite Nanocrystals via Multi-amine Chelating Ligands. *ACS Energy Lett.* **2022**, *7*, 1963.
- (189) Wang, Y.; Yuan, J.; Zhang, X.; Ling, X.; Larson, B. W.; Zhao, Q.; Yang, Y.; Shi, Y.; Luther, J. M.; Ma, W. Surface Ligand Management Aided by a Secondary Amine Enables Increased Synthesis Yield of CsPbI<sub>3</sub> Perovskite Quantum Dots and High Photovoltaic Performance. *Adv. Mater.* **2020**, *32*, 2000449.
- (190) Wang, H.; Ye, F.; Sun, J.; Wang, Z.; Zhang, C.; Qian, J.; Zhang, X.; Choy, W. C. H.; Sun, X. W.; Wang, K.; Zhao, W. Efficient CsPbBr<sub>3</sub> Nanoplatelet-Based Blue Light-Emitting Diodes Enabled by Engineered Surface Ligands. *ACS Energy Lett.* **2022**, *7*, 1137.
- (191) Zhang, C.; Wan, Q.; Wang, B.; Zheng, W.; Liu, M.; Zhang, Q.; Kong, L.; Li, L. Surface Ligand Engineering toward Brightly Luminescent and Stable Cesium Lead Halide Perovskite Nanoplatelets for Efficient Blue-Light-Emitting Diodes. *J. Phys. Chem. C* **2019**, *123*, 26161.
- (192) Pan, J.; Quan, L. N.; Zhao, Y.; Peng, W.; Murali, B.; Sarmah, S. P.; Yuan, M.; Sinatra, L.; Alyami, N. M.; Liu, J.; Yassitepe, E.; Yang, Z.; Voznyy, O.; Comin, R.; Hedhili, M. N.; Mohammed, O. F.; Lu, Z. H.; Kim, D. H.; Sargent, E. H.; Bakr, O. M. Highly Efficient Perovskite-Quantum-Dot Light-Emitting Diodes by Surface Engineering. *Adv. Mater.* **2016**, *28*, 8718.
- (193) He, H.; Mei, S.; Chen, Z.; Liu, S.; Wen, Z.; Cui, Z.; Yang, D.; Zhang, W.; Xie, F.; Yang, B.; Guo, R.; Xing, G. Thioacetamide-ligand-mediated synthesis of CsPbBr<sub>3</sub>-CsPbBr<sub>3</sub> homostructured nanocrystals with enhanced stability. *J. Mater. Chem. C* **2021**, *9*, 11349.
- (194) Zhang, Q.; Jiang, M.; Yan, G.; Feng, Y.; Zhang, B. Surface ligand engineering involving fluorophenethyl ammonium for stable and strong emission CsPbBr<sub>3</sub> quantum dots and high-performance QLEDs. *J. Mater. Chem. C* **2022**, *10*, 5849.
- (195) Lu, M.; Guo, J.; Sun, S.; Lu, P.; Zhang, X.; Shi, Z.; Yu, W. W.; Zhang, Y. Surface ligand engineering-assisted CsPbI<sub>3</sub> quantum dots enable bright and efficient red light-emitting diodes with a top-emitting structure. *Chem. Eng. J.* **2021**, *404*, 126563.
- (196) Lu, C.; Li, H.; Kolodziejski, K.; Dun, C.; Huang, W.; Carroll, D.; Geyer, S. M. Enhanced stabilization of inorganic cesium lead triiodide (CsPbI<sub>3</sub>) perovskite quantum dots with tri-octylphosphine. *Nano Res.* **2018**, *11*, 762.
- (197) Wang, C.; Chesman, A. S. R.; Jasieniak, J. J. Stabilizing the cubic perovskite phase of CsPbI<sub>3</sub> nanocrystals by using an alkyl phosphonic acid. *Chem. Commun.* **2017**, *53*, 232.
- (198) Mubiyi, K. P.; Moloto, N.; Moloto, M. J. Effect of diphenylphosphinic acid on cesium lead iodide perovskite stability. *CrystEngComm* **2018**, *20*, 5275.
- (199) Wang, T.; Li, X.; Fang, T.; Wang, S.; Song, J. Room-temperature synthesis of perovskite-phase CsPbI<sub>3</sub> nanocrystals for optoelectronics via a ligand-mediated strategy. *Chem. Eng. J.* **2021**, *418*, 129361.
- (200) Baek, S.; Kim, Y.; Kim, S.-W. Highly photo-stable CsPbI<sub>3</sub> perovskite quantum dots via thiol ligand exchange and their polymer film application. *J. Industrial and Engineering Chem.* **2020**, *83*, 279.
- (201) Min, X.; Xie, Q.; Wang, Z.; Wang, X.; Chen, M. Improving the stability and optical properties of CsPbI<sub>3</sub> perovskite nanocrystals by 1-Octadecanethiol through surface modification. *Mater. Chem. Phys.* **2022**, *276*, 125404.
- (202) Khan, J.; Zhang, X.; Yuan, J.; Wang, Y.; Shi, G.; Patterson, R.; Shi, J.; Ling, X.; Hu, L.; Wu, T.; Dai, S.; Ma, W. Tuning the Surface-Passivating Ligand Anchoring Position Enables Phase Robustness in CsPbI<sub>3</sub> Perovskite Quantum Dot Solar Cells. *ACS Energy Lett.* **2020**, *5*, 3322.
- (203) Zhang, J.; Yin, C.; Yang, F.; Yao, Y.; Yuan, F.; Chen, H.; Wang, R.; Bai, S.; Tu, G.; Hou, L. Highly Luminescent and Stable CsPbI<sub>3</sub> Perovskite Nanocrystals with Sodium Dodecyl Sulfate Ligand Passivation for Red-Light-Emitting Diodes. *J. Phys. Chem. Lett.* **2021**, *12*, 2437.
- (204) Lan, Y.-F.; Yao, J.-S.; Yang, J.-N.; Song, Y.-H.; Ru, X.-C.; Zhang, Q.; Feng, L.-Z.; Chen, T.; Song, K.-H.; Yao, H.-B. Spectrally Stable and Efficient Pure Red CsPbI<sub>3</sub> Quantum Dot Light-Emitting Diodes Enabled by Sequential Ligand Post-Treatment Strategy. *Nano Lett.* **2021**, *21*, 8756.
- (205) Huynh, K. A.; Bae, S.-R.; Nguyen, T. V.; Do, H. H.; Heo, D. Y.; Park, J.; Lee, T.-W.; Le, Q. V.; Ahn, S. H.; Kim, S. Y. Ligand-Assisted Sulfide Surface Treatment of CsPbI<sub>3</sub> Perovskite Quantum Dots to Increase Photoluminescence and Recovery. *ACS Photonics* **2021**, *8*, 1979.
- (206) Sim, K. M.; Swarnkar, A.; Nag, A.; Chung, D. S. Phase Stabilized  $\alpha$ -CsPbI<sub>3</sub> Perovskite Nanocrystals for Photodiode Applications. *Laser Photonics Rev.* **2018**, *12*, 1700209.
- (207) Cai, Y.; Li, W.; Tian, D.; Shi, S.; Chen, X.; Gao, P.; Xie, R.-J. Organic Sulfonium-Stabilized High-Efficiency Cesium or Methylammonium Lead Bromide Perovskite Nanocrystals. *Angew. Chem., Int. Ed.* **2022**, *61*, e202209880.
- (208) Lai, H. M.; Lu, Z.; Choi, C. K. K.; Zhou, W.; Ngo Yau, C.; Tang, B. Z.; Ko, H. Direct Room Temperature Synthesis of  $\alpha$ -CsPbI<sub>3</sub> Perovskite Nanocrystals with High Photoluminescence Quantum Yields: Implications for Lighting and Photovoltaic Applications. *ACS Appl. Nano Mater.* **2022**, *5*, 12366.
- (209) Yan, D.; Shi, T.; Zang, Z.; Zhou, T.; Liu, Z.; Zhang, Z.; Du, J.; Leng, Y.; Tang, X. Ultrastable CsPbBr<sub>3</sub> Perovskite Quantum Dot and Their Enhanced Amplified Spontaneous Emission by Surface Ligand Modification. *Small* **2019**, *15*, 1901173.
- (210) Dutt, V. G. V.; Akhil, S.; Singh, R.; Palabathuni, M.; Mishra, N. Year-Long Stability and Near-Unity Photoluminescence Quantum Yield of CsPbBr<sub>3</sub> Perovskite Nanocrystals by Benzoic Acid Post-treatment. *J. Phys. Chem. C* **2022**, *126*, 9502.
- (211) Shi, J.; Li, F.; Jin, Y.; Liu, C.; Cohen-Kleinstein, B.; Yuan, S.; Li, Y.; Wang, Z. K.; Yuan, J.; Ma, W. J. A. C. In Situ Ligand Bonding Management of CsPbI<sub>3</sub> Perovskite Quantum Dots Enables High-Performance Photovoltaics and Red Light-Emitting Diodes. *Angew. Chem., Int. Ed.* **2020**, *132*, 22414.
- (212) Jia, D.; Chen, J.; Yu, M.; Liu, J.; Johansson, E. M. J.; Hagfeldt, A.; Zhang, X. Dual Passivation of CsPbI<sub>3</sub> Perovskite Nanocrystals with Amino Acid Ligands for Efficient Quantum Dot Solar Cells. *Small* **2020**, *16*, 2001772.
- (213) Bi, C.; Kershaw, S. V.; Rogach, A. L.; Tian, J. Improved Stability and Photodetector Performance of CsPbI<sub>3</sub> Perovskite Quantum Dots by Ligand Exchange with Aminoethanethiol. *Adv. Funct. Mater.* **2019**, *29*, 1902446.
- (214) Qiao, Q.; Shen, Z.; Jiang, N.; Song, P.; Song, D.; Qiao, B.; Zhao, S.; Xu, Z. Synergistic effect of multidentate ligands on CsPbI<sub>3</sub> perovskite nanocrystals surface for high efficiency deep red light-emitting diode. *Org. Electron.* **2022**, *107*, 106550.
- (215) Tang, C.; Shen, X.; Yu, S.; Zhong, Y.; Wang, Z.; Hu, J.; Lu, M.; Wu, Z.; Zhang, Y.; Yu, W. W.; Bai, X. Post-treatment of CsPbI<sub>3</sub> nanocrystals by p-iodo-D-Phenylalanine for efficient perovskite LEDs. *Mater. Today Phys.* **2021**, *21*, 100555.

- (216) Zu, Y.; Dai, J.; Li, L.; Yuan, F.; Chen, X.; Feng, Z.; Li, K.; Song, X.; Yun, F.; Yu, Y.; Jiao, B.; Dong, H.; Hou, X.; Ju, M.; Wu, Z. Ultra-stable CsPbBr<sub>3</sub> nanocrystals with near-unity photoluminescence quantum yield via postsynthetic surface engineering. *J. Mater. Chem. A* **2019**, *7*, 26116.
- (217) Yin, W.; Li, M.; Dong, W.; Luo, Z.; Li, Y.; Qian, J.; Zhang, J.; Zhang, W.; Zhang, Y.; Kershaw, S. V.; Zhang, X.; Zheng, W.; Rogach, A. L. Multidentate Ligand Polyethylenimine Enables Bright Color-Saturated Blue Light-Emitting Diodes Based on CsPbBr<sub>3</sub> Nanoplatelets. *ACS Energy Lett.* **2021**, *6*, 477.
- (218) Mir, W. J.; Alamoudi, A.; Yin, J.; Yorov, K. E.; Maity, P.; Naphade, R.; Shao, B.; Wang, J.; Lintangpradipto, M. N.; Nematulloev, S.; Emwas, A.-H.; Genovese, A.; Mohammed, O. F.; Bakr, O. M. Lecithin Capping Ligands Enable Ultrastable Perovskite-Phase CsPbI<sub>3</sub> Quantum Dots for Rec. 2020 Bright-Red Light-Emitting Diodes. *J. Am. Chem. Soc.* **2022**, *144*, 13302.
- (219) Zhang, Y.; Li, G.; Hou, G.; Lin, J.; Chen, M.; Liu, S.; Lin, H.; Fang, J.; Jing, C.; Chu, J. Multidentate Ligand Passivated CsPbBr<sub>3</sub> Perovskite Nanocrystals with Near-Unity Quantum Yield and Improved Stability for High-Efficiency White Light-Emitting Diodes. *SSRN*, February 16, 2022..
- (220) Qiao, Q.; Shen, Z.; Jiang, N.; Song, P.; Song, D.; Qiao, B.; Zhao, S.; Xu, Z. Synergistic effect of multidentate ligands on CsPbI<sub>3</sub> perovskite nanocrystals surface for high efficiency deep red light-emitting diode. *Org. Electronics* **2022**, *107*, 106550.
- (221) Meyns, M.; Perálvarez, M.; Heuer-Jungemann, A.; Hertog, W.; Ibáñez, M.; Nafria, R.; Genç, A.; Arbiol, J.; Kovalenko, M. V.; Carreras, J.; Cabot, A.; Kanaras, A. G. Polymer-Enhanced Stability of Inorganic Perovskite Nanocrystals and Their Application in Color Conversion LEDs. *ACS Appl. Mater. Interfaces* **2016**, *8*, 19579.
- (222) Dutta, A.; Pradhan, N. Phase-Stable Red-Emitting CsPbI<sub>3</sub> Nanocrystals: Successes and Challenges. *ACS Energy Lett.* **2019**, *4*, 709.
- (223) Swarnkar, A.; Mir, W. J.; Nag, A. Can B-Site Doping or Alloying Improve Thermal- and Phase-Stability of All-Inorganic CsPbX<sub>3</sub> (X = Cl, Br, I) Perovskites? *ACS Energy Lett.* **2018**, *3*, 286.
- (224) Masi, S.; Gualdrón-Reyes, A. F.; Mora-Seró, I. Stabilization of Black Perovskite Phase in FAPbI<sub>3</sub> and CsPbI<sub>3</sub>. *ACS Energy Lett.* **2020**, *5*, 1974.
- (225) Ye, F.; Zhang, H.; Li, W.; Yan, Y.; Cai, J.; Gurney, R. S.; Pearson, A. J.; Liu, D.; Wang, T. Ligand-Exchange of Low-Temperature Synthesized CsPbBr<sub>3</sub> Perovskite toward High-Efficiency Light-Emitting Diodes. *Small Methods* **2019**, *3*, 1800489.
- (226) Song, J.; Fang, T.; Li, J.; Xu, L.; Zhang, F.; Han, B.; Shan, Q.; Zeng, H. Organic-Inorganic Hybrid Passivation Enables Perovskite QLEDs with an EQE of 16.48%. *Adv. Mater.* **2018**, *30*, 1805409.
- (227) Shin, Y. S.; Yoon, Y. J.; Lee, K. T.; Jeong, J.; Park, S. Y.; Kim, G.-H.; Kim, J. Y. Vivid and Fully Saturated Blue Light-Emitting Diodes Based on Ligand-Modified Halide Perovskite Nanocrystals. *ACS Appl. Mater. Interfaces* **2019**, *11*, 23401.
- (228) Bodnarchuk, M. I.; Boehme, S. C.; ten Brinck, S.; Bernasconi, C.; Shynkarenko, Y.; Krieg, F.; Widmer, R.; Aeschlimann, B.; Günther, D.; Kovalenko, M. V.; Infante, I. Rationalizing and Controlling the Surface Structure and Electronic Passivation of Cesium Lead Halide Nanocrystals. *ACS Energy Lett.* **2019**, *4*, 63.
- (229) Balakrishnan, S. K.; Kamat, P. V. Ligand Assisted Transformation of Cubic CsPbBr<sub>3</sub> Nanocrystals into Two-Dimensional CsPb<sub>2</sub>Br<sub>5</sub> Nanosheets. *Chem. Mater.* **2018**, *30*, 74.
- (230) Quarta, D.; Imran, M.; Capodilupo, A.-L.; Petralanda, U.; van Beek, B.; De Angelis, F.; Manna, L.; Infante, I.; De Trizio, L.; Giansante, C. Stable Ligand Coordination at the Surface of Colloidal CsPbBr<sub>3</sub> Nanocrystals. *J. Phys. Chem. Lett.* **2019**, *10*, 3715.
- (231) Uddin, M. A.; Mobley, J. K.; Masud, A. A.; Liu, T.; Calabro, R. L.; Kim, D.-Y.; Richards, C. I.; Graham, K. R. Mechanistic Exploration of Dodecanethiol-Treated Colloidal CsPbBr<sub>3</sub> Nanocrystals with Photoluminescence Quantum Yields Reaching Near 100%. *J. Phys. Chem. C* **2019**, *123*, 18103.
- (232) Uddin, M. A.; Glover, J. D.; Park, S. M.; Pham, J. T.; Graham, K. R. Growth of Highly Stable and Luminescent CsPbX<sub>3</sub> (X = Cl, Br, and I) Nanoplates via Ligand Mediated Anion Exchange of CsPbCl<sub>3</sub> Nanocubes with AlX<sub>3</sub>. *Chem. Mater.* **2020**, *32*, 5217.
- (233) Zhang, B.-B.; Yuan, S.; Ma, J.-P.; Zhou, Y.; Hou, J.; Chen, X.; Zheng, W.; Shen, H.; Wang, X.-C.; Sun, B.; Bakr, O. M.; Liao, L.-S.; Sun, H.-T. General Mild Reaction Creates Highly Luminescent Organic-Ligand-Lacking Halide Perovskite Nanocrystals for Efficient Light-Emitting Diodes. *J. Am. Chem. Soc.* **2019**, *141*, 15423.
- (234) McGrath, F.; Ghorpade, U. V.; Ryan, K. M. Synthesis and dimensional control of CsPbBr<sub>3</sub> perovskite nanocrystals using phosphorous based ligands. *J. Chem. Phys.* **2020**, *152*, 174702.
- (235) Xu, Y.; Li, H.; Ramakrishnan, S.; Song, D.; Zhang, Y.; Cotlet, M.; Yu, Q. Ion-Assisted Ligand Exchange for Efficient and Stable Inverted FAPbI<sub>3</sub> Quantum Dot Solar Cells. *ACS Appl. Energy Mater.* **2022**, *5*, 9858.
- (236) Lu, H.; Zhu, X.; Miller, C.; Martin, J. S.; Chen, X.; Miller, E. M.; Yan, Y.; Beard, M. C. Enhanced photoredox activity of CsPbBr<sub>3</sub> nanocrystals by quantitative colloidal ligand exchange. *J. Chem. Phys.* **2019**, *151*, 204305.
- (237) Jiang, S.; Song, Y.; Kang, H.; Li, B.; Yang, K.; Xing, G.; Yu, Y.; Li, S.; Zhao, P.; Zhang, T. Ligand Exchange Strategy to Achieve Chiral Perovskite Nanocrystals with a High Photoluminescence Quantum Yield and Regulation of the Chiroptical Property. *ACS Appl. Mater. Interfaces* **2022**, *14*, 3385.
- (238) Jin, X.; Ma, K.; Chakkamalayath, J.; Morsby, J.; Gao, H. In Situ Photocatalyzed Polymerization to Stabilize Perovskite Nanocrystals in Protic Solvents. *ACS Energy Lett.* **2022**, *7*, 610.
- (239) Wang, S.; Wang, W.; Donmez, S.; Xin, Y.; Mattoussi, H. Engineering Highly Fluorescent and Colloidally Stable Blue-Emitting CsPbBr<sub>3</sub> Nanoplatelets Using Polysalt/PbBr<sub>2</sub> Ligands. *Chem. Mater.* **2022**, *34*, 4924.
- (240) Wheeler, L. M.; Sanehira, E. M.; Marshall, A. R.; Schulz, P.; Suri, M.; Anderson, N. C.; Christians, J. A.; Nordlund, D.; Sokaras, D.; Kroll, T.; Harvey, S. P.; Berry, J. J.; Lin, L. Y.; Luther, J. M. Targeted Ligand-Exchange Chemistry on Cesium Lead Halide Perovskite Quantum Dots for High-Efficiency Photovoltaics. *J. Am. Chem. Soc.* **2018**, *140*, 10504.
- (241) Udayabhaskararao, T.; Houben, L.; Cohen, H.; Menahem, M.; Pinkas, I.; Avram, L.; Wolf, T.; Teitelboim, A.; Leskes, M.; Yaffe, O.; Oron, D.; Kazes, M. A Mechanistic Study of Phase Transformation in Perovskite Nanocrystals Driven by Ligand Passivation. *Chem. Mater.* **2018**, *30*, 84.
- (242) Hintermayr, V. A.; Richter, A. F.; Ehrat, F.; Döblinger, M.; Vanderlinden, W.; Sichert, J. A.; Tong, Y.; Polavarapu, L.; Feldmann, J.; Urban, A. S. Tuning the Optical Properties of Perovskite Nanoplatelets through Composition and Thickness by Ligand-Assisted Exfoliation. *Adv. Mater.* **2016**, *28*, 9478.
- (243) Palazon, F.; Almeida, G.; Akkerman, Q. A.; De Trizio, L.; Dang, Z.; Prato, M.; Manna, L. Changing the dimensionality of cesium lead bromide nanocrystals by reversible postsynthesis transformations with amines. *Chem. Mater.* **2017**, *29*, 4167.
- (244) Chen, X.; Chen, D.; Li, J.; Fang, G.; Sheng, H.; Zhong, J. Tunable CsPbBr<sub>3</sub>/Cs<sub>4</sub>PbBr<sub>6</sub> phase transformation and their optical spectroscopic properties. *Dalton Trans.* **2018**, *47*, 5670.
- (245) Li, G.; Wang, H.; Zhu, Z.; Chang, Y.; Zhang, T.; Song, Z.; Jiang, Y. Shape and phase evolution from CsPbBr<sub>3</sub> perovskite nanocubes to tetragonal CsPb<sub>2</sub>Br<sub>5</sub> nanosheets with an indirect bandgap. *Chem. Commun.* **2016**, *52*, 11296.
- (246) Balakrishnan, S. K.; Kamat, P. V. Ligand assisted transformation of cubic CsPbBr<sub>3</sub> nanocrystals into two-dimensional CsPb<sub>2</sub>Br<sub>5</sub> nanosheets. *Chem. Mater.* **2018**, *30*, 74.
- (247) Fanizza, E.; Cascella, F.; Altamura, D.; Giannini, C.; Panniello, A.; Triggiani, L.; Panzarea, F.; Depalo, N.; Grisorio, R.; Suranna, G. P.; et al. Post-synthesis phase and shape evolution of CsPbBr<sub>3</sub> colloidal nanocrystals: The role of ligands. *Nano Res.* **2019**, *12*, 1155.
- (248) Rossi, A.; Price, M. B.; Hardy, J.; Gorman, J.; Schmidt, T. W.; Davis, N. Energy Transfer between Perylene Diimide Based Ligands and Cesium Lead Bromide Perovskite Nanocrystals. *J. Phys. Chem. C* **2020**, *124*, 3306.



- (249) Hofmann, F. J.; Bodnarchuk, M. I.; Dirin, D. N.; Vogelsang, J.; Kovalenko, M. V.; Lupton, J. M. Energy Transfer from Perovskite Nanocrystals to Dye Molecules Does Not Occur by FRET. *Nano Lett.* **2019**, *19*, 8896.
- (250) Liu, M.; Xia, P.; Zhao, G.; Nie, C.; Gao, K.; He, S.; Wang, L.; Wu, K. Energy-Transfer Photocatalysis Using Lead Halide Perovskite Nanocrystals: Sensitizing Molecular Isomerization and Cycloaddition. *Angew. Chem., Int. Ed.* **2022**, *61*, e202208241.
- (251) Liao, J.; Guo, W.; Luo, X. Triplet energy transfer between inorganic nanocrystals and organic molecules. *J. Photochem. Photobiol.* **2022**, *11*, 100128.
- (252) Lu, H.; Chen, X.; Anthony, J. E.; Johnson, J. C.; Beard, M. C. Sensitizing Singlet Fission with Perovskite Nanocrystals. *J. Am. Chem. Soc.* **2019**, *141*, 4919.
- (253) He, S.; Han, Y.; Guo, J.; Wu, K. Entropy-Powered Endothermic Energy Transfer from CsPbBr<sub>3</sub> Nanocrystals for Photon Upconversion. *J. Phys. Chem. Lett.* **2022**, *13*, 1713.
- (254) Ghosh, G.; Marjit, K.; Ghosh, S.; Ghosh, A.; Ahammed, R.; De Sarkar, A.; Patra, A. Hot Hole Cooling and Transfer Dynamics from Lead Halide Perovskite Nanocrystals Using Porphyrin Molecules. *J. Phys. Chem. C* **2021**, *125*, 5859.
- (255) Chen, Z.; Hu, Y.; Wang, J.; Shen, Q.; Zhang, Y.; Ding, C.; Bai, Y.; Jiang, G.; Li, Z.; Gaponik, N. Boosting Photocatalytic CO<sub>2</sub> Reduction on CsPbBr<sub>3</sub> Perovskite Nanocrystals by Immobilizing Metal Complexes. *Chem. Mater.* **2020**, *32*, 1517.
- (256) Luo, X.; Liang, G.; Han, Y.; Li, Y.; Ding, T.; He, S.; Liu, X.; Wu, K. Triplet Energy Transfer from Perovskite Nanocrystals Mediated by Electron Transfer. *J. Am. Chem. Soc.* **2020**, *142*, 11270.
- (257) DuBose, J. T.; Kamat, P. V. Directing Energy Transfer in Halide Perovskite–Chromophore Hybrid Assemblies. *J. Am. Chem. Soc.* **2021**, *143*, 19214.
- (258) Martin, J. S.; Zeng, X.; Chen, X.; Miller, C.; Han, C.; Lin, Y.; Yamamoto, N.; Wang, X.; Yazdi, S.; Yan, Y.; Beard, M. C.; Yan, Y. A Nanocrystal Catalyst Incorporating a Surface Bound Transition Metal to Induce Photocatalytic Sequential Electron Transfer Events. *J. Am. Chem. Soc.* **2021**, *143*, 11361.
- (259) Luo, X.; Han, Y.; Chen, Z.; Li, Y.; Liang, G.; Liu, X.; Ding, T.; Nie, C.; Wang, M.; Castellano, F. N.; et al. Mechanisms of triplet energy transfer across the inorganic nanocrystal/organic molecule interface. *Nat. Commun.* **2020**, *11*, 28.
- (260) De, A.; Das, S.; Samanta, A. Hot Hole Transfer Dynamics from CsPbBr<sub>3</sub> Perovskite Nanocrystals. *ACS Energy Lett.* **2020**, *5*, 2246.
- (261) He, S.; Han, Y.; Guo, J.; Wu, K. Long-Lived Delayed Emission from CsPbBr<sub>3</sub> Perovskite Nanocrystals for Enhanced Photochemical Reactivity. *ACS Energy Lett.* **2021**, *6*, 2786.
- (262) De, A.; Mondal, N.; Samanta, A. Hole Transfer Dynamics from Photoexcited Cesium Lead Halide Perovskite Nanocrystals: 1-Aminopyrene as Hole Acceptor. *J. Phys. Chem. C* **2018**, *122*, 13617.
- (263) DuBose, J. T.; Kamat, P. V. Probing Perovskite Photocatalysis. Interfacial Electron Transfer between CsPbBr<sub>3</sub> and Ferrocene Redox Couple. *J. Phys. Chem. Lett.* **2019**, *10*, 6074.
- (264) Wu, K.; Liang, G.; Shang, Q.; Ren, Y.; Kong, D.; Lian, T. Ultrafast Interfacial Electron and Hole Transfer from CsPbBr<sub>3</sub> Perovskite Quantum Dots. *J. Am. Chem. Soc.* **2015**, *137*, 12792.
- (265) DuBose, J. T.; Kamat, P. V. Surface Chemistry Matters. How Ligands Influence Excited State Interactions between CsPbBr<sub>3</sub> and Methyl Viologen. *J. Phys. Chem. C* **2020**, *124*, 12990.
- (266) DuBose, J. T.; Kamat, P. V. Efficacy of Perovskite Photocatalysis: Challenges to Overcome. *ACS Energy Lett.* **2022**, *7*, 1994.
- (267) Palabathuni, M.; Akhil, S.; Singh, R.; Mishra, N. Charge Transfer in Photoexcited Cesium–Lead Halide Perovskite Nanocrystals: Review of Materials and Applications. *ACS Appl. Nano Mater.* **2022**, *5*, 10097.
- (268) Shyamal, S.; Pradhan, N. Halide Perovskite Nanocrystal Photocatalysts for CO<sub>2</sub> Reduction: Successes and Challenges. *J. Phys. Chem. Lett.* **2020**, *11*, 6921.
- (269) Wang, J.; Shi, Y.; Wang, Y.; Li, Z. Rational Design of Metal Halide Perovskite Nanocrystals for Photocatalytic CO<sub>2</sub> Reduction: Recent Advances, Challenges, and Prospects. *ACS Energy Lett.* **2022**, *7*, 2043.
- (270) Zhu, X.; Lin, Y.; San Martin, J.; Sun, Y.; Zhu, D.; Yan, Y. Lead halide perovskites for photocatalytic organic synthesis. *Nat. Commun.* **2019**, *10*, 2843.
- (271) Wang, J.; Liu, J.; Du, Z.; Li, Z. Recent advances in metal halide perovskite photocatalysts: Properties, synthesis and applications. *J. Energy Chem.* **2021**, *54*, 770.
- (272) Wang, K.; Lu, H.; Zhu, X.; Lin, Y.; Beard, M. C.; Yan, Y.; Chen, X. Ultrafast Reaction Mechanisms in Perovskite Based Photocatalytic C–C Coupling. *ACS Energy Lett.* **2020**, *5*, 566.
- (273) Akhil, S.; Dutt, V. G. V.; Mishra, N. Surface modification for improving the photoredox activity of CsPbBr<sub>3</sub> nanocrystals. *Nanoscale Adv.* **2021**, *3*, 2547.
- (274) DuBose, J. T.; Kamat, P. V. Surface Chemistry Matters. How Ligands Influence Excited State Interactions between CsPbBr<sub>3</sub> and Methyl Viologen. *J. Phys. Chem. C* **2020**, *124*, 12990.
- (275) Lin, Y.; Guo, J.; San Martin, J.; Han, C.; Martinez, R.; Yan, Y. Photoredox Organic Synthesis Employing Heterogeneous Photocatalysts with Emphasis on Halide Perovskite. *Chem. Eur. J.* **2020**, *26*, 13118.
- (276) Guo, Y.; Lou, Y.; Chen, J.; Zhao, Y. Lead-Free Cs<sub>2</sub>AgSbCl<sub>6</sub> Double Perovskite Nanocrystals for Effective Visible-Light Photocatalytic C–C Coupling Reactions. *ChemSusChem* **2022**, *15*, e202102334.
- (277) Zhu, Y.; Liu, Y.; Miller, K. A.; Zhu, H.; Egap, E. Lead Halide Perovskite Nanocrystals as Photocatalysts for PET-RAFT Polymerization under Visible and Near-Infrared Irradiation. *ACS Macro Lett.* **2020**, *9*, 725.
- (278) Mase, K.; Okumura, K.; Yanai, N.; Kimizuka, N. Triplet sensitization by perovskite nanocrystals for photon upconversion. *Chem. Commun.* **2017**, *53*, 8261.
- (279) Yuan, Y.; Zhu, H.; Hills-Kimball, K.; Cai, T.; Shi, W.; Wei, Z.; Yang, H.; Candler, Y.; Wang, P.; He, J.; Chen, O. Stereoselective C–C Oxidative Coupling Reactions Photocatalyzed by Zwitterionic Ligand Capped CsPbBr<sub>3</sub> Perovskite Quantum Dots. *Angew. Chem., Int. Ed.* **2020**, *59*, 22563.
- (280) Lin, Y.; Avvacumova, M.; Zhao, R.; Chen, X.; Beard, M. C.; Yan, Y. Triplet Energy Transfer from Lead Halide Perovskite for Highly Selective Photocatalytic 2 + 2 Cycloaddition. *ACS Appl. Mater. Interfaces* **2022**, *14*, 25357.
- (281) Hardy, J.; Brett, M. W.; Rossi, A.; Wagner, I.; Chen, K.; Timmer, M. S. M.; Stocker, B. L.; Price, M. B.; Davis, N. J. L. K. Energy Transfer between Anthracene-9-carboxylic Acid Ligands and CsPbBr<sub>3</sub> and CsPbI<sub>3</sub> Nanocrystals. *J. Phys. Chem. C* **2021**, *125*, 1447.
- (282) He, S.; Han, Y.; Guo, J.; Wu, K. Entropy-Gated Thermally Activated Delayed Emission Lifetime in Phenanthrene-Functionalized CsPbBr<sub>3</sub> Perovskite Nanocrystals. *J. Phys. Chem. Lett.* **2021**, *12*, 8598.
- (283) Luo, X.; Lai, R.; Li, Y.; Han, Y.; Liang, G.; Liu, X.; Ding, T.; Wang, J.; Wu, K. Triplet Energy Transfer from CsPbBr<sub>3</sub> Nanocrystals Enabled by Quantum Confinement. *J. Am. Chem. Soc.* **2019**, *141*, 4186.
- (284) Kong, Z.-C.; Zhang, H.-H.; Liao, J.-F.; Dong, Y.-J.; Jiang, Y.; Chen, H.-Y.; Kuang, D.-B. Immobilizing Re(CO)<sub>3</sub>Br(dcbpy) Complex on CsPbBr<sub>3</sub> Nanocrystal for Boosted Charge Separation and Photocatalytic CO<sub>2</sub> Reduction. *Solar RRL* **2020**, *4*, 1900365.
- (285) De, A.; Das, S.; Samanta, A. Hot Hole Transfer Dynamics from CsPbBr<sub>3</sub> Perovskite Nanocrystals. *ACS Energy Lett.* **2020**, *5*, 2246.
- (286) Kobosko, S. M.; DuBose, J. T.; Kamat, P. V. Perovskite Photocatalysis. Methyl Viologen Induces Unusually Long-Lived Charge Carrier Separation in CsPbBr<sub>3</sub> Nanocrystals. *ACS Energy Lett.* **2020**, *5*, 221.
- (287) Akhil, S.; Dutt, V. G. V.; Singh, R.; Mishra, N. Surface-State-Mediated Interfacial Hole Transfer Dynamics between CsPbBr<sub>3</sub> Perovskite Nanocrystals and Phenothiazine Redox Couple. *J. Phys. Chem. C* **2021**, *125*, 22133.

- (288) Gandini, M.; Villa, I.; Beretta, M.; Gotti, C.; Imran, M.; Carulli, F.; Fantuzzi, E.; Sassi, M.; Zaffalon, M.; Brofferio, C.; Manna, L.; Beverina, L.; Vedda, A.; Fasoli, M.; Gironi, L.; Brovelli, S. Efficient, fast and reabsorption-free perovskite nanocrystal-based sensitized plastic scintillators. *Nat. Nanotechnol.* **2020**, *15*, 462.
- (289) Ma, J.; Fang, C.; Chen, C.; Jin, L.; Wang, J.; Wang, S.; Tang, J.; Li, D. Chiral 2D perovskites with a high degree of circularly polarized photoluminescence. *ACS Nano* **2019**, *13*, 3659.
- (290) Hubley, A.; Bensalah-Ledoux, A.; Baguenard, B.; Guy, S.; Abécassis, B.; Mahler, B. Chiral perovskite nanoplatelets exhibiting circularly polarized luminescence through ligand optimization. *Adv. Opt. Mater.* **2022**, *10*, 2200394.
- (291) Shi, Y.; Duan, P.; Huo, S.; Li, Y.; Liu, M. Endowing perovskite nanocrystals with circularly polarized luminescence. *Adv. Mater.* **2018**, *30*, 1705011.
- (292) Liu, P.; Chen, W.; Okazaki, Y.; Battie, Y.; Brocard, L.; Decossas, M.; Pouget, E.; Müller-Buschbaum, P.; Kauffmann, B.; Pathan, S.; et al. Optically active perovskite CsPbBr<sub>3</sub> nanocrystals helically arranged on inorganic silica nanohelices. *Nano Lett.* **2020**, *20*, 8453.
- (293) Ma, W.; Xu, L.; de Moura, A. F.; Wu, X.; Kuang, H.; Xu, C.; Kotov, N. A. Chiral Inorganic Nanostructures. *Chem. Rev.* **2017**, *117*, 8041.
- (294) Wei, Q.; Ning, Z. Chiral Perovskite Spin-Optoelectronics and Spintronics: Toward Judicious Design and Application. *ACS Mater. Lett.* **2021**, *3*, 1266.
- (295) Hu, Y.; Florio, F.; Chen, Z.; Phelan, W. A.; Siegler, M. A.; Zhou, Z.; Guo, Y.; Hawks, R.; Jiang, J.; Feng, J.; Zhang, L.; Wang, B.; Wang, Y.; Gall, D.; Palermo, E. F.; Lu, Z.; Sun, X.; Lu, T.-M.; Zhou, H.; Ren, Y.; Wertz, E.; Sundararaman, R.; Shi, J. A chiral switchable photovoltaic ferroelectric 1D perovskite. *Sci. Adv.* **2020**, *6*, eaay4213.
- (296) Ma, J.; Wang, H.; Li, D. Recent Progress of Chiral Perovskites: Materials, Synthesis, and Properties. *Adv. Mater.* **2021**, *33*, 2008785.
- (297) Rajput, P. K.; Poonia, A. K.; Mukherjee, S.; Sheikh, T.; Shrivastava, M.; Adarsh, K. V.; Nag, A. Chiral Methylbenzylammonium Bismuth Iodide with Zero-Dimensional Perovskite Derivative Structure. *J. Phys. Chem. C* **2022**, *126*, 9889.
- (298) Billing, D. G.; Lemmerer, A. Bis[(S)-β-phenethylammonium] Tribromoplumbate(II). *Acta Crystallogr. E* **2003**, *59*, m381.
- (299) Ma, J.; Fang, C.; Chen, C.; Jin, L.; Wang, J.; Wang, S.; Tang, J.; Li, D. Chiral 2D perovskites with a high degree of circularly polarized photoluminescence. *ACS Nano* **2019**, *13*, 3659.
- (300) Wang, L.; Xue, Y.; Cui, M.; Huang, Y.; Xu, H.; Qin, C.; Yang, J.; Dai, H.; Yuan, M. A Chiral Reduced-Dimension Perovskite for an Efficient Flexible Circularly Polarized Light Photodetector. *Angew. Chem., Int. Ed.* **2020**, *132*, 6504.
- (301) Chen, C.; Gao, L.; Gao, W.; Ge, C.; Du, X.; Li, Z.; Yang, Y.; Niu, G.; Tang, J. N. c. Circularly Polarized Light Detection Using Chiral Hybrid Perovskite. *Nat. Commun.* **2019**, *10*, 1927.
- (302) Ahn, J.; Lee, E.; Tan, J.; Yang, W.; Kim, B.; Moon, J. J. M. H. A New Class of Chiral Semiconductors: Chiral-organic-molecule-Incorporating Organic–inorganic Hybrid Perovskites. *Mater. Horiz.* **2017**, *4*, 851.
- (303) Ahn, J.; Ma, S.; Kim, J.-Y.; Kyhm, J.; Yang, W.; Lim, J. A.; Kotov, N. A.; Moon, J. Chiral 2D Organic Inorganic Hybrid Perovskite with Circular Dichroism Tunable over Wide Wavelength Range. *J. Am. Chem. Soc.* **2020**, *142*, 4206.
- (304) Di Nuzzo, D.; Cui, L.; Greenfield, J. L.; Zhao, B.; Friend, R. H.; Meskers, S. C. Circularly Polarized Photoluminescence from Chiral Perovskite Thin Films at Room Temperature. *ACS Nano* **2020**, *14*, 7610.
- (305) Liu, T.; Shi, W.; Tang, W.; Liu, Z.; Schroeder, B. C.; Fenwick, O.; Fuchter, M. J. High Responsivity Circular Polarized Light Detectors based on Quasi Two-Dimensional Chiral Perovskite Films. *ACS Nano* **2022**, *16*, 2682.
- (306) Jana, M. K.; Song, R.; Liu, H.; Khanal, D. R.; Janke, S. M.; Zhao, R.; Liu, C.; Valy Vardeny, Z.; Blum, V.; Mitzi, D. B. Organic-to-inorganic structural chirality transfer in a 2D hybrid perovskite and impact on Rashba-Dresselhaus spin-orbit coupling. *Nat. Commun.* **2020**, *11*, 4699.
- (307) Zhao, L.; Han, X.; Zheng, Y.; Yu, M.-H.; Xu, J. Tin-Based Chiral Perovskites with Second-Order Nonlinear Optical Properties. *Adv. Photon. Res.* **2021**, *2*, 2100056.
- (308) Moon, T. H.; Oh, S.-J.; Ok, K. M. [(R)-C<sub>8</sub>H<sub>12</sub>N<sub>4</sub>][Bi<sub>2</sub>Br<sub>10</sub>] and [(S)-C<sub>8</sub>H<sub>12</sub>N<sub>4</sub>][Bi<sub>2</sub>Br<sub>10</sub>]: chiral hybrid bismuth bromides templated by chiral organic cations. *ACS omega* **2018**, *3*, 17895.
- (309) Yao, L.; Zeng, Z.; Cai, C.; Xu, P.; Gu, H.; Gao, L.; Han, J.; Zhang, X.; Wang, X.; Wang, X.; Pan, A.; Wang, J.; Liang, W.; Liu, S.; Chen, C.; Tang, J. Strong Second- and Third-Harmonic Generation in 1D Chiral Hybrid Bismuth Halides. *J. Am. Chem. Soc.* **2021**, *143*, 16095.
- (310) Kim, Y.-H.; Zhai, Y.; Gaubling, E. A.; Habisreutinger, S. N.; Moot, T.; Rosales, B. A.; Lu, H.; Hazarika, A.; Brunecky, R.; Wheeler, L. M.; Berry, J. J.; Beard, M. C.; Luther, J. M. Strategies to Achieve High Circularly Polarized Luminescence from Colloidal Organic–Inorganic Hybrid Perovskite Nanocrystals. *ACS Nano* **2020**, *14*, 8816.
- (311) Ye, C.; Jiang, J.; Zou, S.; Mi, W.; Xiao, Y. Core–Shell Three-Dimensional Perovskite Nanocrystals with Chiral-Induced Spin Selectivity for Room-Temperature Spin Light-Emitting Diodes. *J. Am. Chem. Soc.* **2022**, *144*, 9707.
- (312) Georgieva, Z. N.; Bloom, B. P.; Ghosh, S.; Waldeck, D. H. Imprinting Chirality onto the Electronic States of Colloidal Perovskite Nanoplatelets. *Adv. Mater.* **2018**, *30*, 1800097.
- (313) Hubley, A.; Bensalah-Ledoux, A.; Baguenard, B.; Guy, S.; Abécassis, B.; Mahler, B. Chiral Perovskite Nanoplatelets Exhibiting Circularly Polarized Luminescence through Ligand Optimization. *Adv. Opt. Mater.* **2022**, *10*, 2200394.
- (314) Kim, Y.-H.; Zhai, Y.; Gaubling, E. A.; Habisreutinger, S. N.; Moot, T.; Rosales, B. A.; Lu, H.; Hazarika, A.; Brunecky, R.; Wheeler, L. M.; et al. Strategies to achieve high circularly polarized luminescence from colloidal organic–inorganic hybrid perovskite nanocrystals. *ACS Nano* **2020**, *14*, 8816.
- (315) Ren, H.; Wu, Y.; Wang, C.; Yan, Y. 2D Perovskite Nanosheets with Intrinsic Chirality. *J. Phys. Chem. Lett.* **2021**, *12*, 2676.
- (316) Chen, W.; Zhang, S.; Zhou, M.; Zhao, T.; Qin, X.; Liu, X.; Liu, M.; Duan, P. Two-Photon Absorption-Based Upconverted Circularly Polarized Luminescence Generated in Chiral Perovskite Nanocrystals. *J. Phys. Chem. Lett.* **2019**, *10*, 3290.
- (317) Debnath, G. H.; Georgieva, Z. N.; Bloom, B. P.; Tan, S.; Waldeck, D. H. Using Post-synthetic Ligand Modification to Imprint Chirality onto the Electronic States of Cesium Lead Bromide (CsPbBr<sub>3</sub>) Perovskite Nanoparticles. *Nanoscale* **2021**, *13*, 15248.
- (318) Kim, Y.-H.; Song, R.; Hao, J.; Zhai, Y.; Yan, L.; Moot, T.; Palmstrom, A. F.; Brunecky, R.; You, W.; Berry, J. J.; Blackburn, J. L.; Beard, M. C.; Blum, V.; Luther, J. M. The Structural Origin of Chiroptical Properties in Perovskite Nanocrystals with Chiral Organic Ligands. *Adv. Funct. Mater.* **2022**, *32*, 2200454.
- (319) He, T.; Li, J.; Li, X.; Ren, C.; Luo, Y.; Zhao, F.; Chen, R.; Lin, X.; Zhang, J. Spectroscopic studies of chiral perovskite nanocrystals. *Appl. Phys. Lett.* **2017**, *111*, 151102.
- (320) Zhao, B.; Gao, X.; Pan, K.; Deng, J. Chiral Helical Polymer/Perovskite Hybrid Nanofibers with Intense Circularly Polarized Luminescence. *ACS Nano* **2021**, *15*, 7463.
- (321) Wang, C. T.; Chen, K.; Xu, P.; Yeung, F.; Kwok, H. S.; Li, G. Fully chiral light emission from CsPbX<sub>3</sub> perovskite nanocrystals enabled by cholesteric superstructure stacks. *Adv. Funct. Mater.* **2019**, *29*, 1903155.
- (322) Dong, Y.; Zhang, Y.; Li, X.; Feng, Y.; Zhang, H.; Xu, J. Chiral Perovskites: Promising Materials Toward Next-generation Optoelectronics. *Small* **2019**, *15*, 1902237.
- (323) Long, G.; Sabatini, R.; Saidaminov, M. I.; Lakhwani, G.; Rasmita, A.; Liu, X.; Sargent, E. H.; Gao, W. Chiral-perovskite optoelectronics. *Nat. Rev. Mater.* **2020**, *5*, 423.
- (324) Ma, S.; Ahn, J.; Moon, J. Chiral Perovskites for Next-Generation Photonics: From Chirality Transfer to Chiroptical Activity. *Adv. Mater.* **2021**, *33*, 2005760.

(325) Georgieva, Z. N.; Zhang, Z.; Zhang, P.; Bloom, B. P.; Beratan, D. N.; Waldeck, D. H. Ligand Coverage and Exciton Delocalization Control Chiral Imprinting in Perovskite Nanoplatelets. *J. Phys. Chem. C* **2022**, *126*, 15986.

## Recommended by ACS

### Colloidal CsPbX<sub>3</sub> Nanocrystals with Thin Metal Oxide Gel Coatings

Dominic Guggisberg, Dmitry N. Dirin, *et al.*

MARCH 20, 2023  
CHEMISTRY OF MATERIALS

READ 

### Halide-Driven Halogen-Hydrogen Bonding versus Chelation in Perovskite Nanocrystals: A Concept of Charge Transfer Bridging

Mihir Manna, Tushar Debnath, *et al.*

JANUARY 06, 2023  
THE JOURNAL OF PHYSICAL CHEMISTRY LETTERS

READ 

### Surface Reconstruction of CsPbBr<sub>3</sub> Nanocrystals by the Ligand Engineering Approach for Achieving High Quantum Yield and Improved Stability

Yu Zhang, Junhao Chu, *et al.*

APRIL 20, 2023  
LANGMUIR

READ 

### Highly Stable Perovskite Nanocrystals with Pure Red Emission for Displays

Xue Ren, Feng-Lei Jiang, *et al.*

MARCH 17, 2023  
ACS APPLIED NANO MATERIALS

READ 

Get More Suggestions >